To the Graduate Council:

I am submitting herewith a thesis written by Joel Lee McDuffee entitled "Pressure Gradient Modeling During Subcooled Boiling in High Heat Flux and High Mass Flux Systems." I have examined the final copy of this thesis for form and content and recommend that it be accepted in partial fulfillment of the requirements for the degree of Master of Science, with a major in Engineering Science.

Arthur E. Ruggles

Arthur E. Ruggles, Major Professor

We have read this thesis
and recommend its acceptance:

A J Baker

Matt Fontana

Accepted for the Council:

C W Minkel

Associate Vice Chancellor
and Dean of The Graduate School

PRESSURE GRADIENT MODELING DURING SUBCOOLED BOILING IN HIGH HEAT FLUX AND HIGH MASS FLUX SYSTEMS

A Thesis

Presented For The

Master Of Science

Degree

The University Of Tennessee, Knoxville

Joel Lee McDuffee

December 1995

Dedication

This thesis is dedicated

to my wife, Genia, for her love, support, and confidence

and

to my father, Kenneth, who never doubts his abilities and taught me never to doubt my own

and

to my mother, Ruth, who taught me to read, to question, to think, and to learn.

Acknowledgments

I would like to thank my research advisors, Dr. Arthur E. Ruggles at the University of Tennessee and Dr. Moshe Siman-Tov at Oak Ridge National Laboratory, for providing support and guidance for this thesis.

I would also like to thank the Thermal Systems Section of the Engineering Technology Division of Oak Ridge National Laboratory both for funding this research and for providing a creative atmosphere in which to work.

Abstract

A historical overview of the methods used to predict the channel pressure drop in subcooled boiling is given in this study. It is recommended for the conditions of the Advanced Neutron Source reactor that the drift-flux model developed by Avdeev [1982-1988] be used to predict the local pressure gradient. This reactor has fuel cooling channels with a 1.27 mm gap, 80 mm span, and 0.507 m length. The average heat flux is 6 MW/m^2, the channel inlet temperature is 45°C, the nominal mass flux is 25,000 kg/m^2 s, and the exit pressure is 1.7 MPa. The model predictions using the recommended correlations are about 6% high on average with a standard deviation of 0.10 in the single-phase and partially developed subcooled boiling regions. When the fully developed boiling region is included, the average prediction of pressure drop is 13% high with a standard deviation of 0.12.

Three mechanistic approaches are developed that predict the increase in wall shear due to bubble ebullition. These models are shown to produce trends consistent with existing data. It is also shown that the combination of high heat flux, high mass flux, and small equivalent diameter causes the bubble departure size and the laminar sublayer to be roughly equal based on conventional models. It is demonstrated experimentally that bubble ebullition at the channel surface of the THTL test section disrupts the oxide layer and creates a surface with a roughness scale two or three times the predicted laminar sublayer thickness.

It is established that under low pressure and high Reynolds number flows, the onset of net vapor generation (ONVG) is a good approximation to the location of the minimum in the channel demand curve. Alternatively, ONVG precedes the minimum in the demand curve significantly for

conditions of high pressure and low Reynolds number, as long as the flow Peclet number remains above 70,000.

Table of Contents

List of Tables

List of Figures

List of Symbols and Abbreviations

Symbols

A	area (m^2)
A_s	surface area (m^2)
A_{xs}	cross sectional area (m^2)
c_0	void distribution parameter
C_p	liquid specific heat (J/kg °C)
C_{vm}	virtual mass coefficient
d	equivalent diameter (m)
E	energy (J)
f	frequency (1/s)
f	function
F_{τ_w}	general force due to wall shear (N)
F_{Mi}	general force due to interphase momenta transfer (N)
F_{fi}	general force due to interphase drag (N)
F_{τ_i}	general force due to interphase shear (N)
F_{vm}	general force due to liquid resistance to bubble motion (N)
F_σ	bubble force due to surface tension (N)
F_{bu}	bubble force due to buoyancy (N)
F_{in}	bubble force due to inertial growth (N)
F_p	bubble force due to normal pressure differences (N)
F_τ	bubble force due to tangential pressure (shear) (N)
F_{lift}	bubble force due to lift (N)
FDB	Fully Developed Subcooled Boiling
G	mass flux (kg/m^2 s)
g	acceleration due to gravity (m/s^2)
h	liquid enthalpy (J/kg)
$h_{1\phi}$	single-phase, forced-convective heat transfer coefficient (W/m^2 °C)
h_{fg}	latent heat of evaporation (J/kg)
IB	Incipience of Boiling
k	conductivity (W/m °C)
K	constant
l	mixing length (m)
$\dot{m}$	mass flow rate (kg/s)
m_{vm}	virtual mass (kg)
n	bubble area number density (1/m^2)
$\mathbf{n}$, $\mathbf{t}$	unit vectors for the directions normal and tangential to the wall, respectively
OBB	Onset of Bulk Boiling
ONVG	Onset of Net Vapor Generation

P	pressure (Pa)
PDB	Partially Developed Subcooled Boiling
P_h	heated perimeter (m)
q, $q_{applied}$	applied heat flux (W/m²)
q_{evap}	heat flux due to bubble evaporation (W/m²)
q_{pump}	heat flux due to bubble ebullition (W/m²)
q_{core}	portion of the applied heat flux used to increase bulk temperature
q_{cond}	heat supplied to bulk flow via bubble condensation, normalized to wall area
r	radius (m)
r_c	cavity radius (m)
s	arbitrary state space
T	temperature (°C)
t	time (s)
t_{life}	bubble lifetime (s)
u	velocity (m/s)
u'	velocity perturbation tangential to the wall (m/s)
u_{kd}	drift velocity (m/s)
u_m	mixture velocity (m/s)
V	volume (m³)
v^*	friction velocity, $(\tau_w / \rho_l)^{1/2}$
v'	velocity perturbation normal to the wall (m/s)
y	coordinate normal to the wall (m)

Greek Symbols

μ	dynamic viscosity (kg/m s)
ψ	contact angle (rad)
ϕ, θ	angle (rad)
α_l	thermal diffusivity (m²/s)
δ	reference thickness (m)
δ_{lam}	laminar sublayer thickness (m)
$\Delta\rho$	$\rho_l - \rho_v$
ΔT_{wall}	wall superheat (°C)
ε_H, ε_M	eddy viscosity for heat transfer and momentum, respectively (m²/s)
Γ	volumetric mass generation rate (kg/m³ s)
Γ_{ig}	interfacial volumetric mass generation rate for vapor (kg/m³ s)
λ	subcooling (°C)
ν	kinematic viscosity (m²/s)
ρ	density (kg/m³)
σ	surface tension (N/m)
τ	shear stress (Pa)

Dimensionless Numbers and Groups

α	void fraction
Bo	Boiling Number, $q / G\, h_{fg}$
f	friction factor
g'	non-dimensional gravity, $g\, d\, (\rho_l\, d / \mu)^2$
Ja	Jacob number, $(T_w - T_s)\, C_p\, \rho_l / \rho_v\, h_{fg}$
k^+	non-dimensional roughness height, $k\, v^* / \nu$
l	length to diameter ratio, L/d
M_0	$\mu\, (\sigma\, d\, \rho_l)^{-1/2}$
M_1	$q\, d / \mu\, h_{fg}$
M_2	$(\rho_v\, d / \mu)\, (\sigma\, g\, \Delta\rho / \rho_l^2)^{1/4}$
Nu_{si}	Nusselt number based on the inlet subcooling, $q\, d / k\, \lambda_i$
P'	non-dimensional pressure, $\Delta P\, d^2\, \rho_l / \mu^2$
Pe	Peclet number, Re Pr, $G\, d\, C_p / k$
Pr	Prandtl number, $\mu\, C_p / k$
Pr_T	turbulent Prandtl number, $\varepsilon_M / \varepsilon_H$
R	ratio of channel radius to bubble diameter, r / d_b
Re	Reynolds number, $G\, d / \mu$
St	Stanton number, $q / G\, C_p\, \lambda$
T^+	normalized two-phase temperature profile, $(T(z^+) - T_{ONVG}) / (T_s - T_{ONVG})$
T_P^*	$(\mu^2 / \lambda_i\, d^2\, \rho_l)\, (dT_s / dP)$
u^+	non-dimensional velocity, u / v^*
x	mass quality
x_{eq}	equilibrium mass quality
y^+	non-dimensional distance from the wall, $y\, v^* / \nu$
z^+	normalized two-phase length, $(z - z_{ONVG}) / (z_{sat} - z_{ONVG})$

Subscripts

0	value at a reference position
1, 1ϕ	single-phase
2ϕ	two-phase
a	acceleration
av	average
b	bubble
cond	condensation
core	value at the channel core
d	departure
f	friction
g	gravitational
h	heated

i	inlet
l	liquid
m	maximum
ONVG	Onset of Net Vapor Generation
s	saturation
σ	surface tension
t	turbulent
v	vapor
w	wall
wet	wetted

Introduction And Background

There are an increasing number of devices that require the removal of very high power densities. Some examples include the Advanced Neutron Source (ANS) reactor, hypersonic aircraft, beam dumps in fusion energy, spallation neutron sources, and plasma arc torches. One of the most efficient ways to remove high power densities is forced convection using a high mass flux and a highly subcooled flow in parallel cooling channels. These cooling channels must often operate at low to intermediate pressures (i.e., less than 5 MPa) to reduce the conduction lengths associated with the pressure boundaries. The design limit for these systems is usually a static flow instability first described by Ledinegg [1932] and commonly known as a flow excursion. This instability is shown schematically in Figure 1 and Figure 2.

In Figure 1, a parallel channel assembly is shown with shared plenums at the inlet and exit and an average applied heat load for the entire system. The pressure drop across the assembly is common to all the channels and is not significantly affected by any single channel. Also shown in Figure 1 is a blowup of two channels from the assembly designated as channel I and channel II. Channel I represents a reference channel in the assembly with an average applied heat flux. The heat flux applied to channel II is slightly larger than the average and is sufficient for boiling to occur at the exit.

Figure 2 shows the demand curves for channels I and II. The system pressure drop, ΔP_{system}, corresponds to the minimum in the demand curve for channel II while the reference channel is still single phase. The minimums in the demand curves occur because the production of void after the onset of boiling results in a substantial increase in the convective acceleration of the

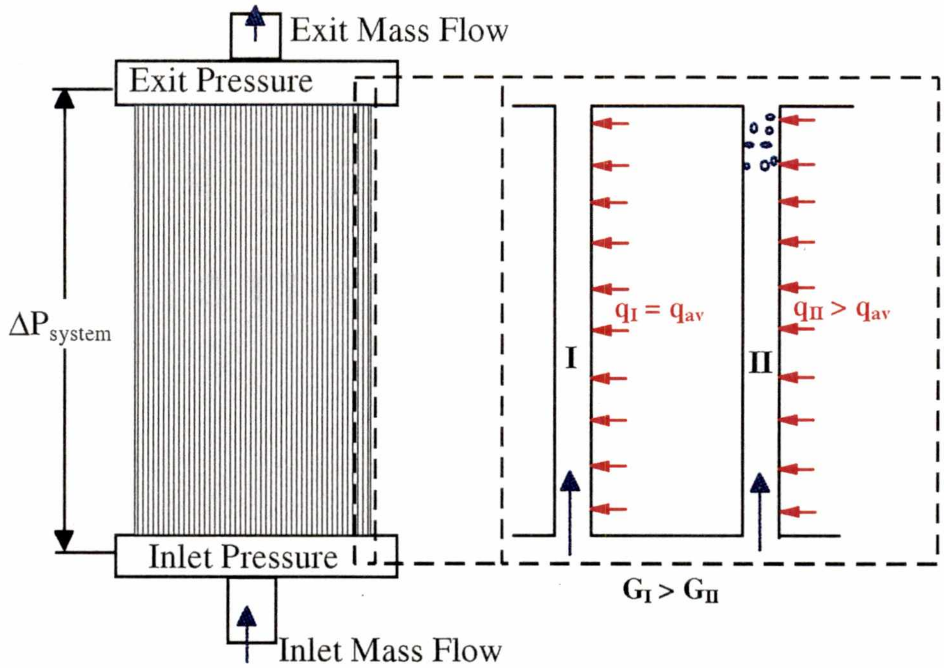

Figure 1. A Flow Excursion Schematic for Parallel Channels.

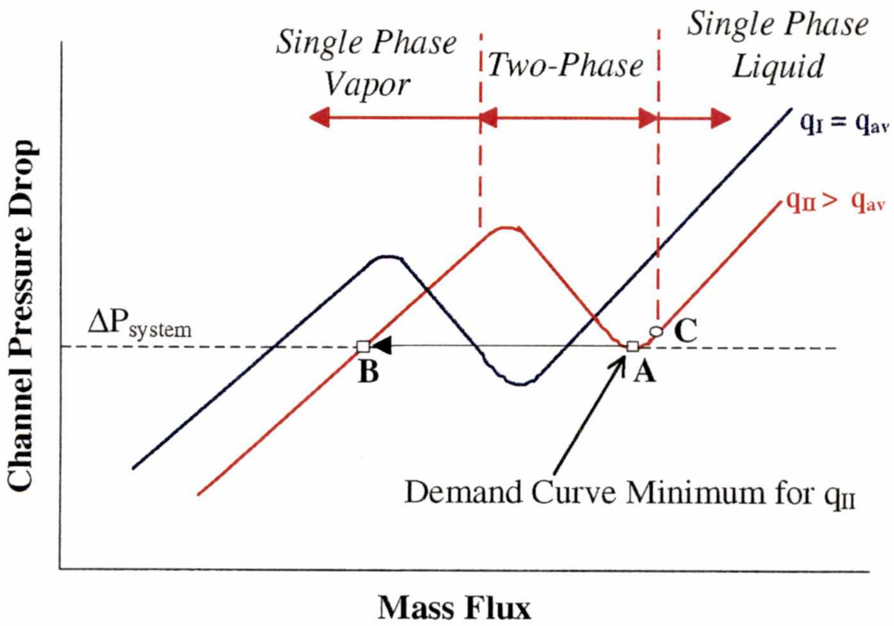

Figure 2. Demand Curve Schematic.

flows and a corresponding increase in the channel flow resistances. Since the pressure drop in the assembly is common for all channels and not significantly affected by a single channel, the mass flux in channel II will decrease in an attempt to regain equilibrium. Therefore, if the heat flux in channel II is perturbed from the minimum, the mass flux in channel II will follow the line **AB** to a corresponding point on the single phase vapor line (point B) at a significantly lower mass flux. The lower mass flux in channel II is usually insufficient to absorb the applied heat load, and channel II will fail during the flow excursion due to a primary departure from nucleate boiling.

The mass flux at the minimum in the pressure demand curve can be predicted if accurate models exist for the resistance to flow in the channel in the single-phase and two-phase regions. The mass flux at the minimum in the pressure demand characteristic is closely connected to the conditions that generate significant void at the channel exit in high mass flux and low pressure systems (point **C** in Figure 2). Accurate prediction of the mass flux that allows significant void to appear in the channel requires accurate models for the flow resistance in the channel, both in the single-phase region and in the region between the Incipience of Boiling (IB) and the Onset of Net Vapor Generation (ONVG). Otherwise, the exit enthalpy and subcooling cannot be calculated accurately, and the onset of significant void cannot be known.

This situation is exacerbated in systems where the applied heat flux is tailored to provide a constant margin to ONVG, or to IB, as is done in the Advanced Neutron Source (ANS) reactor fuel design [Yoder, et al, 1994]. This approach peaks the applied flux at the inlet of the cooling channel to take advantage of the higher subcooling available there. This causes a large portion of the cooling channel to be beyond IB prior to the occurrence of ONVG when off-normal conditions are considered. The flow resistance in the region from IB to ONVG is more significant to the evaluation of the thermal limits in such systems.

Conventional pressure drop modeling in high heat flux and mass flux systems relies on several general assumptions in concert with empirical correlations. Unfortunately, these correlations are often extrapolated beyond the flow situations for which they were developed. The purpose of this study is to evaluate existing methods for predicting the pressure drop in a coolant channel and to recommend a method that can be used for the conditions of high mass flux, small hydraulic diameter, and high, non-uniform heat flux. The specific application for this effort is the fuel cooling system for the ANS reactor. This reactor has fuel cooling channels with a 1.27 mm gap, 80 mm span, and 0.507 m length. The coolant channel cross-section is involute, but may be considered rectangular without significant error. The average heat flux is 6 MW/m^2, but the heat flux profile is peaked at the inlet with a peak-to-average ratio of about 2. The channel inlet temperature is 45°C, the nominal mass flux is 25,000 kg/m^2 s, and the exit pressure is 1.7 MPa.

The methods traditionally used to predict the pressure drop in a heated channel are described herein, and one of the methods is recommended for the flow conditions of the ANS reactor. Additionally, the development of some constitutive models that describe the increase in the pressure gradient in the partially developed boiling region are considered. Finally, the recommended pressure drop model is compared with data collected at the Thermal-Hydraulic Test Loop (THTL) facility by the ANS design team.

Because of the complexity of solving for the pressure gradient in a subcooled boiling flow, many approximations and assumptions are necessary to obtain a solution. The assumptions used in the derivations are considered in detail. This includes an evaluation of length scales and interfacial forces in the bubble boundary layer.

In many cases the data indicate that the point of ONVG coincides closely with the demand curve minimum. Since ONVG correlations are usually explicit and algebraic, there is a significant benefit for using ONVG as a conservative predictor to the demand curve minimum. The relationship between these two phenomena is established and conditions when ONVG is a reasonable predictor of the demand curve minimum are presented.

Chapter 1. Two-Phase Pressure Gradient Modeling

There are five flow situations that must be considered in modeling two-phase pressure drop that are defined by three lines of demarcation. The first line of demarcation is the point of IB which represents the set of flow and fluid conditions that allows the formation of vapor at the wall. IB separates single-phase forced-convection from partially developed subcooled boiling. The second line of demarcation is ONVG which represents the set of conditions that allow vapor bubbles at the wall to move into the bulk flow. ONVG separates the regions of partially developed subcooled boiling and fully developed subcooled boiling. The third line of demarcation is the onset of bulk boiling (OBB) where the bulk fluid has reached the saturation temperature. OBB separates the regions of fully developed subcooled boiling and bulk boiling. The fifth flow situation is the condensation region where the IB criterion is not met locally, but there is some void in the bulk fluid convected from upstream. These regions are shown schematically in Figure 3. This analysis concentrates on the regions of partially developed subcooled boiling (PDB) and fully developed subcooled boiling (FDB).

1.1 Conventional Modeling Techniques

There are many methods used to describe two-phase flow. The simplest model is the Homogeneous Equilibrium Model where the single-phase flow equations are solved for a hypothetical fluid with properties determined from an average of the liquid and vapor phases. The most complex is the completely Separated Flow Model where the field equations (continuity,

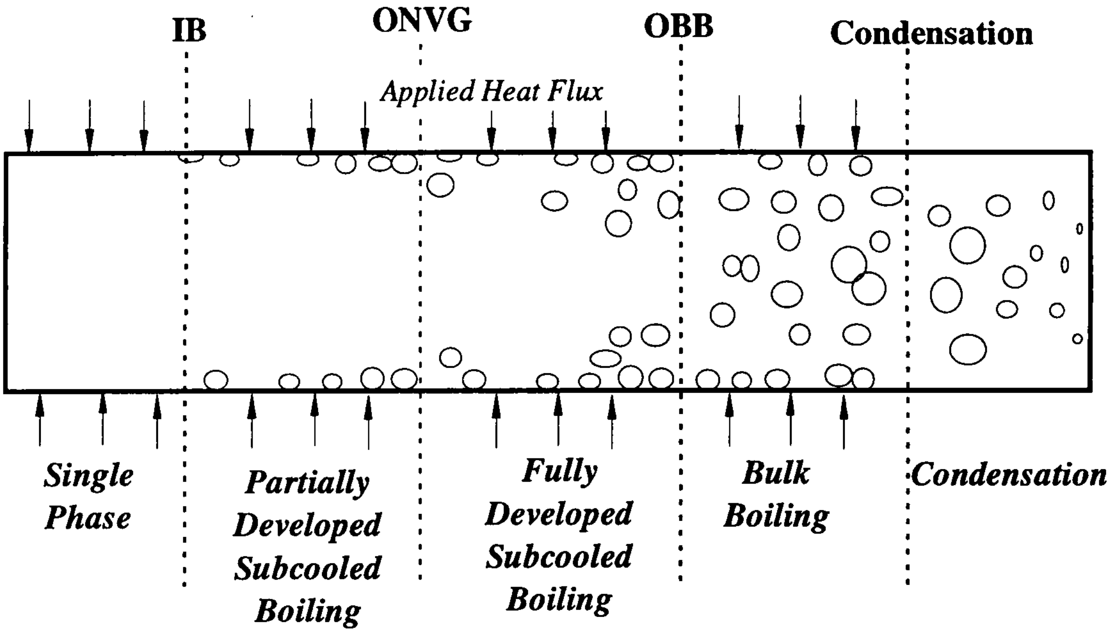

Figure 3. Boiling Regions.

momentum, and energy) are solved separately. However, the practical application of these models usually takes one of three forms: the boiling length approach, the drift-flux model (global and local), and the two-fluid model.

The boiling length approach has the significant advantage of simplicity and numerical stability, but contains limited flow physics. The global drift-flux models have considerable mechanistic basis but rely on global parameters that are ill defined. The local drift-flux models are generally more mechanistic than the global drift-flux models, but are also based on empirically defined parameters and are sometimes numerically unstable. The two-fluid models attempt to solve the field equations for both the fluid and vapor phases with no assumption of homogeneity or equilibrium. They are the most mechanistic of all the models, but the interfacial and fluid structure interaction terms (constitutive models) are often based on the same correlations used in the drift-flux models.

1.1.1 The Boiling Length

The boiling length model is an empirical approximation of the integral of the pressure over the channel length. It was originally developed by Reynolds [1954] and is characterized by the ratio of the two-phase pressure gradient to the single-phase pressure gradient.

$$\frac{(dP/dz)_{2\phi}}{(dP/dz)_{1\phi}} = f(z^+, \bar{s}) \qquad 1$$

where z^+ is the fractional distance between the onset of boiling and the bulk saturation point. The earliest forms of $f(z^+, s)$ were hyperbolic or exponential functions of z^+ alone. Recent uses of the boiling length approach are more sophisticated, but even the most advanced forms of this approach are simpler than the drift-flux models, which make them attractive for analysis of flow situations where large amounts of data have been taken. However, this approach is purely empirical which makes extrapolation to conditions beyond existing data impossible to defend. Table 1 presents a list of forms for $f(z^+, s)$ given by Hahne, et al [1993]. These models do not include gravitational effects.

1.1.2 The Drift-flux Model

The drift-flux model is significantly more mechanistic than the boiling length approach in that it considers non-equilibrium between the vapor and liquid, velocity differences between the vapor and liquid, radial vapor concentration profiles, and axial temperature profiles. More

Table 1. Pressure Drop Correlation Summary for Boiling Length Models.

Investigator	$f(z^+, s)$
Reynolds [1954]	$\cosh[(1.2 + 1.458\frac{q}{10^6})z^+]$
Owens & Schrock [1960]	$0.97 + 0.028\exp(6.13\, z^+)$
Rohde [1962]	$\exp\left[\frac{26.48}{P}\left(\frac{q}{q_m} - 1\right)\right]$ where $q_m = \frac{\lambda_i + \lambda}{4z^+/(\dot{m}C_p d) + 1/h_{1\phi}}$
Tarasova & Orlov [1962]	$1 + 3.09\left(\frac{\rho_l}{\rho_v}Bo\right)^{0.7}\left[7 - \sqrt{1.48\frac{x_{eq}(z^+)}{x_{eq}(z^+_{ONVG})}}\right]\frac{d_h}{d_{wet}}$
Tarasova, et al [1966]	$1 + Bo^{0.7}\left(\frac{\rho_l}{\rho_v}\right)^{0.78}\frac{20z^+}{1.315 - z^+}$
Hahne, et al [1993]	$1 + 80Bo^{1.6}Ja^{-1.2}\frac{\rho_l}{\rho_v}\frac{d_h}{d_{wet}}$

importantly, this model separates the very different effects of wall shear and flow acceleration on the overall pressure gradient, as shown in Equations 2 through 4.

$$\left.\frac{\Delta P}{\Delta z}\right|_{friction} = -\frac{1}{2}\frac{f_{2\phi}}{d}\frac{G^2}{\rho_l} \qquad (2)$$

$$\left.\frac{\Delta P}{\Delta z}\right|_{gravity} = -g[\alpha\rho_g + (1-\alpha)\rho_l] \qquad (3)$$

$$\left.\frac{\Delta P}{\Delta z}\right|_{acceleration} = -G^2\frac{d}{dz}\left[\frac{[1-x]^2}{[1-\alpha]\rho_l} + \frac{x^2}{\alpha\rho_g}\right] \qquad (4)$$

The channel averaged void fraction, α, is a crucial parameter in Equations 3 and 4 and is dependent on both the radial void distribution and the velocity difference between the vapor and liquid. The continuity equation for the two phase system (in indicial notation) is

$$\frac{\partial}{\partial t}(\alpha_k \rho_k) + \frac{\partial}{\partial x_j}(\alpha_k u_k) = 0 \tag{5}$$

where k represents the phase and j represents direction.

Assuming constant liquid and vapor density and noting that $\alpha_l + \alpha_v = 1$, a mixture velocity, u_m, can be defined

$$u_m = \alpha_k u_k \tag{6}$$

such that

$$\frac{\partial u_m}{\partial x_j} = 0 \tag{7}$$

This is convenient since u_m is independent of space for one-dimensional flow and is therefore a function of time alone. Multiplying the drift velocity, $u_{kd} = u_k - u_m$, by α_i gives

$$\alpha_k u_k = u_m \alpha_k + \alpha_k u_{kd} \tag{8}$$

Taking the average over the flow cross section (designated by < >) and dividing by $\langle\alpha_k\rangle\langle u_m\rangle$ yields

$$\frac{\langle \alpha_k u_k \rangle}{\langle \alpha_k \rangle \langle u_m \rangle} = \frac{\langle \alpha_k u_m \rangle}{\langle \alpha_k \rangle \langle u_m \rangle} + \frac{\langle \alpha_k u_{id} \rangle}{\langle \alpha_k \rangle \langle u_m \rangle} \tag{9}$$

If the void distribution in the channel is known, then the first term on the right hand side is also known due to the spatial independence of u_m.

$$\frac{\langle \alpha_k u_m \rangle}{\langle \alpha_k \rangle \langle u_m \rangle} = c_0 \tag{10}$$

Zuber and Findlay [1964] showed through further manipulation of Equations 9 and 10 that

$$\frac{\langle \alpha_k u_k \rangle}{\langle \alpha_k \rangle} = c_0 \langle u_m \rangle + \frac{\langle \alpha_k u_{kd} \rangle}{\langle \alpha_k \rangle} \qquad 11$$

This function is important since it allows the flow rates for each phase to be determined if the void profile, the total flow rate, and the drift velocity are known. Zuber further postulated that the drift velocity in bubbly flow is

$$\langle u_{kd} \rangle = 1.41 \left[\frac{\sigma g(\rho_l - \rho_v)}{\rho_l^2} \right] \qquad 12$$

Combining Equations 9 through 12 leads to a solution for the area averaged void fraction in a subcooled channel.

$$\langle \alpha \rangle = \frac{x}{c_0 \frac{\Delta\rho}{\rho_l} x + \left(c_0 + \frac{\langle u_{kd} \rangle}{\overline{u}_i} \right) \frac{\rho_v}{\rho_l}} \qquad 13$$

The drift-flux model is a popular method for calculating pressure drop in subcooled boiling and is referenced extensively in the literature [Maitra & Raju, 1975; Jia & Schrock, 1986; Hoffman & Wong, 1992]. The use of the method requires only that a correlation for the distribution parameter, c_0, and drift-flux, u_{id}, be chosen, of which there are numerous in the available literature. The method is relatively stable and easy to use.

The difference between the global and local drift-flux models is the way the channel quality and temperature profiles are treated. The global applications generally use empirical formulations that involve little flow physics. The local applications use quasi-mechanistic models for these profiles.

1.1.2.1 Global Models

The fundamental assumption in most global models is that the axial temperature profile can be modeled as a simple empirical function. Kroeger & Zuber [1968] recommend one of the following forms for the non-equilibrium temperature profile.

$$T^+ = \frac{T(z^+) - T_0}{T_s - T_0} \approx 1 - \exp(-z^+) \quad \textit{or} \quad \approx \tanh(z^+) \qquad 14$$

where z^+ is the fractional distance between IB and the bulk saturation point. Ahmad [1970] showed that the subcooling profile in the subcooled boiling regions may be an exponential function under certain limiting conditions; however, most investigators recommend the hyperbolic form of the profile [Jia & Schrock, 1986; Hoffman & Wong, 1992].

The local bulk quality is calculated with

$$x(z^+) = \frac{C_p \lambda_{ONVG}(z^+ - T^+)}{h_{fg} + C_p \lambda_{ONVG}(1 - T^+)} \qquad 15$$

The major deficiency of the method is the assumed form of the temperature profile since the true functional form will change when a non-uniform heat flux is applied. This is troublesome when many different axial heat flux profiles must be considered as is the case for a reactor fuel assembly.

1.1.2.2 Local Models

The purpose of the local conditions approach is to improve the drift-flux model by providing a more mechanistic basis for the mass quality development. Naturally, this leads to more equations and greater complexity. However, it also leads to formulations that are based on local flow conditions so they may be extended to non-uniform heat fluxes or unusual geometries.

Studies of boiling heat transfer often partition the locally applied heat flux into component parts. For subcooled boiling the heat flux may be divided into a single-phase component for the areas not affected by boiling, an evaporation heat flux that is used to create new vapor, and a pumping component due to the liquid displaced during the ebullition cycle [Lahey, 1974].

$$q_{applied} = q_{1\phi} + q_{evap} + q_{pump} \qquad 16$$

In a developed boiling situation, condensation from vapor bubbles in the liquid core region also adds enthalpy to the flow.

For boiling quality and void development, the particular microscopic effects of boiling are not of primary concern. Therefore, a bubble boundary layer is used to make ensemble averages for the flow behavior. Before ONVG, the bubbles form and collapse but remain attached to the wall. The bubble boundary layer will continuously grow as the average bubble diameter and bubble number density increase. Since the bubbles are attached to the wall, there is no condensation heat addition to the liquid internal energy from upstream. Additionally, all the applied heat flux, whether through single-phase convection, bubble evaporation, or local condensation, is directed into the liquid core region in a time averaged sense. There is some increase in the frictional pressure gradient due to bubble induced eddy transport in the bubble region. There is also some additional flow acceleration due to the decrease in liquid flow area.

Beyond ONVG the bubble boundary layer thickness remains roughly constant as the bubbles are free to escape into the flow and be replaced at the wall. There is an increase in the evaporation component of the heat flux as the bubbles are allowed to convect heat away from the surface through mass transfer. Condensation must be considered since the bubbles in the core region are surrounded by highly subcooled liquid, resulting in very short lifetimes.

The local conditions approach to modeling assumes that the particular modes of heat transfer mentioned above can be treated separately. The resulting heat transfer correlations are semi-empirical and based on inference from bubble lifetime data since direct measurements are rarely possible. In addition, they are usually functions of the local quality and void fraction, making the resulting formulation implicit.

Once the applied heat flux is partitioned, the local quality and temperature may be determined. The bulk temperature will increase in response to the part of the heat flux that proceeds to the bulk core and in response to vapor condensation. Vapor is produced by direct evaporation at the wall and consumed by condensation. The local quality is therefore given by the solution of

$$\frac{dx}{dz} = \frac{P_h}{GA_{xs}h_{fg}}(q_{applied} - q_{core} - q_{cond}) \qquad 17$$

while the local liquid bulk temperature is given by the solution of

$$\frac{dT}{dz} = \frac{P_h}{GA_{xs}C_p}(q_{core} + q_{cond}) \qquad 18$$

The specific correlations that are used to model the heat transfer modes vary widely. Table 2 gives a brief summary of the models used in three such investigations.

1.1.3 The Two-Fluid Model

The two-fluid model is the most ambitious of the predictive methods for calculating pressure gradients and is used extensively in the nuclear industry for safety analysis. It includes

Table 2. Heat Flux Partition Correlation Summary for Local Conditions Modeling.

Investigator	q_{core} or q_{evap}	q_{cond}
Rouhani & Axelsson [1970] (q_{evap} & q_{cond})	$\frac{q - h_{1\phi}\lambda(1-\alpha/\alpha_{core})}{\rho_v h_{fg} + C_p \rho_l \lambda}\rho_v h_{fg} P_h$	$30.0\lambda\frac{k}{Pr}\left(\frac{\rho_v}{\rho_l}\right)^2 A_{xs}^{2/3}\alpha^{2/3}\,Re\left[\frac{q\mu}{h_{fg}\sigma\Delta\rho}\right]^{-0.5}$
Larson & Tong [1969] (q_{core})	$-\rho_l C_p \frac{K}{Pr_T}\frac{u^+ R}{\ln(1-R)}\lambda$	condensation not included
Avdeev [1986] (q_{core} & q_{cond})	$\frac{G h_{fg}}{(6.28\log_{10} R + 1.28)^2}$	$0.007 G h_{fg}\alpha_{core} R\left(1-\frac{2}{R}\right)Re^{-0.3}\,Pr^{-0.5}\left(\frac{\alpha}{1-\alpha}\right)$

the two-fluid field equations without assumptions regarding homogeneity or equilibrium. One of the most popular forms is included in the RELAP5 code, which is a time-dependent, one-dimensional two-fluid model developed by the Idaho National Engineering Laboratory for the Nuclear Regulatory Agency. The following discussion is based primarily on the RELAP5/MOD3 Code Manual [Carlson, et al, 1990].

The continuity equations for one-dimensional flow with two fluids is

$$\frac{\partial}{\partial t}(\alpha_v \rho_v) + \frac{1}{A}\frac{\partial}{\partial x}(\alpha_v \rho_v u_v A) = \Gamma_v \qquad 19$$

$$\frac{\partial}{\partial t}(\alpha_l \rho_l) + \frac{1}{A}\frac{\partial}{\partial x}(\alpha_l \rho_l u_l A) = -\Gamma_v \qquad 20$$

where Γ_v is the vapor volumetric mass generation rate. The associated momentum equations can be written as

$$\alpha_v\rho_v A\frac{\partial u_v}{\partial t}+\frac{1}{2}\alpha_v\rho_v A\frac{\partial u_v^2}{\partial x}=-\alpha_v A\frac{\partial P}{\partial x}+\alpha_v\rho_v g_x A+F_{v,\tau_{wall}}+F_{v,Mi}+F_{v,fi}+F_{v,\tau i}+F_{v,vm} \quad 21$$

$$\alpha_l\rho_l A\frac{\partial u_l}{\partial t}+\frac{1}{2}\alpha_l\rho_l A\frac{\partial u_l^2}{\partial x}=-\alpha_l A\frac{\partial P}{\partial x}+\alpha_l\rho_l g_x A+F_{l,\tau_{wall}}+F_{l,Mi}+F_{l,fi}+F_{l,\tau i}+F_{l,vm} \quad 22$$

where

$F_{\tau_{wall}}$: wall friction force

F_{Mi} : momenta due to interphase transfer

F_{fi} : interphase frictional drag

F_{τ_i} : interphase shear

F_{vm} : virtual mass force

The models that represent the various forces in Equations 21 through 22 are presented in the RELAP5/MOD3 code manual [Carlson, et al, 1990]. The models are empirical and vary with flow regime.

Of particular concern for subcooled boiling are the mass generation rates since they are essential to the void development in the two-fluid model. In RELAP5 these rates are partitioned into a bulk fluid component, Γ_{ig}, and a wall component, Γ_w, similar to that described in the previous section. It should be noted that RELAP5 does not consider void until the criteria for ONVG is met according to the correlation of Saha & Zuber [1974].

$$St_{ONVG}=\frac{q}{GC_p\lambda}=0.0065 \qquad \text{(for Pe > 70,000)} \quad 23$$

$$Nu_{ONVG}=\frac{qd_e}{k\lambda}=455 \qquad \text{(for Pe < 70,000)} \quad 24$$

The wall component of the mass generation rate is taken from Lahey [1974], who superimposes the Saha & Zuber critical enthalpy with a microscopic bubble pumping term.

$$\Gamma_w = \frac{q''A_s}{h_{fg}V} \frac{(h_l - h_{ONVG})}{(h_{sat,l} - h_{ONVG})(1+\varepsilon)} \qquad 25$$

where

$$\varepsilon = \frac{\rho_l (h_{sat,l} - h_{ONVG})}{\rho_v h_{fg}} \qquad 26$$

The bulk mass generation rate is taken from Unal [1976] as modified by Riemke [1993]. The actual correlation used in RELAP is for the condensation heat transfer coefficient at the liquid-vapor interface. It is assumed that the implementation of this is

$$\Gamma_{ig} = \frac{h_c (T_v - T_l)}{Vh_{fg}} \qquad 27$$

The condensation heat transfer coefficient, h_c, is a semi-empirically determined factor given by

$$h_c = \frac{C\Phi h_{fg} d_b}{2(1/\rho_v - 1/\rho_l)} \qquad 28$$

where Φ is a velocity dependent parameter and C is a pressure dependent parameter. The bubble departure diameter given by Unal [1976] is based on a thermally controlled mechanism and assumes that departure occurs when the bubble can no longer sustain its growth. Unal shows that his model predicts data over a broad range of conditions including pressures from 0.1 to 17.7 MPa, heat fluxes from 0.45 to 10.64 MW/m^2, velocities from 0.8 to 9.15 m/s, and subcoolings from 3 to 86 °K. However, the data do not include the combination of high velocity and intermediate subcooling (i.e., 25 m/s and 9 degrees Kelvin) characteristic of the ANS reactor at full flow and full power just prior to ONVG.

Although the two-fluid model is generally accepted as the most correct of the available predictive tools, the implementation of hundreds of models for different flow situations into code requires intricate smoothing strategies and interpolation techniques to ensure computational reliability. For example, vapor is first predicted by RELAP5/MOD3 at ONVG. ONVG introduces strong nonlinearities, especially in low pressure, high heat flux situations where the wall void fraction is expected to be significant. Time smoothing strategies are employed in the RELAP5/MOD3 code to help deal with these nonlinearities without requiring excessively small time steps. These time smoothing strategies compromise the physics embodied in the conservation and constitutive models. Therefore, the steady-state performance of the models in RELAP5-MOD3 may not be directly related to the actual performance of the code during a fast transient such as a rapid depressurization.

1.1.4 Recommended Pressure Gradient Model

A local conditions model is desired since the heat flux profile to be considered is both non-uniform and time varying. A model due to Avdeev [1982-1988] is chosen for close examination and comparison to data since it was developed for flow conditions similar to those present in the ANS fuel cooling channels. The model by Avdeev [1982-1988] is chosen for several reasons. First, it has a good mechanistic basis, and the models are generally consistent at the flow regime boundaries. Second, the models were developed using a database that included data with high velocity and high heat flux. Third, it does a reasonably good job of correlating the experimental data obtained by the ANS design team.

Avdeev [1982-1988] uses R, which is the ratio of the channel radius to bubble diameter, as a non-dimensional parameter that carries through all the calculations and defines the character of the model. The R parameter is based entirely on local conditions. This allows for much greater flexibility in treating heat flux and temperature profiles. This flexibility is need for modeling situations such as those present in the ANS reactor because the heat flux and temperature profiles in the ANS are very different from situations commonly found in the literature, as shown in Figure 4 and Figure 5.

The bulk temperature rises sharply in the first half of the channel, as shown in Figure 5, and much more slowly in the second half of the channel where boiling could be expected to begin. The onset of boiling will flatten the temperature profile further as some of the applied heat flux is diverted to vapor formation. In addition, the ANS flux profile changes substantially during the fuel cycle. The calculations shown in Figure 4 and Figure 5 were based on an approximate beginning-of-life profile for the ANS fuel design.

The R parameter is central to the model proposed by Avdeev. This parameter is correlated for partially developed boiling by

$$St = \frac{q}{GC_p\lambda} = \left[6.28\log_{10}\left(\frac{d}{2d_{b,av}}\right) + 1.28\right]^{-2} = \left[6.28\log_{10}(R_{av}) + 1.28\right]^{-2} \qquad 29$$

while for fully developed boiling,

$$R_{max} = \frac{d}{d_{b,m}} = (0.93 + 0.65A^{0.25})^4 \qquad 30$$

where

$$A = \frac{Gd(h_s - h_{bulk})}{2k\Delta T_w} \qquad 31$$

and ΔT_w is correlated by [Mikheev & Mikheeva, 1973]

$$\Delta T_w = q_w^{0.33}\left[\frac{1 - 0.0045P}{3.4P^{0.18}}\right] \qquad 32$$

where P is the pressure in bar.

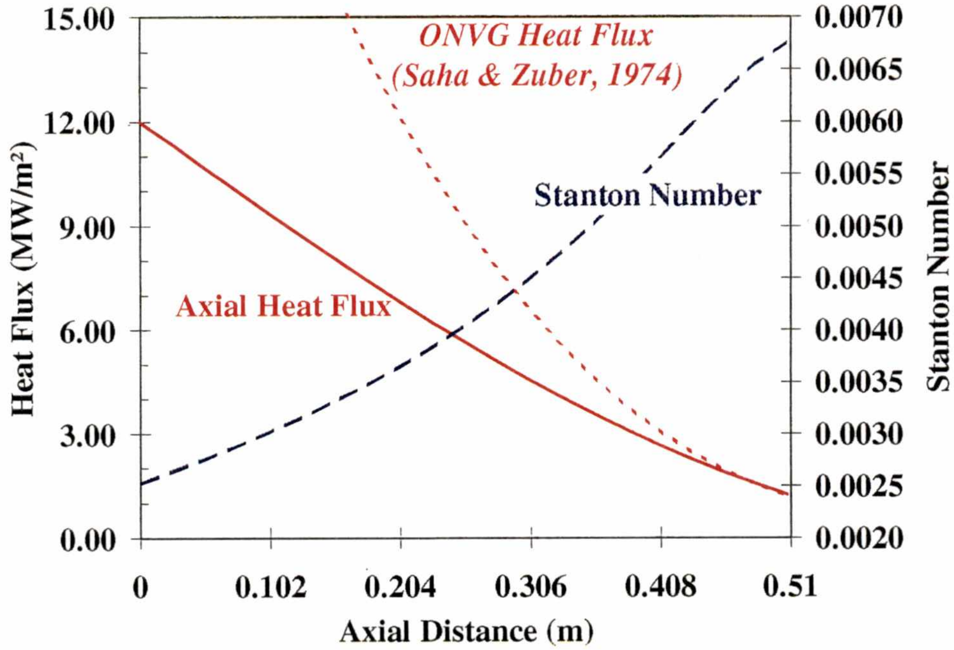

Figure 4. Heat Flux and Stanton Number Profile for an ANS Type Channel during Off-Normal Condition with an Average Heat Flux of 6 MW/m².

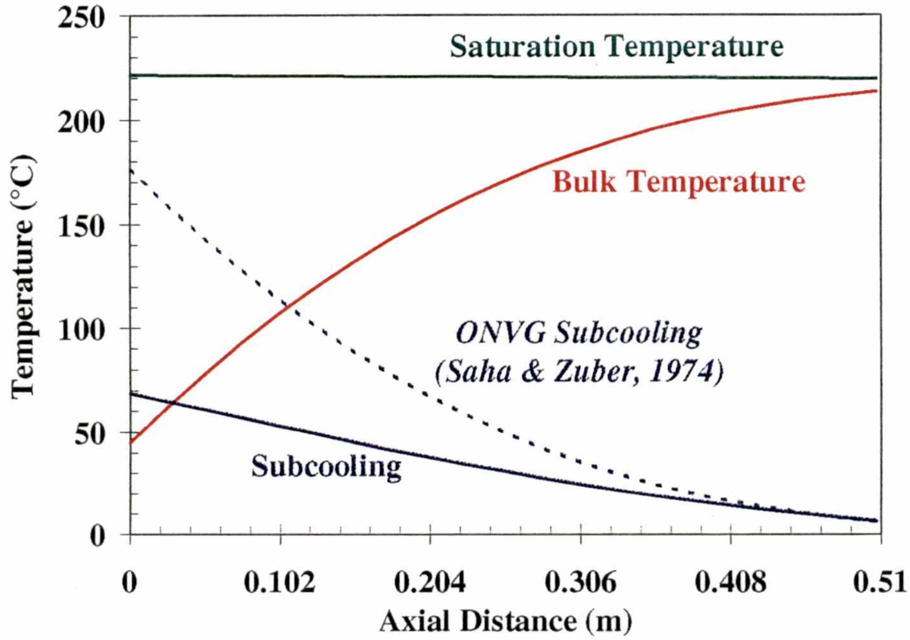

Figure 5. ANS Type Temperature Profile for an Off-Normal Condition with an Average Heat Flux of 6 MW/m².

In partially developed boiling, there is no net condensation or evaporation. The Stanton Number (St) in Equation 29 is therefore known and the *average* R can be calculated. The *maximum* R in fully developed boiling is correlated by Equation 30, and Avdeev recommends that Equation 30 be multiplied by a factor of 2.0 to obtain the *average* R ($d_{b,av} = 0.5 d_{b,m}$). For partially developed boiling, Equation 30 underpredicts R because Equation 32 overpredicts ΔT_w. In fully developed boiling, Equation 29 underpredicts R because it assumes that evaporation is at steady state and that there is no condensation. The greater of the two predictions from Equation 29 and 30 is taken as the best prediction for R in the model implementation. The transition from partially to fully developed subcooled boiling is defined by the point at which Equations 29 and 30 yield equivalent results for R_{av}.

The parameter R is especially useful since it allows the Reynolds analogy to be invoked to describe the relationship between the friction factor and heat transfer, hence the heat flux components are correlated in terms of the Stanton number. This is reasonable for water flows where the Prandtl number is close to unity. The two-phase friction factor used by Avdeev [1986] is derived by treating the bubble region as a rough surface.

$$f_{2\phi} = \left[1.74 - 2\log_{10}\left(\frac{1}{3.9R_{av}} + \frac{49}{Re^{0.91}}\right)\right]^{-2} \qquad 33$$

This formulation is convenient since R_{av} approaches infinity as the bubble diameter approaches zero, and the friction factor approaches the single-phase friction factor from Filonenko [1954], which is known to work well for high velocity flows [Siman-Tov, 1991].

$$\begin{aligned} f_{1\phi} &= \left[1.82\log_{10}(Re) - 1.64\right]^{-2} \\ &\approx \left[1.74 - 2\log_{10}\left(\frac{49}{Re^{0.91}}\right)\right]^{-2} \end{aligned} \qquad 34$$

Because there is no net evaporation or condensation before ONVG, it is not necessary to partition the heat flux into components in partially developed boiling. In a time averaged sense, all the heat flux applied to the wall is used to increase the bulk fluid enthalpy. In fully developed subcooled boiling, some of the applied heat will convect axially as vapor. Similarly, some heat will be supplied by bubbles that were created upstream and are condensing locally as shown in Figure 6. It is necessary to correlate the component of the locally applied heat flux that serves to raise the bulk temperature, q_{core}, and the heat flux that raises the bulk temperature by condensation, q_{cond} [Avdeev, 1986].

$$\begin{aligned} St_{core} &= \frac{q_{core}}{Gh_{fg}} \\ &= \frac{1}{(6.28\log_{10} R_{av} + 1.28)^2} \end{aligned} \qquad 35$$

$$\begin{aligned} St_{cond} &= \frac{q_{cond}}{Gh_{fg}} \\ &= 0.007\alpha_{core} R_{av}\left(1 - \frac{2}{R_{av}}\right) Re^{-0.3}\, Pr^{-0.5}\left(\frac{\alpha}{1-\alpha}\right)^{1/4} \end{aligned} \qquad 36$$

Note that a distinction is made between the wall and core regions, with the wall region defined as the annular region whose inner diameter is the channel diameter minus twice the bubble diameter. The wall void fraction is taken as constant throughout the subcooled boiling region at the value recommended by Avdeev, $\alpha_w = 0.524$, although the volume of the wall region increases with the average bubble diameter. This is in qualitative agreement with Sultan & Judd [1978] who found that a decrease in subcooling or increase in heat flux generally caused active nucleation sites to become more active, rather than more nucleation sites to become available. However, the

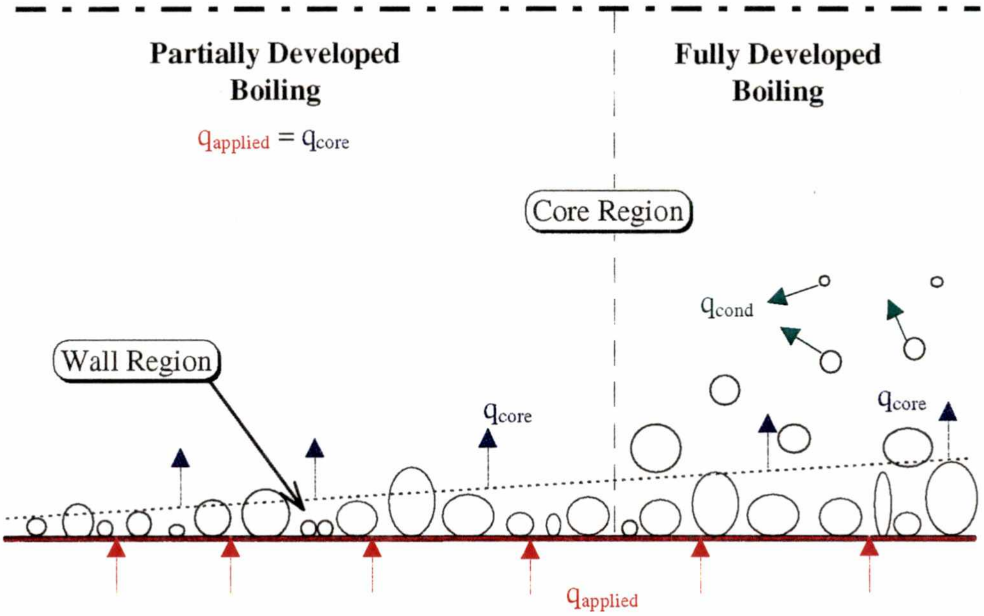

Figure 6. Local Conditions Model Schematic.

variation of the flow resistance with heat flux in the region between IB and ONVG may be sensitive to heater surface characteristics.

Assuming spherical bubbles, a wall void of 50% corresponds geometrically to a bubble separation distance of about 20% of the bubble diameter. Since there are no bubbles in the core flow in partially developed boiling, conservation of area yields that the total void fraction in partially developed boiling is 2 α_w /R.

The flow quality in the wall region is formulated via Reynolds analogy with the relation [Avdeev & Pekhterev, 1986]

$$x_w = 12\sqrt{\frac{f}{8}}\frac{(2/R)\rho_v\alpha_w}{\alpha\rho_v + (1-\alpha)\rho_l} \quad 37$$

The local bulk flow quality is described by the differential Equation 17. The "core" is the turbulent core where bubbles are assumed to be traveling. The void fraction in the core is the source of the condensation heat flux, and it is correlated by [Avdeev & Pekhterev, 1986]

$$\alpha_{core} = \frac{x - x_w}{1.2\left[x + (1-x)\dfrac{\rho_v}{\rho_l} - \dfrac{x_w}{\alpha_w}\right] + \left(1 - \dfrac{2}{R}\right)\dfrac{\rho_v W_t}{G}} \qquad 38$$

where,

$$W_t = \frac{0.48gd}{2}\frac{(1-\rho_v)}{\rho_l} \qquad 39$$

Finally, the channel averaged void fraction, α, can be calculated by an area weighted sum of the void fraction at the wall and the void fraction in the core [Avdeev & Pekhterev, 1987].

$$\alpha = \alpha_{core}\left(1 - \frac{2}{R}\right) + \alpha_w\left(\frac{2}{R}\right) \qquad 40$$

Considering the large values of mass flux of interest and the small equivalent diameter, it is easy to see that the slip velocity term, W_t, is not of great importance. For high velocity water flows, it is generally at least two orders of magnitude smaller than the first term in the denominator of Equation 38, and could be safely neglected.

Equations 29 - 40 are used to calculate the axial flow characteristics during subcooled boiling. Since many of these correlations are implicit, a simple iteration scheme with convergence criteria is used in the program to ensure agreement between variables.

1.2 Development of Mechanistic Constitutive Models

The acceleration pressure drop associated with vapor generation beyond ONVG overwhelms the effects of flow disturbance due to bubble ebullition in flows where the vapor density is small relative to the liquid density. However, in partially developed subcooled boiling the two-phase shear term is often of the same order as the acceleration term in the momentum equation and must be considered in more detail. The bubble growth in a high heat flux and high mass flux channel is inertially controlled, which allows a simple formulation of the momentum exchange between a growing bubble and the surrounding liquid.

The augmentation in heat transfer is related to the augmentation in the wall shear associated with the presence of subcooled void on the wall through the Reynolds analogy. The augmentation in wall shear is modeled by considering parameters such as the wall void or active nucleation site density along with the bubble departure diameter to establish an effective wall roughness. The augmentation in wall roughness is then related to the wall shear using conventional single-phase flow modeling techniques. The Reynolds analogy then prescribes the augmentation in the heat transfer coefficient. This general strategy appears several times in the literature [Larson and Tong, 1969; Avdeev, 1986].

It should be noted that the use of wall roughness implicitly assumes that the bubble growth rate is slower than the fluid velocity near the wall. This condition is rarely met, especially in situations of high heat flux where the bubble departure frequencies are large.

Vapor bubbles form and collapse on and near the heater surface during subcooled boiling in the wall void region as is evidenced by several experimental studies [Gunther, 1951; Griffith, et al, 1958; Bibeau & Salcudean, 1994; Unal, 1976]. The observed behavior of the bubbles varies.

Sometimes bubbles form and collapse at the nucleation site. Sometimes the bubbles are formed and slide along the heated surface before condensing on or near the wall. Other times the bubbles form and depart from the wall into the flow where they condense rapidly. No generally accepted rules exist to determine when each type of behavior is to be expected. However, it is clear that bubbles form and collapse rapidly in the wall void region.

Many models are available for bubble growth and collapse, as can be found in Carey [1992]. The bubble growth and collapse near the surface is used in the mechanistic models for subcooled boiling to quantify the pumping term associated with the convection of energy due to water displacement by the bubbles near the surface. The liquid displaced by the vapor bubbles also convects momentum. Each bubble growth pushes liquid from a low velocity region near the wall into a higher velocity region away from the wall. Each bubble collapse draws water from the higher velocity region away from the wall to the lower velocity region near the wall. This transfer of momentum normal to the time averaged velocity of the flow produces additional resistance to flow and can be treated in a manner analogous to a turbulent shear stress.

The development that follows uses models for bubble formation, bubble departure diameter, and active nucleation site density to derive a bubble induced turbulent shear stress in the "laminar" sublayer. Both the pressure increase due to mechanical pumping and pressure losses due to bubble induced turbulent shear are considered.

1.2.1 Thermal to Mechanical Energy Conversion via Bubble Ebullition

An oscillating bubble may add energy or momentum to the fluid due to the acceleration of liquid surrounding a bubble during the growth process. The physics of this process can be captured by considering the work done to the surrounding media by a growing bubble.

$$E = \int_0^{r_{max}} \frac{d}{dt}\left(m_{vm}\frac{dr_b}{dt}\right)dr_b \qquad 41$$

where the liquid virtual mass, m_{vm}, is approximated to first order using a virtual mass coefficient.

$$m_{vm} = C_{vm}\rho_l \frac{2}{3}\pi r_b^3 \qquad 42$$

The constant, C_{vm}, represents the ratio of liquid-affected volume surrounding the bubble to the volume of the bubble itself.

The growth equation for heterogeneous bubble growth at a heated surface depends on the flow situation and fluid conditions. The high heat flux and high mass flux in the ANS reactor indicate that rapid, hemispherical bubble growth will occur, and that the growth regime will be inertially controlled. For such conditions Carey [1992] recommends a bubble growth formulation developed by van Stralen [1975] which matches microlayer conduction with the bubble growth rate.

$$r_b(t) = 0.470 Ja\, Pr^{-1/6}\, \alpha_l^{1/2} t^{1/2} \qquad 43$$

$$\frac{dr_b(t)}{dt} = 0.235 Ja\, Pr^{-1/6}\, \alpha_l^{1/2} t^{-1/2} \qquad 44$$

$$\frac{d^2 r_b(t)}{dt^2} = -0.1175 Ja\, Pr^{-1/6}\, \alpha_l^{1/2} t^{-3/2} \qquad 45$$

The relations given by Equation's 41 through 42 with the bubble growth equation given in Equation 44 yield a formula for the mechanical energy transferred to the liquid from the growing bubble.

$$E = 2.548(10^{-3}) C_{vm}\rho_l \pi Ja^5\, Pr^{-5/6}\, \alpha_l^{5/2} t_m^{3/2} \qquad 46$$

The maximum growth time, t_m, is related to the maximum bubble radius, $r_{b,m}$, by Equation 43.

$$t_m = \left(\frac{r_{b,m}}{0.470 Ja\, Pr^{-1/6} \alpha_l^{1/2}} \right)^2 \qquad 47$$

Combining this result with Equation 46 gives,

$$E = 0.0245 C_{vm} \rho_l \pi Ja^2 Pr^{-1/3} \alpha_l r_{b,m}^3 \qquad 48$$

Although Equation 48 is convenient for determining mechanical energy, it is not obvious what effect this energy will have on the flow. Equation 48 can be converted to momentum, and then to a local pressure gradient prediction. If we introduce the area density of bubbles on the channel wall, n, the heated perimeter, P_h, and the bubble formation frequency, f, Equation 48 can be converted to a 2nd order differential in space and time.

$$\begin{aligned} \frac{\partial^2 E}{\partial x \partial t} &= n P_h f E \\ &= 0.0245 C_{vm} n P_h f \rho_l \pi Ja^2 Pr^{-1/3} \alpha_l r_{b,m}^3 \end{aligned} \qquad 49$$

Now dividing through by the mean flow velocity, u = dx/dt, gives

$$\frac{\partial^2 E}{\partial x^2} = \frac{0.0245 C_{vm} n P_h f \rho_l \pi Ja^2 Pr^{-1/3} \alpha_l r_{b,m}^3}{\bar{u}} \qquad 50$$

If it is assumed that the work done on the liquid by the bubbles is an isentropic process, then

$$\frac{\partial^2 E}{\partial x^2} = \frac{\partial}{\partial x}\left(\frac{\partial E}{\partial x}\right) = A_{xs} \frac{\partial P}{\partial x} \qquad 51$$

Combining Equations 50 and 51 and converting the bubble radius to the more commonly measured diameter yields

$$\frac{\partial P}{\partial x} = \frac{0.003 C_{vm} P_h n f \rho_l \pi Ja^2 \alpha_l d_b^3}{\bar{u} A_{xs} Pr^{1/3}} \qquad 52$$

It can be shown that, for ANS nominal conditions, the pressure gradient described by Equation 52 is several orders of magnitude below the single-phase viscous gradient. It is interesting that Equation 52 represents work done on the fluid which results in a positive dP/dx contribution. The bubbles will condense and thereby take energy from the fluid. However, the rate of condensation is usually less than the rate of formation, allowing for net work to be done on the liquid phase.

The bubble growth and collapse is accompanied with dissipative phenomena that increase the pressure gradient in the region from IB to ONVG. These phenomena are considered in the three analyses that follow.

1.2.2 Eddy Viscosity due to Bubble Ebullition

In fully developed turbulent flow, the momentum equation can be recast to include turbulent stresses, <u′v′>. It is common practice to express the inertial terms as an apparent turbulent stress-tensor by redefining the shear stress, τ, as the summation of the Newtonian viscous stresses plus the apparent Reynolds stress. For two-dimensional flow, this is approximately

$$\begin{aligned} \tau &= \tau_{viscous} + \tau_{turbulent} \\ &= \mu \frac{du}{dy} - \rho \overline{u'v'} \end{aligned} \qquad 53$$

Many investigators have offered functional forms for the turbulent shear. This investigation presents three mechanistically based methods to formulate the shear due to dynamic bubbles in the region from IB to ONVG. The methods presented could be extended from ONVG to annular film evaporation with some additional assumptions and appropriate data.

1.2.2.1 Model 1. The Mixing Length

Prandtl postulated that u′ is of the same order as v′ and that u′ is proportional to the product of a mixing length, l, and the local velocity gradient [Schlichting, 1979].

$$u' \approx v' \approx l\frac{du}{dy} \qquad 54$$

For subcooled boiling, the length scale can be approximated by evaluating the distance that an arbitrary fluid "lump" would be moved by an expanding or contracting bubble,

$$l = K\left|\frac{dr_b}{dt}\right|\Delta t = K\left|\frac{dr_b}{dt}\right|\frac{2r_b}{u(r_b)} \qquad 55$$

Noting that $u(r_b)$ is related to the velocity gradient,

$$u(r_b) = r_b\frac{du}{dy} \qquad 56$$

Equation 54 leads directly to an approximation for the turbulent shear due to a single pulsating bubble.

$$\tau_{t,b} = 4\rho_l K^2\left|\frac{dr_b}{dt}\right|^2 \qquad 57$$

A total flow turbulent shear is derived by introducing an area and time averaged nucleation site density. Defining α_w as the area void fraction of bubbles on the wall ($\alpha_w = n\ \pi\ r_b^2$) and multiplying by the product of the bubble frequency, f, and bubble lifetime, t_{life}, Equation 57 becomes

$$\tau_t = 4\rho_l\alpha_w f t_{life} K^2\left|\frac{dr_b}{dt}\right|^2 \qquad 58$$

1.2.2.2 Model 2. The Shear Analogy

In this approach, the velocity perturbation in the direction of flow is modeled using the bubble radius as the characteristic length.

$$u' = r_b \frac{du}{dy} \qquad 59$$

Again, for situations where rapid, hemispherical bubble growth occurs, the perturbations in the direction normal to the wall are taken proportional to the bubble growth rate.

$$v' = \frac{dr_b}{dt} \qquad 60$$

After including time and area averaging in a manner identical to that employed for Model 1, the turbulent shear becomes

$$\begin{aligned} \tau_t &= Kft_{life}\rho_l \left|\frac{dr_b}{dt}\right| \left[r_b \frac{du}{dy}\right] \alpha_w \\ &= Kft_{life}\rho_l \left|\frac{dr_b}{dt}\right| \frac{du}{dy} n\pi r_b^3 \end{aligned} \qquad 61$$

Vapor liquid exchange models similar to that proposed herein have been used to model the heat transfer augmentation due to pumping [Forster & Greif, 1959]. It is generally acknowledged that additional subcooling decreases the bubble departure radius and increases the departure frequency such that the energy converted at a given nucleation site,

$$q_b = \rho_l C_p \left(\frac{2\pi}{6}\right) r_b^3 (T_w - T_l) f \qquad 62$$

is approximately constant [Carey, 1992]. If it is assumed this relationship, which was derived for pool boiling, applies for flow boiling then Equation 62 can be used to simplify Equation 61,

$$\tau_t = \frac{3Kq_b\left|\frac{dr_b}{dt}\right|\left[\frac{du}{dy}\right]nt_{life}}{C_p(T_w - T_l)}$$ 63

1.2.2.3 Model 3. Momentum Transfer

The momentum transfer due to bubble formation can be evaluated directly. Considering the liquid mass flux normal to the wall due to bubble formation.

$$G_b = \rho_l nf\frac{4}{3}\pi r_b^3$$ 64

If the displaced liquid is inserted into the flow at position y = r_b, where the mean velocity is given by

$$u(r_b) = r_b\frac{du}{dy}$$ 65

then the momentum per unit wall area provided to the liquid is given by

$$\tau_t = Kfr_b^4 n\frac{4}{3}\pi\rho_l\frac{du}{dy}$$ 66

This model is also simplified by making use of Equation 62, such that

$$\tau_t = \frac{4Kq_b r_b\frac{du}{dy}n}{C_p(T_w - T_l)}$$ 67

It is interesting to note that Models 2 and 3 are equivalent if

$$\frac{dr_b}{dt} \propto \frac{r_b}{t_{life}}$$ 68

1.2.3 Extension to Heat Transfer

Since there is generally more data available for heat transfer in the IB to ONVG region than for skin friction, it is natural to extend the above analysis to formulate a heat transfer coefficient. By dividing Fourier's law by $\rho_l C_p$ and adding an eddy viscosity term, ε_H, to the thermal diffusivity, the heat flow from the wall can be defined as

$$\frac{q}{\rho C_p} = -(\alpha_l + \varepsilon_H)\frac{dT}{dy} \qquad 69$$

In addition, the shear stress can be expressed in terms of the wall velocity gradient.

$$\frac{\tau}{\rho} = -\left(\frac{\mu}{\rho} + \varepsilon_M\right)\frac{du}{dy} \qquad 70$$

Dividing Equation 69 by Equation 70, equating the diffusion coefficients, and integrating the result gives

$$q = \frac{\tau C_p}{\bar{u}}(T_w - T_{bulk}) \qquad 71$$

where

$$\tau = \frac{2f_{1\phi}}{\rho\bar{u}^2} + 0.195K^2 n\pi\rho_l Ja^4 Pr^{-2/3} \qquad 72$$

1.2.4 Model Results

The major difficulty in comparing these models is the large uncertainty associated with some of the parameters. The nucleation site density, for example, has been reported to vary with applied heat flux to some power, where the power ranges from 0.5 to 3. There is also a large uncertainty associated with the wall velocity gradient since very little data exists for this parameter during subcooled boiling.

With these uncertainties in mind the following boundary conditions were assumed.

1) The exponent for the nucleation site density was chosen to be 2 and the constant was adjusted to give a wall void fraction of about 50% at ONVG. The nucleation site density exponent is generally thought to be between 1 and 3 [Hsu & Graham, 1986] and 2 is taken as average. The wall void fraction of 50% is taken from Avdeev [1988].

2) The ratio of the bubble lifetime over the departure period was taken as constant at 0.5.

3) The velocity profile was assumed to be equivalent to the single-phase profile.

With these approximations, the three models were compared to each other and to a wall roughness model. The roughness model is given in Equation 33. The constant, K, was chosen to give reasonable results at ANS conditions. K values were found to be 81, 1.3×10^{-3}, and 5.7×10^{-7} for Models 1, 2, and 3, respectively. Figure 7 through Figure 9 show the results of the comparison for 6 MW/m^2 and for three different values of mass flux.

In every case, Model 2, the shear analogy, proved to be superior to the other two for wide ranges of mass flux and heat flux, assuming the model due to Avdeev is correct over the range of states considered. Model 3, as expected, followed closely with Model 2, but tended to be more sensitive to changes in mass flux.

The heat transfer characteristics of the three models are consistent with those expected for highly subcooled flows. The predicted heat transfer coefficient at ONVG for Model 2 approaches 3 times that of the single-phase heat transfer coefficient. This is somewhat higher than predicted using the subcooled boiling model due to Bergles & Rohsenow [1964]. However, Griffith, et al [1958] reported heat transfer coefficients of 5 times the single-phase value at ONVG.

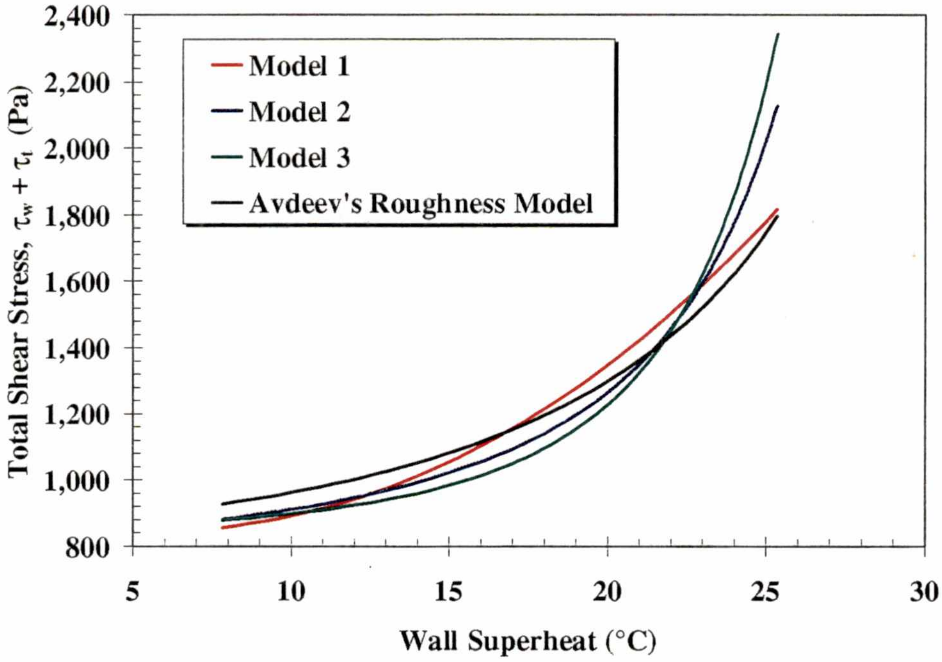

Figure 7. Model Comparison at 20 kg/m²s.

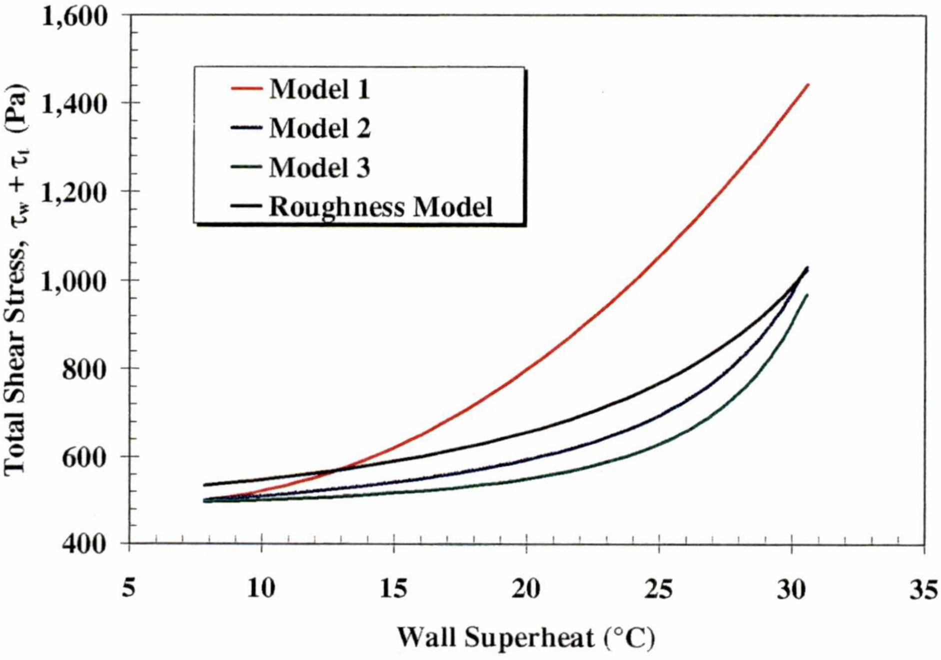

Figure 8. Model Comparison at 15 kg/m²s.

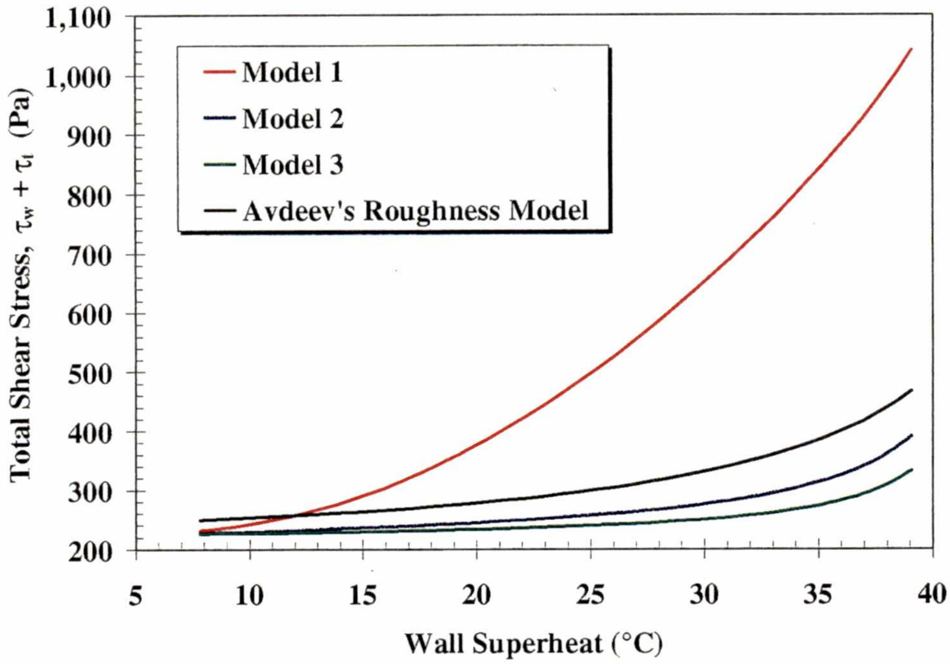

Figure 9. Model Comparison at 10 kg/m²s

1.3 Model Testing With THTL Data

The development in Section 1.2 provides a basis for moving toward more mechanistic models for the wall shear stress in subcooled boiling. However, the Avdeev [1982] model for the shear stress is still recommended for ANS conditions until an database is available which will allow a more thorough analysis of the mechanistic models. To ensure that Avdeev's models work together to form a consistent set of equations, the models must be tested with available data. The data recently collected at the Thermal-Hydraulic Test Loop facility at Oak Ridge National Lab [Siman-Tov, et al, 1995] provides an excellent database for heat fluxes up to 20 MW/m² and mass fluxes up to 30,000 kg/m²s.

Along with testing the model with experimental data, it is also beneficial to compare it with other accepted two-phase flow codes. The RELAP5 [Carlson, et al, 1990] code uses a time dependent, two-fluid model and is a widely used tool in the nuclear industry. The RELAP5 code has been benchmarked to world data, but not at the conditions considered here, and it does not consider void development before the onset of net vapor generation. This will provide a reference from which the additional effects of high heat and mass flux can be evaluated.

1.3.1 THTL Database

Sixteen cases are chosen from the THTL database which are representative of the database. The primary criteria for data inclusion is that the calculated pressure drop agree within 10% to the measured pressure drop for those points that are exclusively single-phase. This is important because it is believed that the channel gap is the primary source of error in single-phase predictions. An error in the gap can cause significant problems throughout the calculations because it effects the calculated mass flux as well as the equivalent diameter and cross sectional area. Table 3 lists the THTL runs used for this comparison.

It is seen in Figure 10 through Figure 20 that an occasional data point will deviate from the demand curve giving the appearance of two minimums. This is the result of a slight increase in pressure during the test and is not of great significance. The true minimum is generally obvious from the overall trend of the data.

1.3.2 Demand Curve Minimum Cases

There are eleven cases in the comparison database that are limited to single-phase and low quality. These cases are the most important for flow excursion limited devices since the instability

Table 3. THTL Database Used for Comparison.

Run	gap (mm)	Mass Flux (kg/m^2 s)	Exit Pressure (MPa)	Average Heat Flux (MW/m^2)	Inlet Temperature (°C)
FED15C	1.229	18,952	1.74	13.02	44.0
FED28B	1.229	20,398	1.74	14.61	44.2
FE114B	1.217	17,832	1.73	10.84	45.4
CF115B	1.217	17,396	1.72	11.77	45.5
FE210B	1.234	17,859	1.73	11.42	45.6
FE212A	1.234	17,020	1.72	12.15	45.7
FE318B	1.199	4,626	0.45	1.89	37.6
FE712B	1.237	2,559	1.70	1.67	42.7
FE713B	1.237	2,712	0.18	0.68	43.3
FE714B	1.237	7,668	1.70	4.33	44.2
FE714C	1.237	10,225	1.71	6.40	45.9
FE719B	1.237	17,912	1.69	11.67	45.9
FE324C	1.245	8,302	1.72	6.17	44.1
CF328A	1.245	17,063	1.72	12.52	44.1
FE620B	1.425	4,379	1.72	4.06	44.5
CF622B	1.425	6,755	1.73	6.12	44.4

will occur almost immediately after a single channel reaches its demand curve minimum. Figure 10 through Figure 20 demonstrate that Avdeev's model for pressure drop fits very well with THTL data for a wide range of heat fluxes and exit pressures.

1.3.3 High Quality Region

There are five cases considered where the test was taken to a CHF burnout. These data give information on the applicability of the model in the high quality and high void fraction region. It should be noted, however, that the Avdeev model is only valid in the bubbly flow regime and limited to void fractions less than about 75%. This corresponds to a mass fraction of about 15% at 2 MPa. Beyond this range, the model predicts a flattened profile and is unable to match the true pressure drop. In Figure 21 through Figure 25, the calculated pressure drops are not shown when the test section conditions are out of the model range.

1.3.4 Error Analysis

The partially developed subcooled boiling model of Avdeev is found to predict the THTL pressure drop 5.7% high with a standard deviation of 0.096. The error distribution appears near normal as shown in Figure 26. More importantly, the error has only a slight increasing trend as the partially developed boiling length increases as shown in Figure 27. High model predictions are not of great concern since the single-phase predictions are high as well. This could be the result of some small consistent measurement error and does not warrant model adjustment.

The Avdeev model predicts pressure drops in the fully developed boiling region that are 13.2% higher than the measured pressure drops on average with a standard deviation of 0.117.

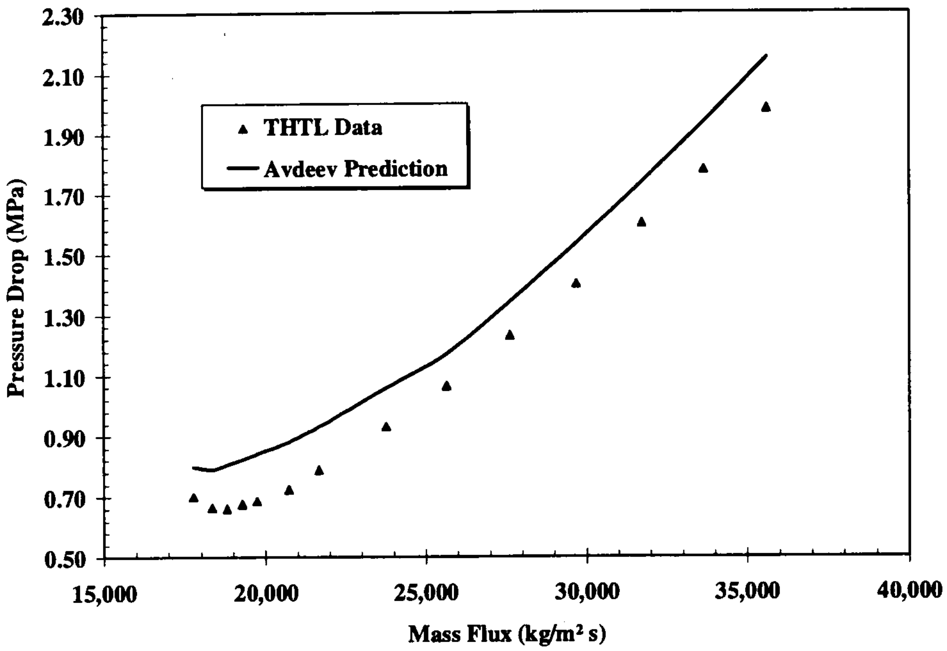

Figure 10. Demand Curve for THTL Case FED15C.

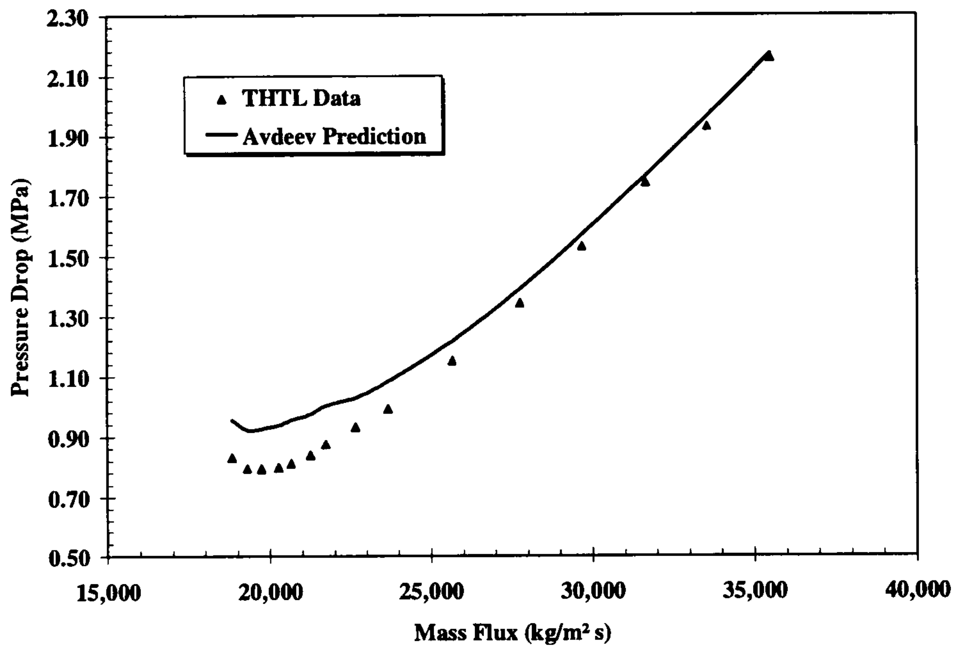

Figure 11. Demand Curve for THTL Case FED28B.

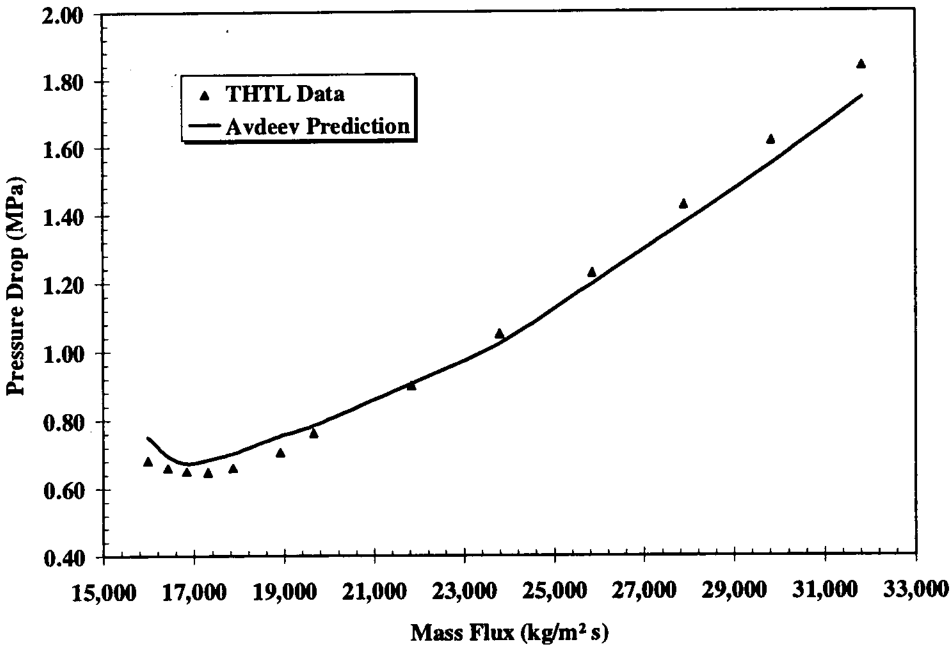

Figure 12. Demand Curve for THTL Case FE210B.

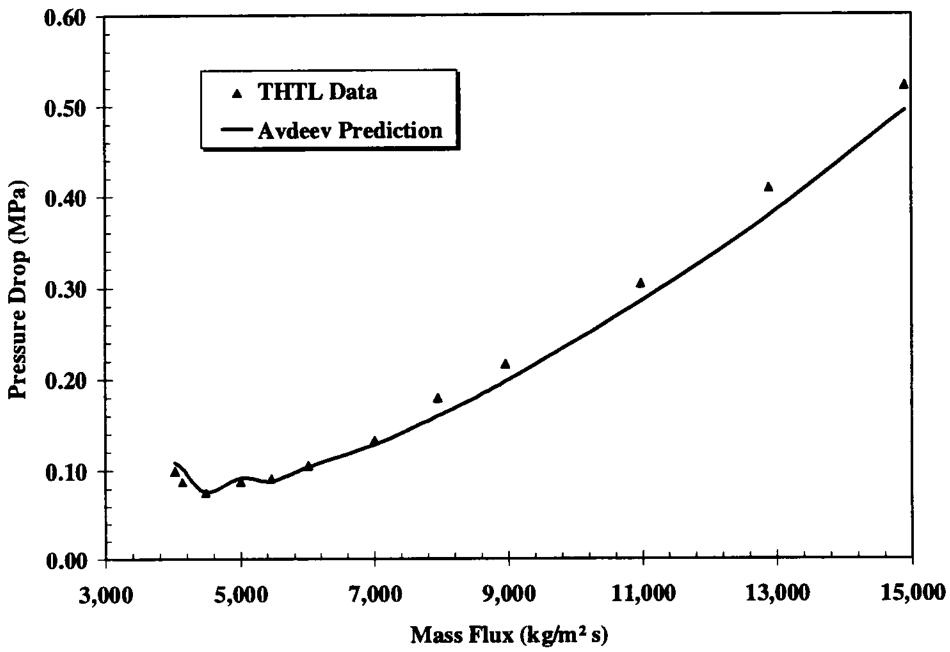

Figure 13. Demand Curve for THTL Case FE318B.

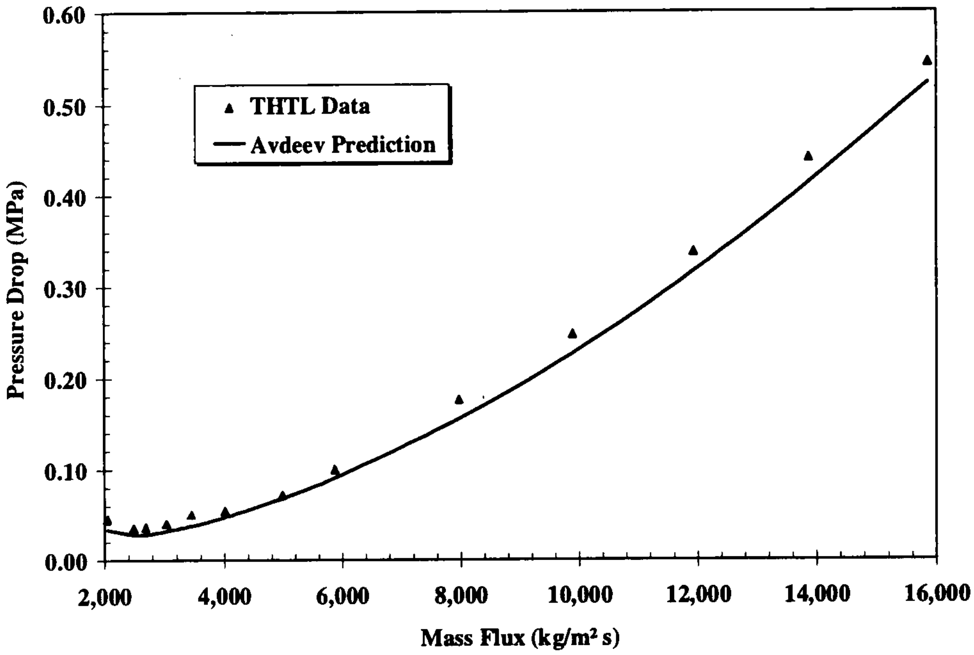

Figure 14. Demand Curve for THTL Case FE712B.

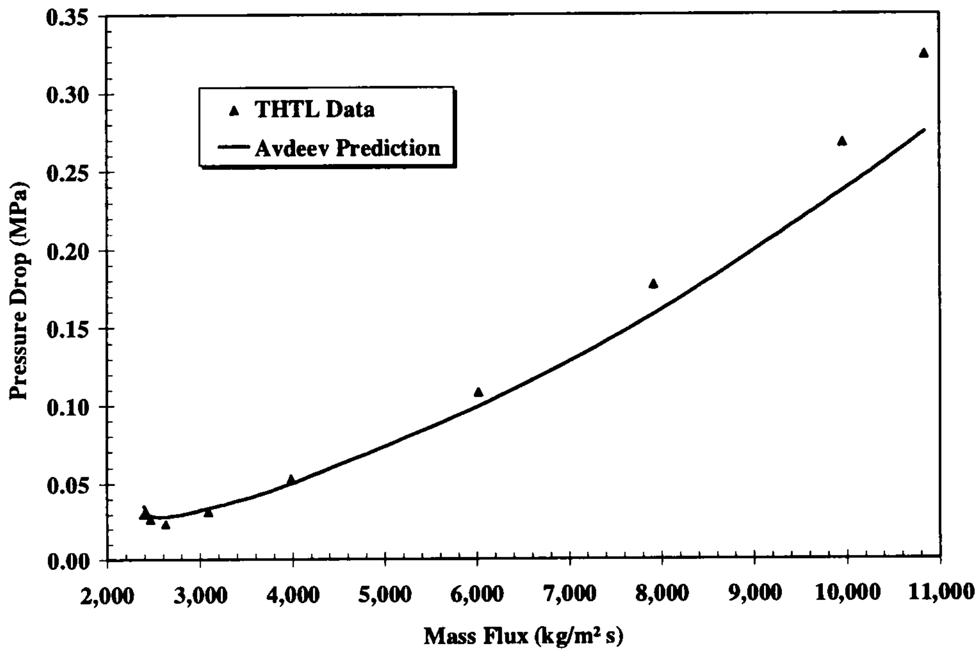

Figure 15. Demand Curve for THTL Case FE713B.

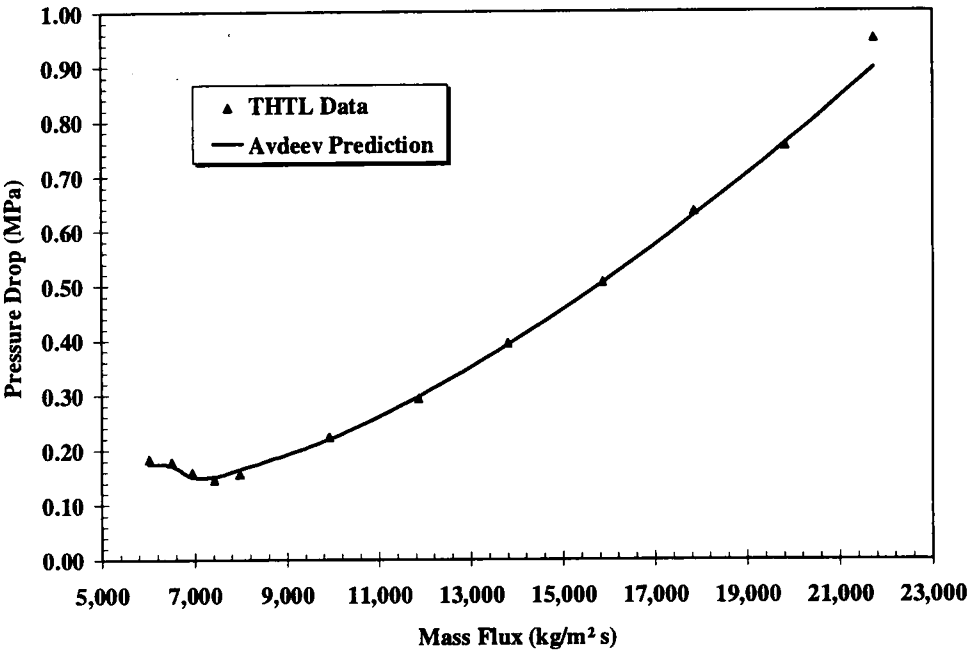

Figure 16. Demand Curve for THTL Case FE714B.

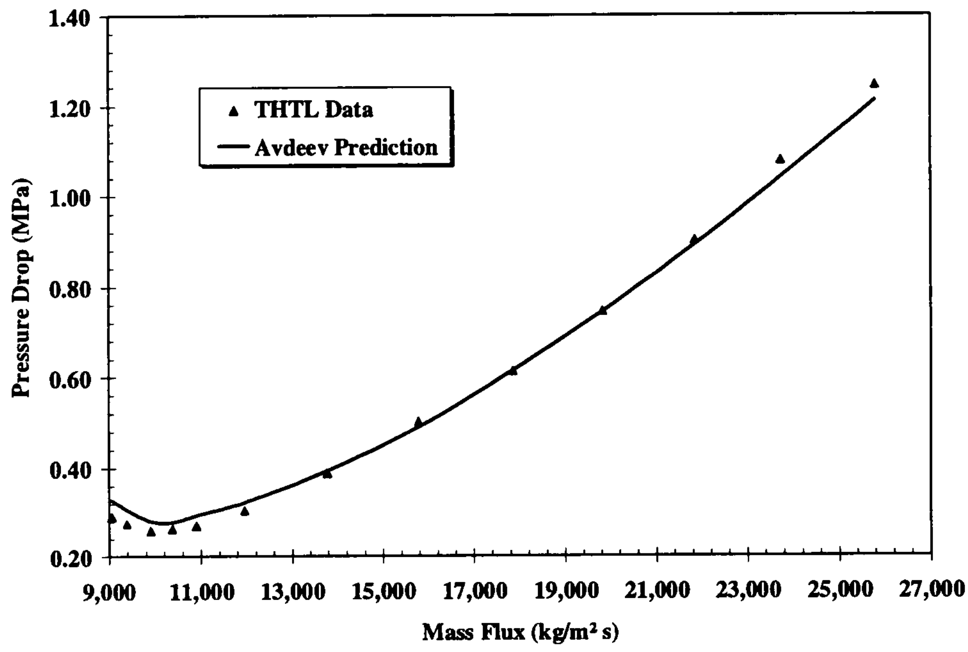

Figure 17. Demand Curve for THTL Case FE714C.

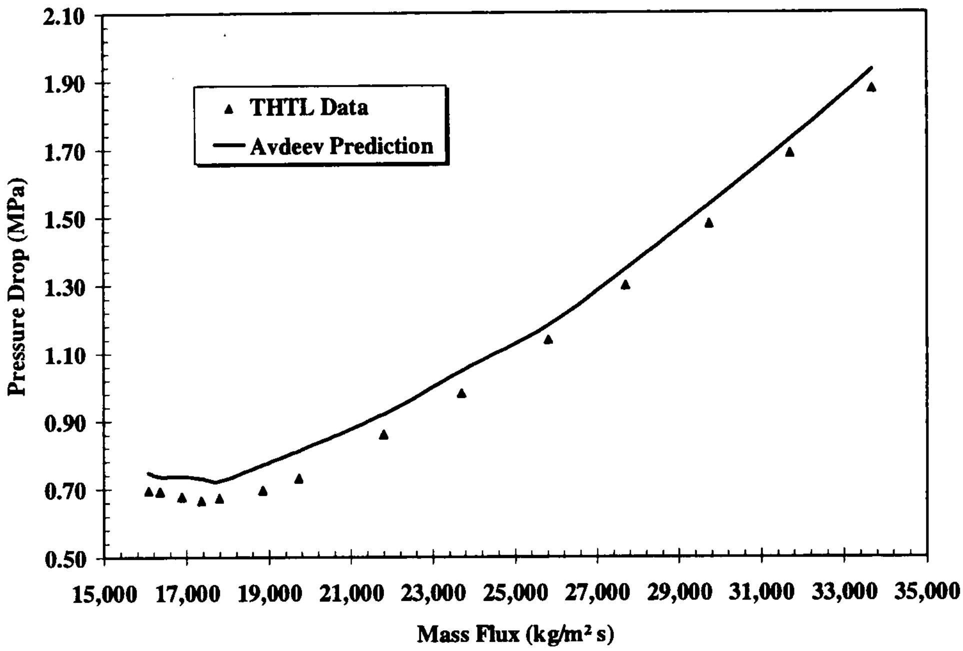

Figure 18. Demand Curve for THTL Case FE719B.

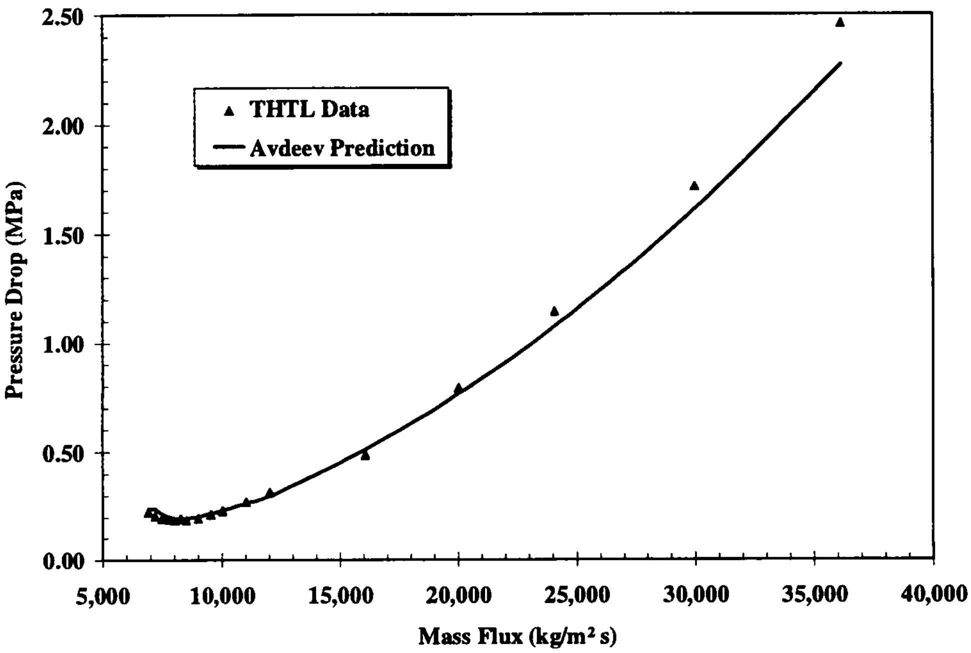

Figure 19. Demand Curve for THTL Case FE324C.

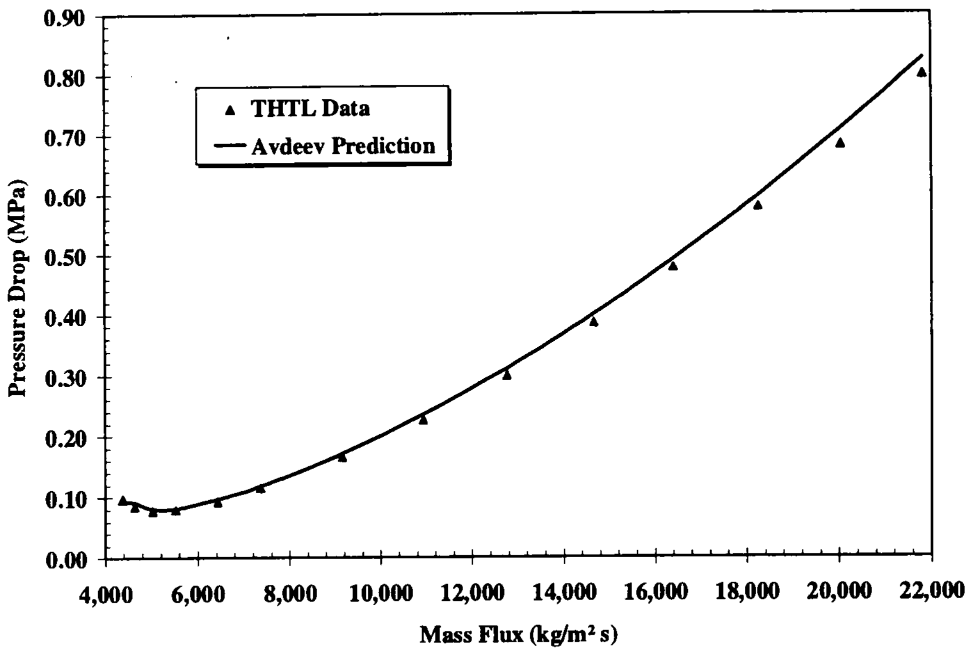

Figure 20. Demand Curve for THTL Case FE620B.

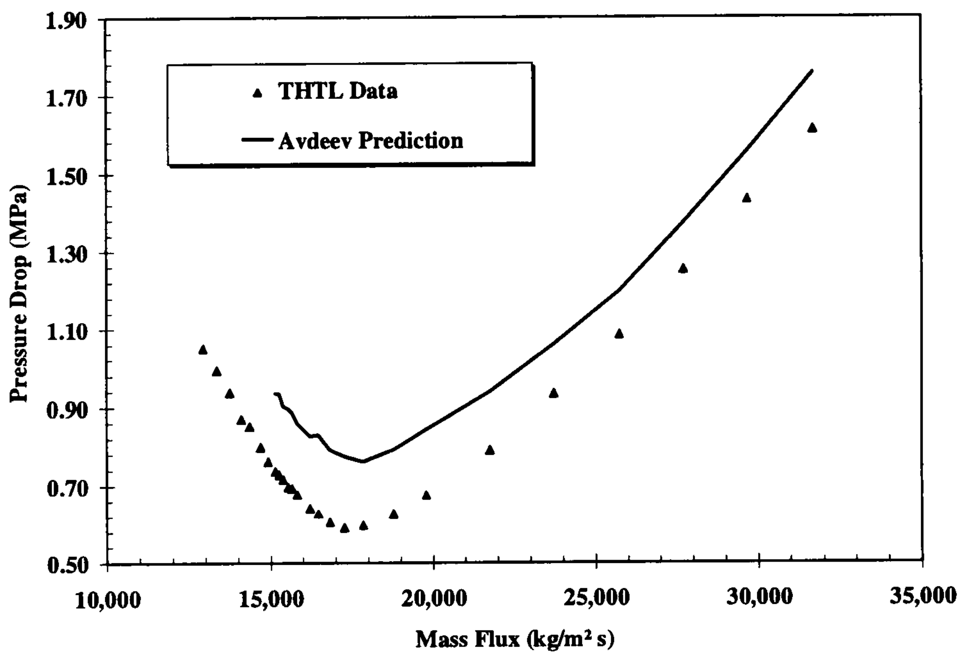

Figure 21. Demand Curve for THTL Case FE114B.

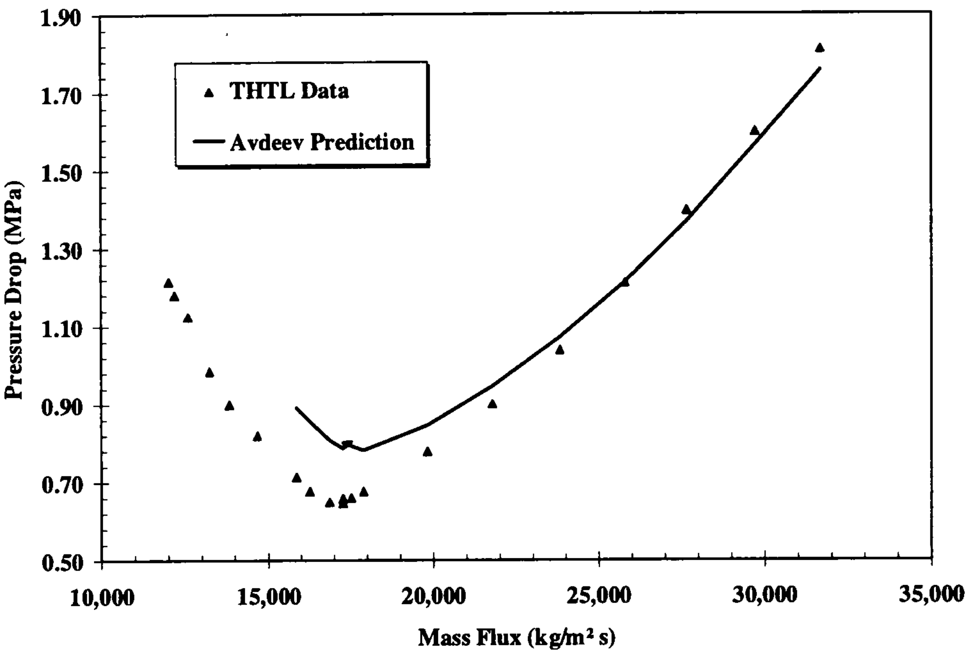

Figure 22. Demand Curve for THTL Case CF115B.

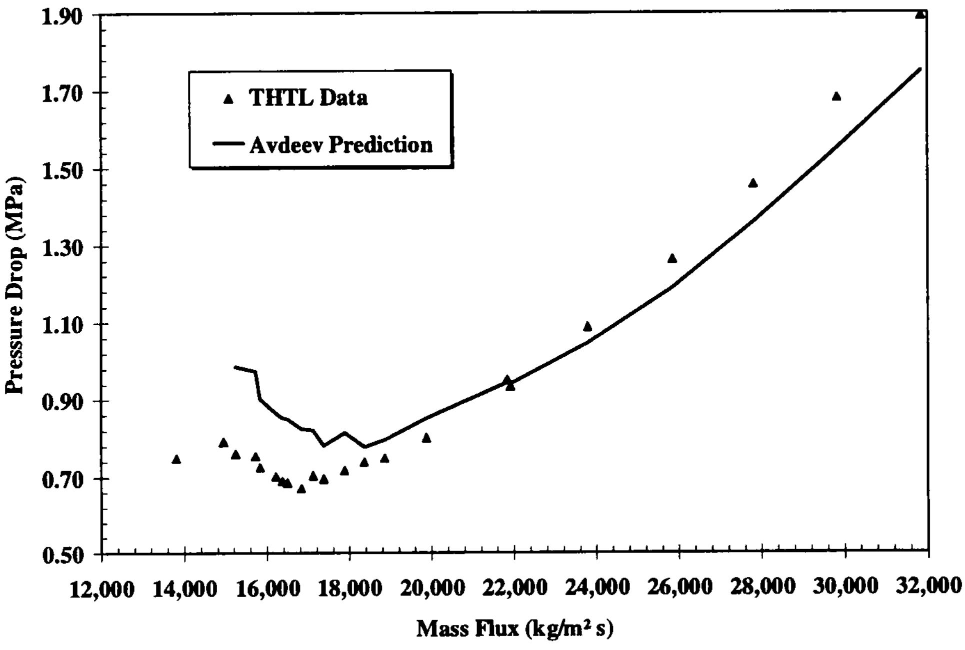

Figure 23. Demand Curve for THTL Case FE212A.

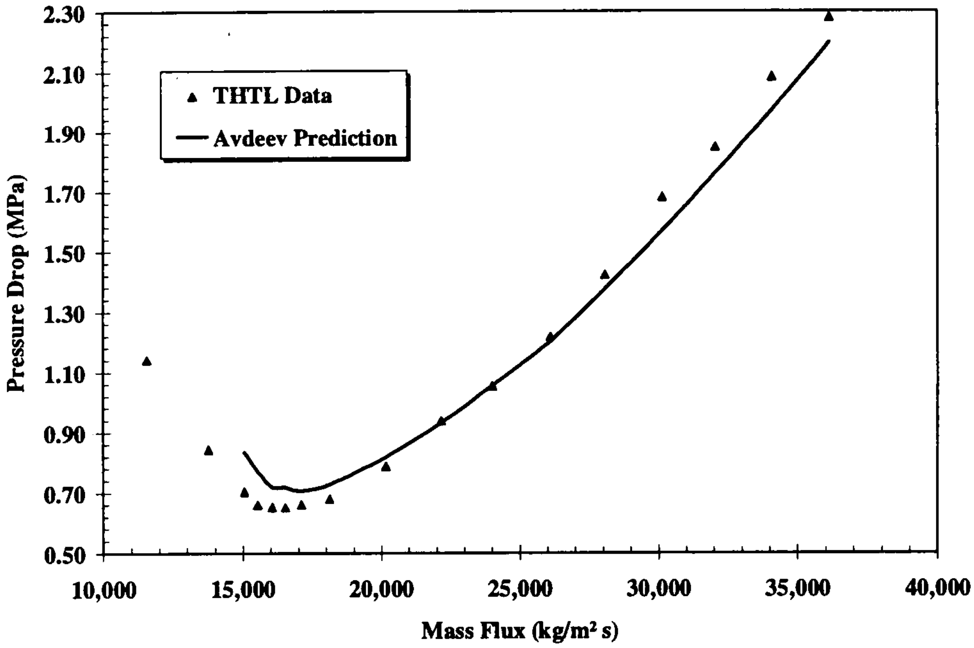

Figure 24. Demand Curve for THTL Case CF328A.

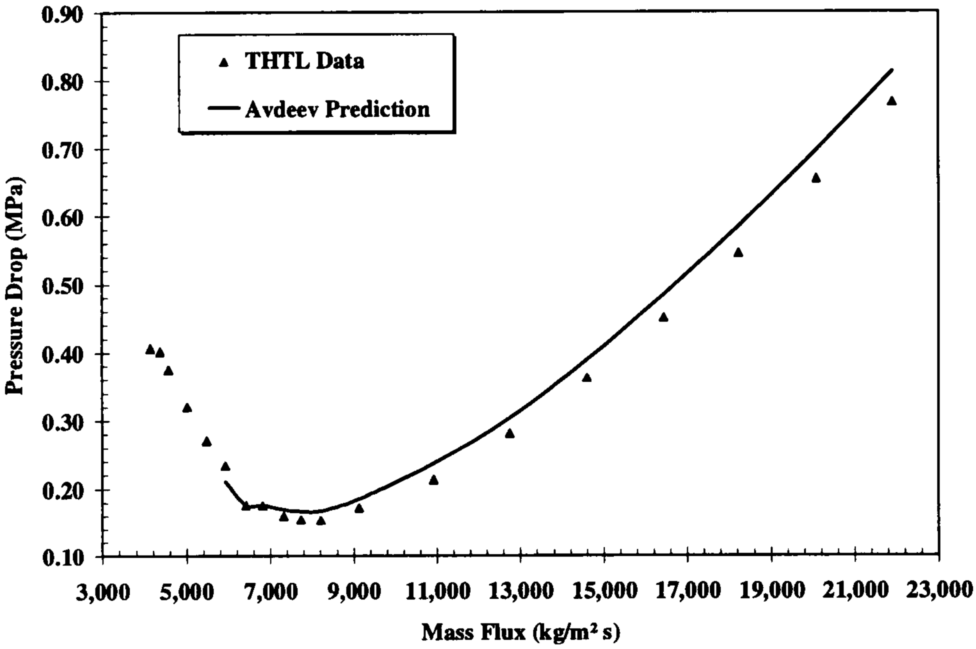

Figure 25. Demand Curve for THTL Case CF622B.

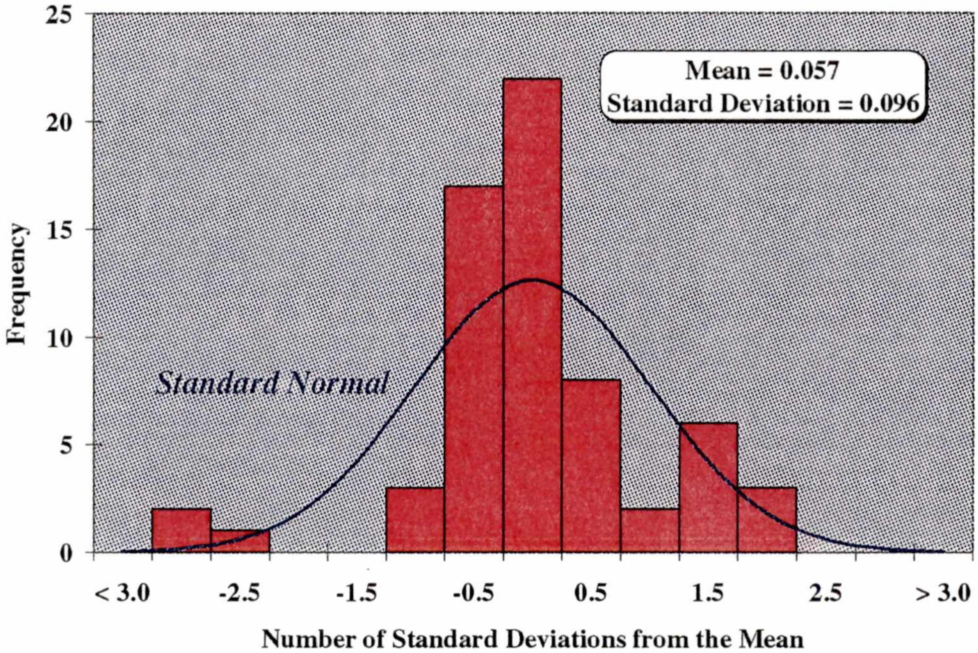

Figure 26. Histogram for the Error Associated with the Partially Developed Boiling Model.

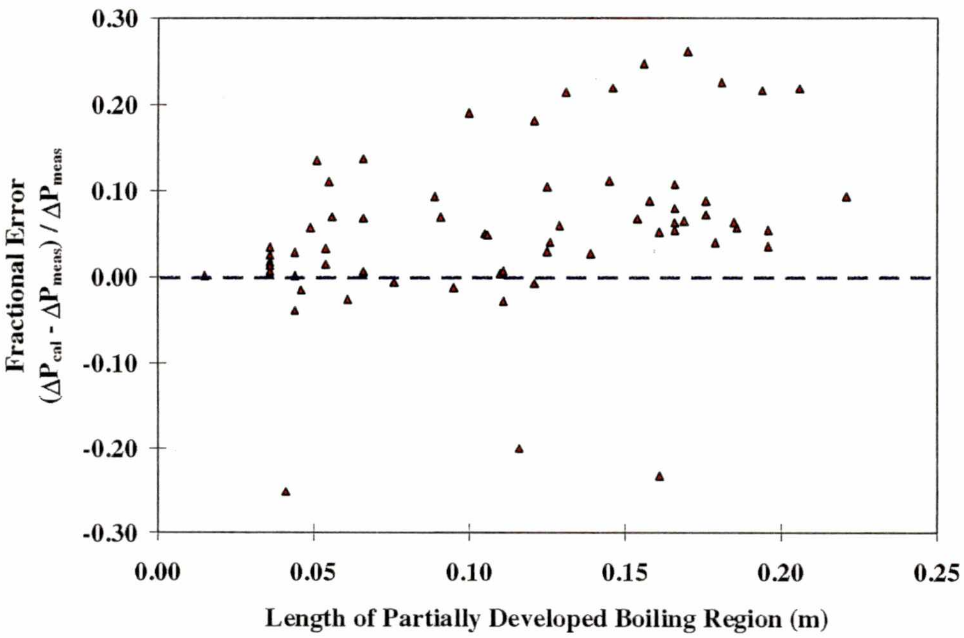

Figure 27. Error Trend with Boiling Length in Partially Developed Boiling.

The distribution of error appears near normal as shown in Figure 28. Again, the error does not show a significant trend as the fully developed boiling length increases as shown in Figure 29.

1.3.5 Comparison with RELAP5/MOD3

A RELAP5/MOD3 simulation of THTL case CF622B is shown in Figure 30 along with the measured data and the Avdeev prediction. Both the RELAP model and the Avdeev model compare well with the measured data. The RELAP model shows significant variation shortly after the demand curve minimum due to the strong nonlinearities associated with void development after ONVG. The average response, however, agrees with the measured trend.

One problem with the RELAP model is that the predicted onset of CHF is highly conservative with respect to the measured data. For cases where the applied heat flux is above 12 MW/m^2, CHF is predicted to occur before void is predicted in the channel (i.e. prior to ONVG) and well before the demand curve minimum. For case CF622B, shown in Figure 30, the CHF point occurs at about the same mass flux that exceeds the limitations of the Avdeev model. The measured data show that the pressure drop continues to increase well beyond this point and burnout does not occur until the mass flux is about 4,000 kg/m^2 s.

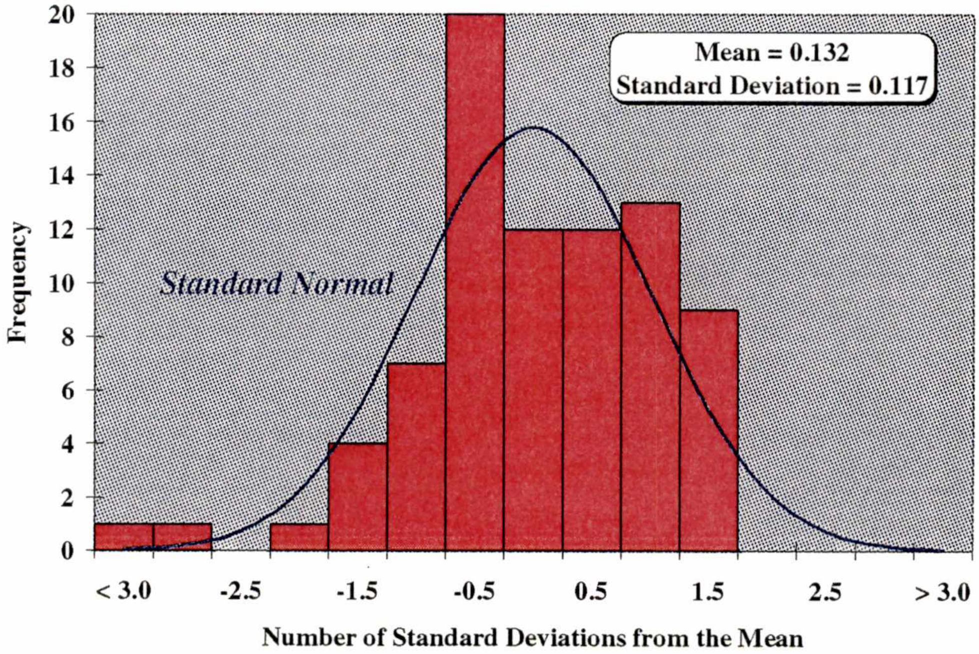

Figure 28. Error Histogram for Fully Developed Subcooled Boiling.

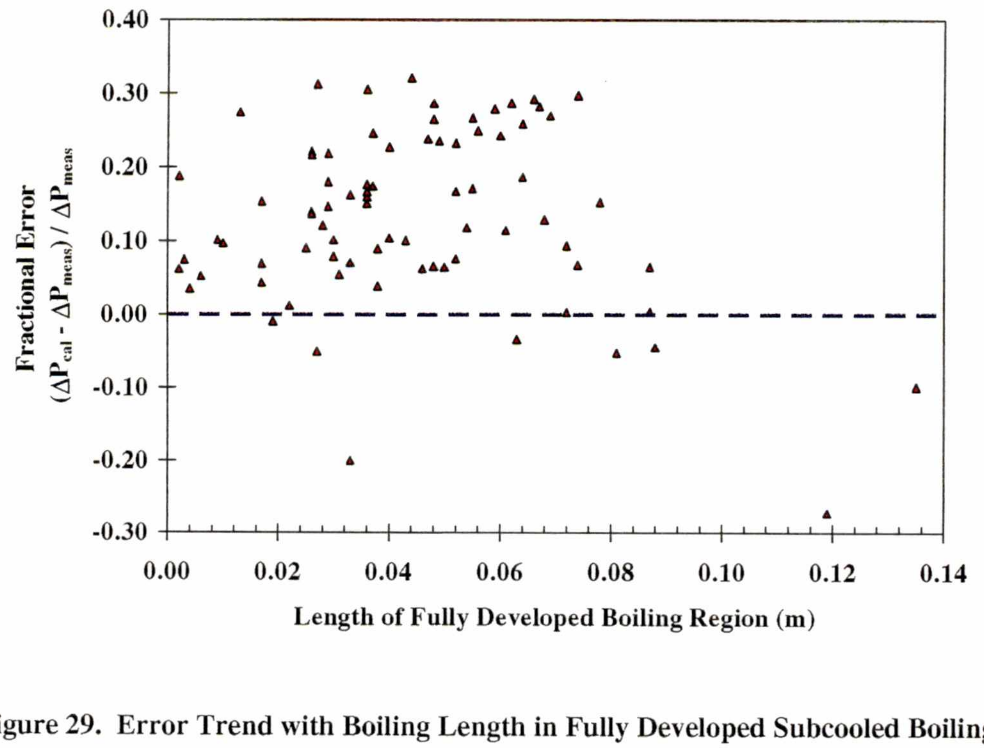

Figure 29. Error Trend with Boiling Length in Fully Developed Subcooled Boiling.

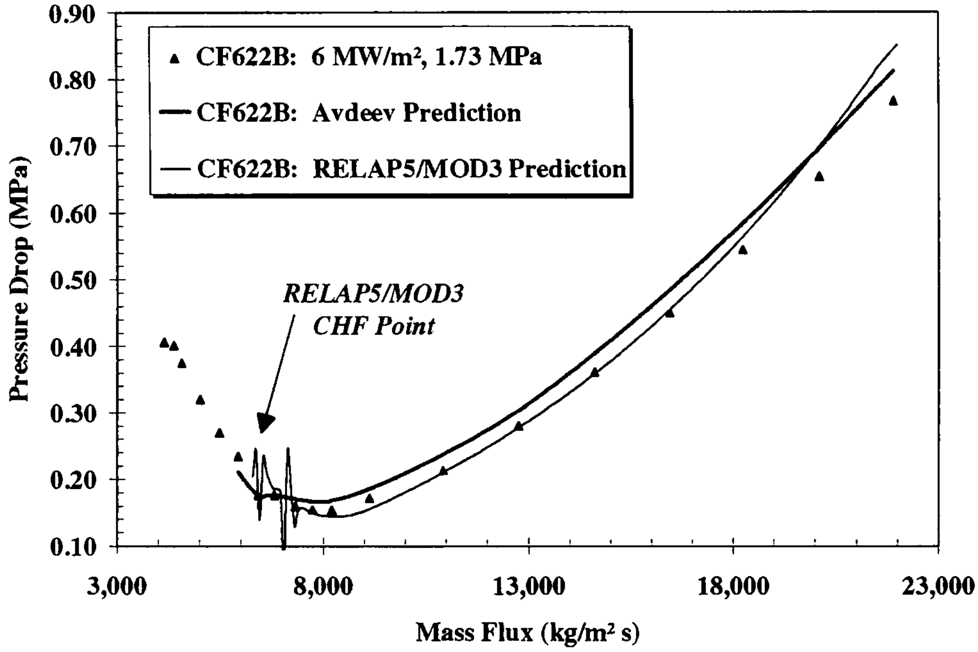

Figure 30. THTL Case CF622B Compared with Avdeev's Model and RELAP5/MOD3.

Chapter 2. Verification of General Assumptions In the Bubble Region

The combination of high heat flux, large mass velocity, and small hydraulic diameter can cause the laminar sublayer thickness, the channel surface roughness, and the bubble departure diameter to be of the same order of magnitude. Use of the universal velocity profile for these situations is questionable, and a clear demarcation between the regions of viscous and turbulent dominated shear is improbable.

It is first necessary to define the range of conditions for which the normal assumptions in the boundary layer are valid. New assumptions and models may be required for conditions beyond this range.

2.1 The Turbulent Bubble Boundary Layer

In single-phase, fully developed turbulent flow, the velocity profile in a rectangular channel is dominated by a central region with negligible spatial deviations in the mean velocity. Due to the no-slip boundary condition, a large velocity gradient exists in a very narrow region at the wall. This region is the turbulent boundary layer and is traditionally divided into three sections. The laminar sublayer is a very thin region next to the wall where the effect of molecular viscosity is much greater than the effect of turbulent viscosity on the local shear stress. The buffer layer exists just outside the laminar sublayer and is defined as the region where the eddy viscosity and the molecular viscosity are of the same order of magnitude. The turbulent layer is the outermost region of the turbulent boundary layer where the contribution of the eddy viscosity to the local shear stress is much greater than the contribution of the molecular viscosity.

The velocity profile in the boundary layer is generally given in terms of a characteristic friction velocity, v*, where

$$v^* = \sqrt{\frac{\tau_w}{\rho_l}} \qquad 73$$

Using the mixing length approach to solve for the velocity distribution in the boundary layer, a universal velocity profile can be developed, as shown in Table 4. The non-dimensional quantities, u^+ and y^+, are the velocity and length parameters scaled with the friction velocity.

$$u^+ = \frac{u}{v^*} = \frac{u}{\sqrt{\tau_w/\rho_l}} \qquad 74$$

$$y^+ = \frac{v^* y}{\nu} = \frac{y\sqrt{\tau_w/\rho_l}}{\nu} \qquad 75$$

Table 4. Universal Velocity Profile for Turbulent Flow.

Region	Limits	Velocity Profile
Laminar Sublayer	$0 < y^+ < 5$	$u^+ = y^+$
Buffer Layer	$5 < y^+ < 30$	$u^+ = 5.0 \ln y^+ - 3.05$
Turbulent Layer	$y^+ > 30$	$u^+ = 2.5 \ln y^+ + 5.5$

from Holman [1990]

The empirical velocity distribution in Table 4 leads to a definition of the laminar sublayer thickness. Using the definition of the friction factor, the laminar sublayer thickness can be expressed as

$$\delta_{lam} = \frac{5\nu}{v^*} = 10\sqrt{\frac{2}{f}}\frac{d}{Re} \qquad 76$$

This definition assumes single-phase flow over a hydraulically smooth wall and is not rigorously applicable beyond IB. The frictional pressure gradient in subcooled boiling has traditionally been modeled as a rough wall [Wallis, 1969; Hsu & Graham, 1986], such that $u^+ = f(y^+, k^+)$ where

$$k^+ = \frac{kv^*}{\nu} \qquad 77$$

and k is the average roughness height. According to White [1991], if

$$\frac{k}{d}Re < 10 \qquad 78$$

then the roughness is not important. If it is greater than 1000 then the surface can be considered fully rough. If the roughness height is equated with the bubble diameter, then Equation 78 can be rearranged so that when

$$d_b > \frac{10d_e}{Re_d} = \delta_{lam}\sqrt{\frac{f}{2}} = \frac{10\mu}{G} \qquad 79$$

the presence of bubbles in the boundary layer must be considered in the development of the velocity profile and wall shear stress. However, there are significant differences between flow over a rough wall and flow through a developing bubble boundary layer, including:

1) The no-slip condition is a tenuous assumption over bubble surfaces and is dependent on impurities in the fluid and bubble surface currents.

2) A bubble growing on a heated wall often has a radial growth rate far greater than the horizontal velocity of the surrounding fluid, causing significant flow redistribution in the bubble affected area.

3) The lifetime of a bubble, whether it departs the wall or collapses, is generally small compared to the waiting time between bubble activities at a nucleation site. The surface roughness imposed by growing bubbles is therefore highly dependent on the time-averaged nucleation site density.

Despite these weaknesses in the wall roughness approximation to subcooled boiling, it is used extensively for typical flow situations. In general, the local bubble diameters will exceed the criteria in Equation 79 sometime between IB and ONVG. It should be noted that the criterion in Equation 79 indicates that high velocity flows may not have to consider the friction due to the bubble layer due to very small bubble departure diameters. However, it will be shown in the next section that the bubble diameter at departure is inversely proportional to the wall shear stress, which is in turn proportional to $G^{3/4}$.

2.2 The Bubble Departure Diameter

Theoretical studies for the diameter of a bubble at departure generally rely on a force balance on the growing bubble [Carey, 1992; Levy, 1967]. Designating **n** to be the direction normal to the wall and **t** to be the direction tangential to the wall and summing the forces indicated in Figure 31 gives.

$$\left[\mathbf{F}_s+\mathbf{F}_{bu}+\mathbf{F}_i+\mathbf{F}_p+\mathbf{F}_\tau\right]\cdot\mathbf{t}=\rho_v V_b \frac{d\,\mathbf{u}_b}{dt}\cdot\mathbf{t} \qquad 80$$

$$\left[\mathbf{F}_s+\mathbf{F}_{bu}+\mathbf{F}_i+\mathbf{F}_{lift}\right]\cdot\mathbf{n}=\rho_v V_b \frac{d\,\mathbf{u}_b}{dt}\cdot\mathbf{n} \qquad 81$$

In general, the vapor acceleration terms in Equations 80 and 81 are neglected since the left hand side forces are associated with ρ_l, which is generally much greater than ρ_v. Some

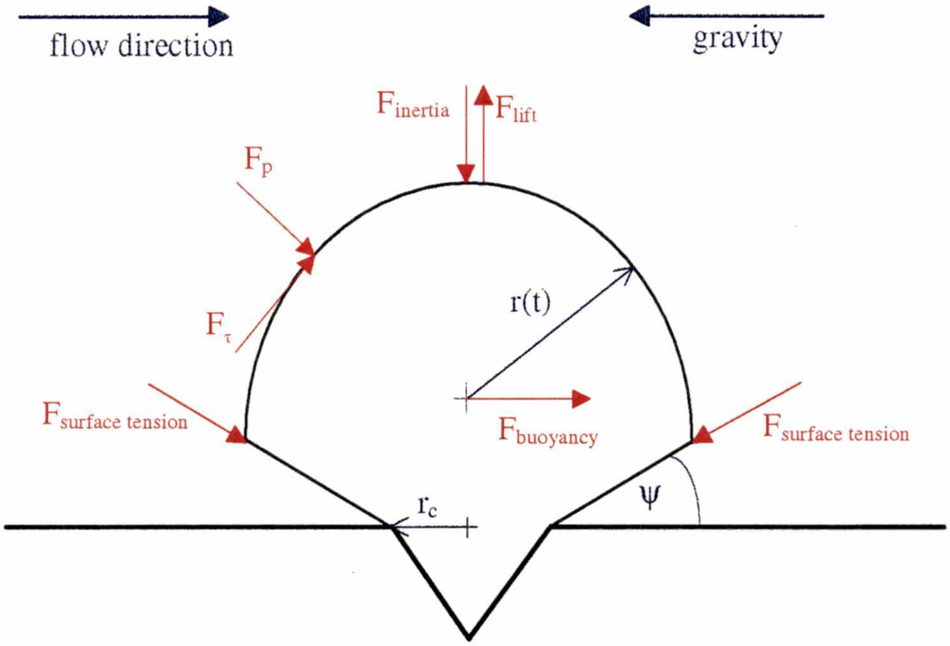

Figure 31. Force Balance on a Bubble.

investigators [Shin & Jones, 1993; Hirata & Nishiwaki, 1963] also include a drag term due the liquid flowing around the bubble during its growth. However, this term presumes that there are streamlines that separate and reconnect behind the bubble. This cannot occur for a hemispherical bubble attached to a wall since the bubble growth rate is much greater than the time average liquid velocity at the maximum bubble diameter. Therefore this force is not included for this analysis. For the present analysis, it is also assumed that the bubble stands vertically with respect to the wall. This should be valid for small, spherical bubbles where surface tension forces are much greater than dynamic pressure forces. This assumption indicates spherically symmetric growth.

2.2.1 Surface Tension

The surface tension force acts along the connective circumference of the bubble/surface interface. It can be modeled as

$$\mathbf{F}_s \cdot \mathbf{t} = -2\pi r_c \sigma \cos\psi \qquad 82$$

$$\mathbf{F}_s \cdot \mathbf{n} = -2\pi r_c \sigma \sin\psi \qquad 83$$

where ψ is the contact angle between the surface and the underside of the bubble and r_c is the connection radius at the bubble / surface interface (which is not, in general, the bubble radius). Although the connection radius is difficult to measure experimentally, a number of studies have determined the minimum and maximum radii available for bubble growth based on thermal and mechanical equilibrium considerations [Hsu & Graham, 1986]. The study by Han & Griffith [1965] proposed the following criteria.

$$r_c = \frac{\delta_{lam}(T_w - T_{sat})}{3(T_w - T_\delta)}\left[1 \pm \sqrt{1 - \frac{12(T_w - T_\delta)T_{sat}\sigma}{(T_w - T_{sat})^2 \delta_{lam}\rho_v h_{fg}}}\right] \qquad 84$$

2.2.2 Shear Forces

Convective flow around a bubble gives rise to a shear force on the bubble. For simplification, the following assumptions are made.

1) The bubble is hemispherical.
2) The shear stress is constant in the bubble region (strictly valid only when the heated surface is not fully rough) and the bubble surface maintains the no-slip condition.

Because of the symmetry of a hemispherical bubble, there is no net shear force in the direction normal to the wall. The force on the bubble tangential to the wall due to the shear stress is found by integrating the tangential component of the shear stress in the boundary layer over the surface of the bubble.

$$\mathbf{F}_\tau \cdot \mathbf{t} = \int_0^\pi \tau \sin(\theta) dA \qquad 85$$

where

$$dA = \pi r^2 \sin\theta d\theta . \qquad 86$$

The solution of Equation 85 is

$$\mathbf{F}_\tau \cdot \mathbf{t} = \frac{\tau_w}{2} \pi^2 r^2 \qquad 87$$

2.2.3 Buoyancy

The buoyancy force is due to the density difference between the vapor and the liquid and to the acceleration due to gravity. For upflow or downflow, the force on the bubble due to buoyancy at a differential area dA is

$$\begin{aligned} d\mathbf{F}_{bu} \cdot \mathbf{t} &= (P_l - P_b)\cos(\theta)(\mathbf{g} \cdot \mathbf{t})dA \\ &= (\rho_l - \rho_v)(\mathbf{g} \cdot \mathbf{t})\pi r^3 \sin(\theta)\cos^2(\theta)d\theta \end{aligned} \qquad 88$$

The net force on the bubble due to buoyancy is found by integrating over the surface of the bubble.

$$\mathbf{F}_{bu} \cdot \mathbf{t} = \frac{2}{3}\pi r^3 (\rho_l - \rho_v)\mathbf{g} \cdot \mathbf{t} \qquad 89$$

2.2.4 Potential Flow Field Around a Bubble

The pressure distribution around a growing bubble can cause a net force both in the normal and tangential directions. If the viscous effects are neglected on the bubble surface and the external velocity field is assumed constant, the pressure field can be modeled according to potential flow theory.

The velocity potential for uniform flow around a sphere is

$$\phi_s(r,\theta) = U\cos(\theta)\left(r + \frac{a(t)^3}{r^2}\right) \tag{90}$$

where a(t) is the bubble radius. The flow field due to the bubble growth is found by superimposing a source such that $u_r\{r = a(t)\} = a'(t)$.

$$\phi_g(r,\theta) = -\frac{a(t)^2 a'(t)}{r} \tag{91}$$

The resulting potential for uniform flow around a growing, spherical bubble is

$$\phi(r,\theta) = U\cos(\theta)\left(r + \frac{a(t)^3}{r^2}\right) - \frac{a(t)^2 a'(t)}{r} \tag{92}$$

Neglecting body forces, the unsteady Bernoulli equation gives the pressure distribution in the fluid surrounding the bubble.

$$P(r,\theta,t) = \rho F(t) - \rho\frac{\partial\phi(r,\theta,t)}{\partial t} - \frac{\rho}{2}\left[\left(\frac{\partial\phi(r,\theta,t)}{\partial r}\right)^2 + \left(\frac{1}{r}\frac{\partial\phi(r,\theta,t)}{\partial\theta}\right)^2\right] \tag{93}$$

The pressure distribution due to viscous shear in the channel can be imposed in Equation 93 if F(t) is chosen correctly.

$$F(t) = -\frac{p'}{\rho}a\cos(\theta)\cos(\varphi) \tag{94}$$

where p' is the viscous pressure gradient in the channel, and the time dependence of the bubble radius, a, is now implied. Note that the pressure field around the bubble is normalized so that the pressure at $r = 0$ is zero. A schematic of this representation is shown in Figure 32.

The derivatives of the velocity potential in Equation 92 are

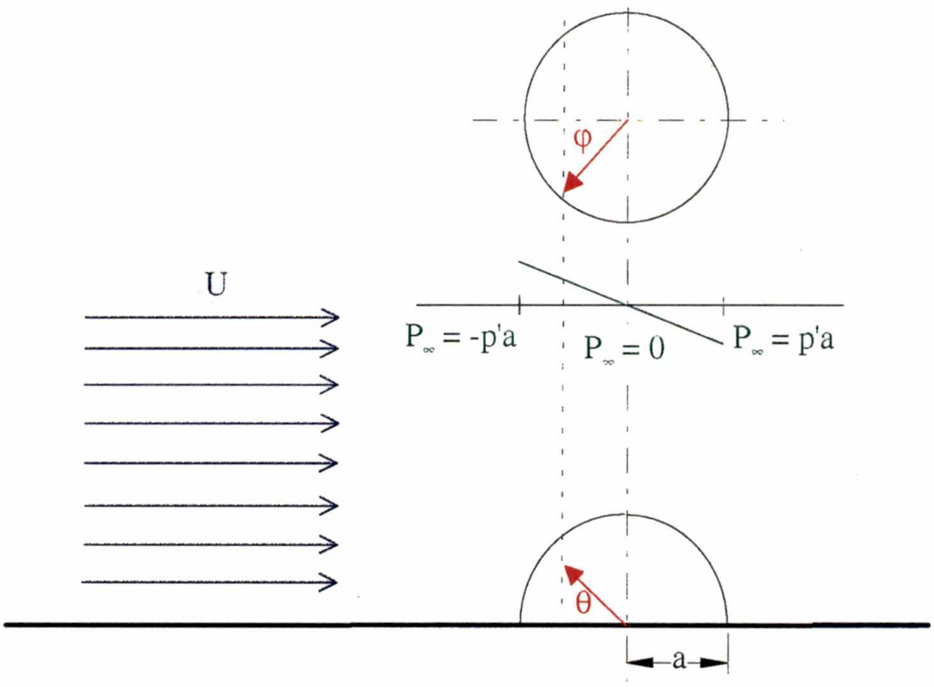

Figure 32. A Representation of the Potential Flow Field Around a Bubble.

$$\frac{\partial\phi(r,\theta,t)}{\partial t} = \frac{3}{2}U\cos(\theta)\frac{a^2a'}{r^2} - \frac{1}{r}(2aa'^2 + a^2a'') \qquad 95$$

$$\left(\frac{\partial\phi(r,\theta,t)}{\partial r}\right)^2 = U^2\cos^2(\theta)\left(1-\frac{a^3}{r^3}\right)^2 + \frac{2U\cos(\theta)a^2a'}{r^2}\left(1-\frac{a^3}{r^3}\right) + \frac{a^4a'^2}{r^4} \qquad 96$$

$$\left(\frac{1}{r}\frac{\partial\phi(r,\theta,t)}{\partial\theta}\right)^2 = U^2\sin^2(\theta)\left(1+\frac{a^3}{2r^3}\right) \qquad 97$$

Combining these derivatives into the Bernoulli equation gives the pressure distribution around the bubble.

$$P(r,\theta,t)=-p'a\cos(\theta)\cos(\varphi)-\frac{3}{2}\rho U\cos(\theta)\frac{a^2a'}{r^2}+\frac{\rho}{r}(2aa'^2+a^2a'')$$

$$-\frac{\rho}{2}\left[\begin{array}{l} U^2\cos^2(\theta)\left(1-\frac{a^3}{r^3}\right)^2+\frac{2U\cos(\theta)a^2a'}{r^2}\left(1-\frac{a^3}{r^3}\right)+\frac{a^4a'^2}{r^4} \\ +U^2\sin^2(\theta)\left(1+\frac{a^3}{2r^3}\right) \end{array}\right] \quad 98$$

Since the force exerted on the bubble is of primary interest, the pressure at the bubble surface is found by setting r = a.

$$P(a,\theta,t)=-p'a\cos(\theta)\cos(\varphi)-\frac{9}{8}\rho U^2\sin^2(\theta)-\frac{3}{2}\rho Ua'\cos(\theta)+\rho aa''+\frac{5}{2}\rho a'^2 \quad 99$$

The force applied to a differential area dA, where $dA = a^2 \sin\theta\, d\theta\, d\varphi$, is simply $-P(a,\theta,\varphi)$ dA. The minus sign indicates that a negative pressure causes a positive force.

2.2.4.1 Tangential Pressure Force

The pressure field induced from the flow around the bubble and from the bubble's growth is symmetric with respect to the normal and does not contribute to a net force in the tangential direction. However, the pressure field due to the externally imposed pressure gradient does have a net force in the tangential direction.

$$
\begin{aligned}
\mathbf{F}\cdot\mathbf{t} &= \int_A -P(a,\theta,\varphi)\cos(\theta)\cos(\varphi)dA \\
&= \int_0^{\pi}\int_0^{\pi} -P(a,\theta,\varphi)\cos(\theta)\cos(\varphi)a^2\sin(\theta)d\theta d\varphi \\
&= \int_0^{\pi}\int_0^{\pi} -(-p'a\cos(\theta)\cos(\varphi))\cos(\theta)\cos(\varphi)a^2\sin(\theta)d\theta d\varphi \\
&= p'a^3\int_0^{\pi}\int_0^{\pi}\sin(\theta)\cos^2(\theta)\cos^2(\varphi)d\theta d\varphi \\
&= \frac{\pi a^3 p'}{3}
\end{aligned}
\qquad 100
$$

2.2.4.2 Lift and Inertial Forces

There are two competing phenomena that contribute to the pressure field around the bubble. The lift force is the result of the liquid which accelerates around the bubble causing a negative pressure above the bubble surface. The inertial force is the result of the work required of the growing bubble to push the liquid away from the surface, causing a positive pressure above the surface. These forces are apparent when the pressure distribution is integrated over the bubble surface.

$$
\begin{aligned}
\mathbf{F}\cdot\mathbf{n} &= \int_0^{\pi}\int_0^{\pi}\frac{9}{8}\rho U^2a^2\sin^4(\theta)d\theta d\varphi \\
&+\int_0^{\pi}\int_0^{\pi}\frac{3}{2}\rho Ua^2a'\sin^2(\theta)\cos(\theta)-\rho a^3a''\sin^2(\theta)-\frac{5}{2}\rho a^2a'^2\sin^2(\theta)d\theta d\varphi
\end{aligned}
\qquad 101
$$

The first integral in Equation 101 is the lift force and the second is the inertial force. The result for the lift force is

$$
F_{lift} = \frac{27}{64}\pi^2\rho U^2a^2 \qquad 102
$$

The result for the inertial force is

$$F_{inertia} = -\frac{\rho\pi^2 a^2}{4}\left[5a'^2 + 2aa''\right] \qquad 103$$

2.2.5 Dominant Forces

For most flow situations, only two or three of the forces described above dominate the criteria for departure of a bubble. Zeng, et al [1993] argue that the surface tension force is generally negligible compared with the inertial force; however, their supporting data are limited to velocities less than 1 m/s. Such low velocities can lead to erroneous conclusions due to the fact that bubbles are normally sheared from the surface at departure but are not quickly accelerated from the nucleation site. Specifically, when

$$\left.\frac{dr}{dt}\right|_{r=r_d} > u(y = r_d) \qquad 104$$

a bubble will grow significantly before leaving the nucleation site after departure, making the determination of the bubble departure diameter difficult.

For higher velocity flows, Levy [1967] proposed a balance of buoyant, surface tension, and pressure forces, noting that the buoyant force played a negligible role even at relatively low velocities. However, Levy only considered the normal pressure distribution similar to that given in Equation 100 and ignored both the imposed shear and the lift force on the bubble surface. In high velocity flows, either the shear force or the lift force is the dominant force acting to overcome the surface tension holding the bubble to the surface. Recall that the derivation of the shear force assumed a no-slip boundary condition on the bubble surface, while the lift force assumed full-slip. The true boundary condition lies somewhere in between, but Figure 33 and Figure 34 demonstrate that the resulting bubble departure diameter is little affected compared with the uncertainties in the

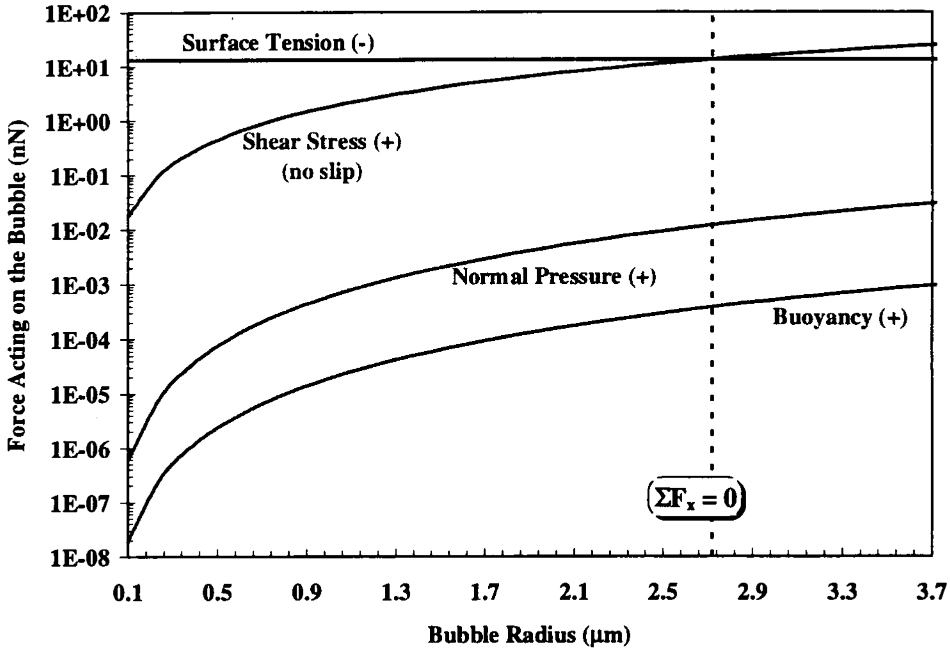

Figure 33. Tangential Forces Acting on a Bubble.

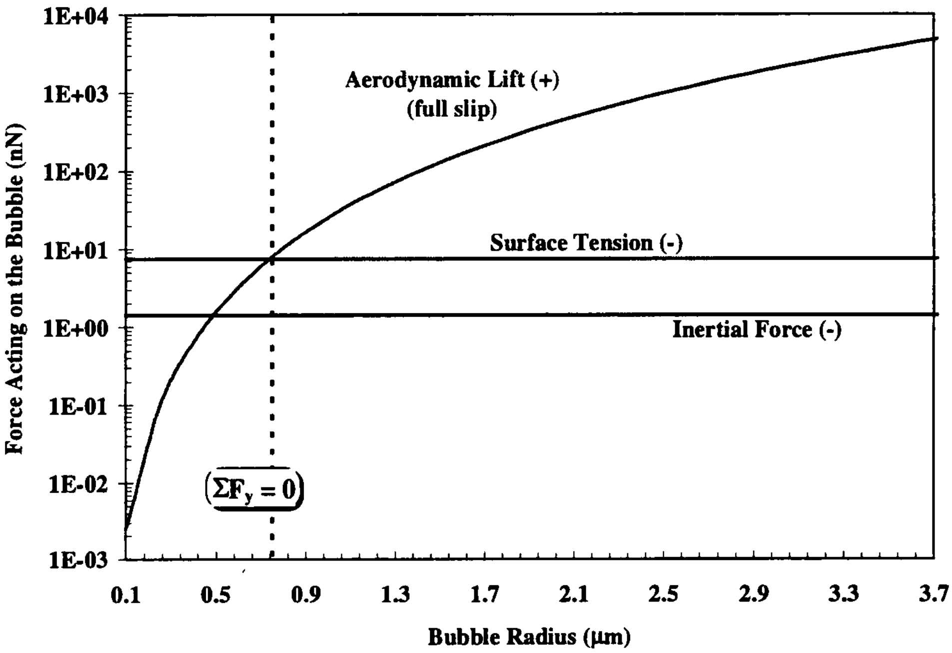

Figure 34. Normal Forces Acting on a Bubble.

calculations. The conditions for Figure 33 and Figure 34 are: Heat Flux, 6 MW/m^2; Mass Flux, 14,000 kg/m^2 s; Equivalent Diameter, 2.5 mm; Pressure, 1.7 MPa; Contact Angle, $\pi/6$.

2.3 Bubble and Boundary Layer Interaction

2.3.1 Ratio at ONVG

The bubble departure diameter decreases with increasing mass flux as shown in Figure 35. For low heat fluxes the change in departure diameter with respect to mass flux is significant, but the effect decreases as the heat flux is increased.

The relationship between the departure diameter and the laminar sublayer thickness is still not clear from Figure 35, so Figure 36 is included to show that the ratio of the departure diameter to the laminar sublayer thickness, d_b / δ_{lam}, is actually much more dependent on heat flux than mass flux. For most situations, the bubble size is greater than the laminar sublayer thickness.

2.3.2 Surface Conditions

The derivations in Sections 2.2 and 2.3 indicate the bubble departure diameter and the laminar sublayer thickness are of the same order of magnitude. However, both calculations assume an idealized heater surface. A post-test inspection of a test section from the THTL facility indicates that this assumption is normally valid, but may be in serious error under certain conditions. The inspection shows that the inlet portion of the test section is covered by a light golden oxide coating that progressively darkens toward the exit. As shown in Figure 37, the

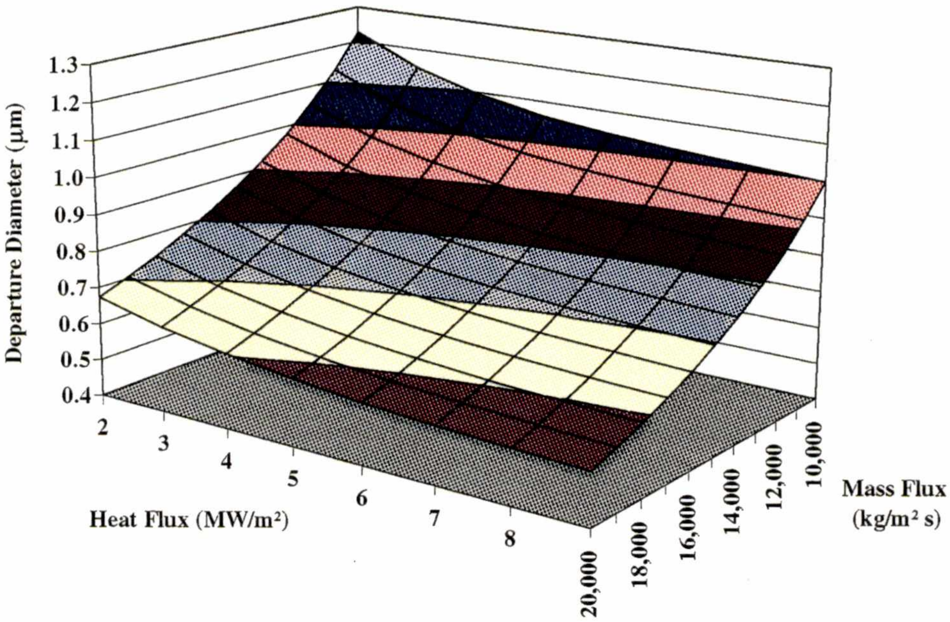

Figure 35. Bubble Departure Diameters at ANS Conditions.

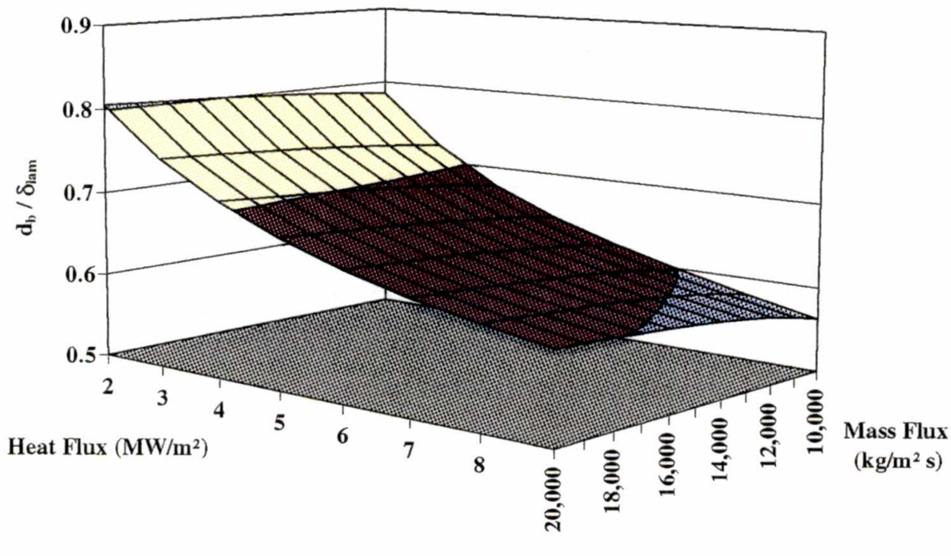

Figure 36. The Ratio between the Bubble Departure Diameter and the Laminar Sublayer Thickness at ANS Conditions.

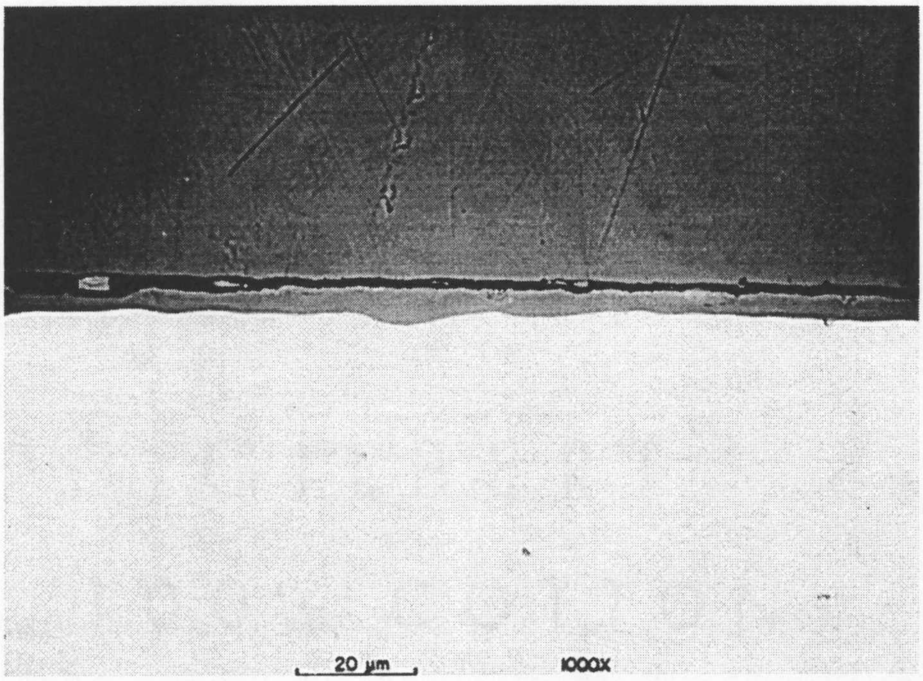

Figure 37. THTL Surface Under Single-phase Flow Conditions.

surface of this section is polished and smooth in agreement with the assumed surface in the previous calculations.

At the axial location that would approximately have been about 25% of the distance between IB and ONVG at the time of the test section burnout, there is a region that appears to have been stripped of all oxide, as shown in Figure 38. The region is curved with the center pointing toward the inlet and spans about 5 mm axially (about 1,000 bubble diameters). The thickness of the affected region appears to be about 10 - 20 µm, or about 5 - 10 times the predicted thicknesses of the laminar sublayer and average bubble diameter.

From the position where the oxide is stripped to the exit, there is gradual re-layering of the surface oxide as shown in Figure 39. The surface just beyond the position where the oxide is stripped has a rougher texture than the other sections, but the surface appears smooth enough to

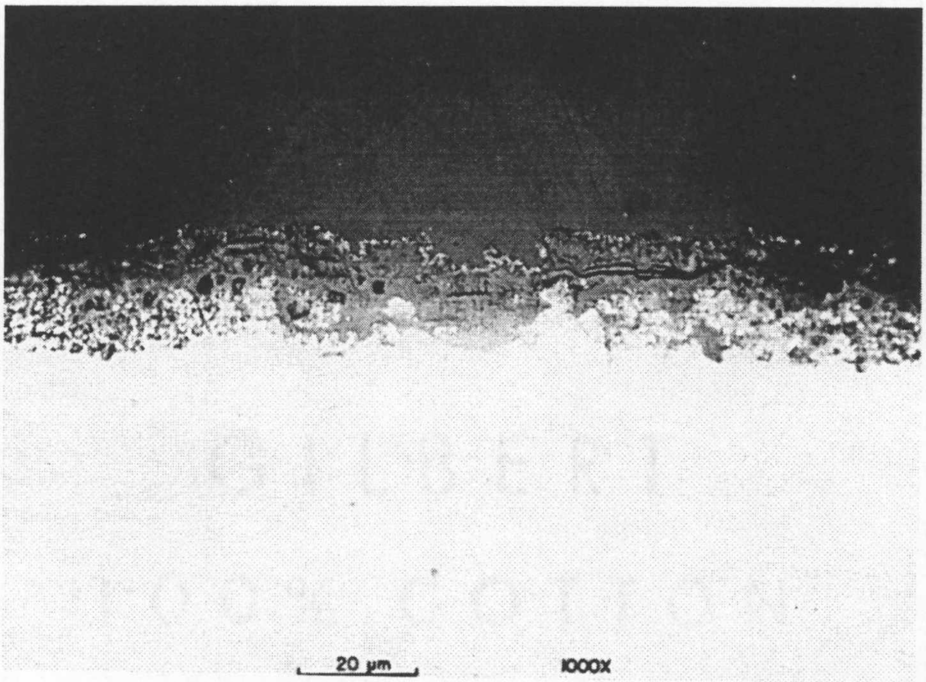

Figure 38. THTL Surface Just Between IB and ONVG.

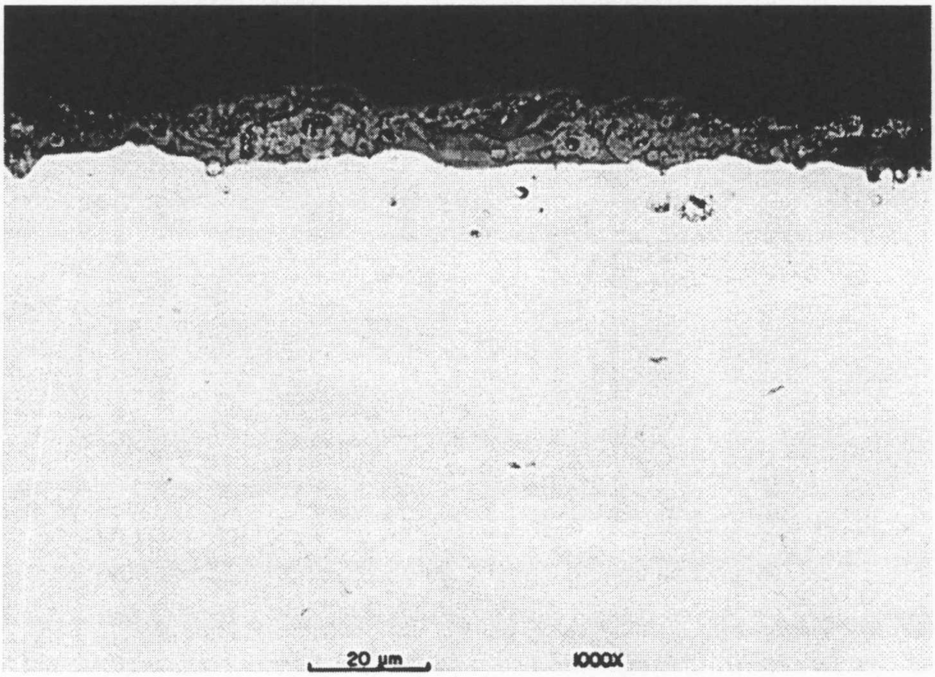

Figure 39. THTL Surface after ONVG.

support the assumptions made in the calculations of the laminar sublayer thickness and average bubble departure diameter.

There are at least two possible reasons for the oxide stripping to occur. The combination of high heat flux and high mass flux leads to large wall superheating at the point of incipient boiling even though the bulk flow is highly subcooled. The high mass flux and small hydraulic diameter in the channel also result in a small laminar sublayer thickness so that the subcooled bulk is very close to the wall. These factors contribute to the probability that rapid bubble collapse near the wall could cause cavitation damage to occur. Another possible mechanism for oxide stripping is that the bubbles are actually forming in pores within the oxide. The rapid vapor expansion during bubble growth may be sufficient to remove the outer oxide layers.

By comparing Figure 35 with Figure 38, it is obvious that normal bubble boundary layer assumptions are invalid in the oxide depleted regions. The bubble departure diameters are generally between 2 and 6 μm, whereas the damaged region is 15 to 20 μm thick. There is no method for predicting the effect of this region on the bubble layer or pressure gradient development. However, the experimental pressure drop data taken in the THTL facility do not indicate the oxide stripping has a large effect on the pressure gradient in the channel.

Chapter 3. Design Methods

For low pressure and high mass flux systems, it is convenient to predict the minimum in the demand curve (pressure drop versus mass flux) with a simple ONVG correlation. Since ONVG is usually a precursor to the minimum in the demand curve, its prediction provides a quick and usually conservative approximation to the conditions at the demand curve minimum. By comparing the conditions at ONVG to those of the demand curve minimum, the flow situations where this approximation can be used can be evaluated.

Another important consideration to the designer is the relative importance of the viscous, acceleration, and gravitational pressure gradients. For many flow situations only one or two of these effects dominate the pressure and velocity field. Flow situations where the acceleration pressure drop is dominant to the onset of Ledinegg flow excursion will be identified.

3.1 The Demand Curve Minimum

A true analytic form of the demand curve minimum can be derived by setting the derivative of the channel pressure drop with respect to mass flux equal to zero. Unfortunately, the governing equations are highly non-linear and do not generally lend themselves to analytical treatments. Under some simplifying assumptions and approximations, however, a form can be derived that can be used for scoping analyses and comparative studies with ONVG. For the following derivation, the following assumptions are made.

1) constant properties, except for the saturation temperature

2) constant heat flux

3.1.1 General Form

The formula for the pressure drop in a two-phase channel is

$$\Delta P=\int_0^{L_1}\left.\frac{\partial P}{\partial z}\right|_{1\phi,f}dz+\int_0^{L_1}\left.\frac{\partial P}{\partial z}\right|_{1\phi,g}dz+\int_{L_1}^{L}\left.\frac{\partial P}{\partial z}\right|_{2\phi,f}dz+\int_{L_1}^{L}\left.\frac{\partial P}{\partial z}\right|_{2\phi,a}dz+\int_{L_1}^{L}\left.\frac{\partial P}{\partial z}\right|_{2\phi,g}dz \qquad 105$$

Using the idea of single-phase and two phase friction factors and expanding the acceleration gradient using the separated flow model, Equation 105 can be expressed as

$$\Delta P=\int_0^{L_1}\frac{f_{1\phi}}{2d}\frac{G^2}{\rho_l}dz+\int_0^{L_1}\rho_l g dz+\int_{L_1}^{L}\frac{f_{2\phi}}{2d}\frac{G^2}{\rho_l}dz+\int_{L_1}^{L}G^2\frac{\partial}{\partial z}\left[\frac{(1-x)^2}{\rho_l(1-\alpha)}+\frac{x^2}{\rho_v\alpha}\right]dz+\int_{L_1}^{L}\rho_{2\phi}g dz \qquad 106$$

Equation 106 can be put in non-dimensional form with the following definitions.

$$P'=\frac{\Delta P d^2\rho_l}{\mu^2} \qquad 107$$

$$\ell_j=\frac{L_j}{d} \qquad 108$$

$$g'=gd\left(\frac{\rho_l d}{\mu}\right)^2 \qquad 109$$

where j represents either the single-phase or the two-phase section. Equation 106 then becomes

$$\begin{aligned}P'=&\int_0^{\ell_1}\frac{f_{1\phi}}{2}Re^2\,d\ell+\int_0^{\ell_1}g'd\ell\\&+\int_{\ell_1}^{\ell}\frac{f_{2\phi}}{2}Re^2\,d\ell+\int_{\ell_1}^{\ell}Re^2\frac{\partial}{\partial\ell}\left[\frac{(1-x)^2}{(1-\alpha)}+\frac{\rho_l}{\rho_v}\frac{x^2}{\alpha}\right]d\ell+\int_{\ell_1}^{\ell}\left[\alpha\left(\frac{\rho_v}{\rho_l}-1\right)+1\right]g'd\ell\end{aligned} \qquad 110$$

For constant properties the minimum in the demand curve will correspond to the zero point of the derivative of P′ with respect to the Reynolds number.

$$\frac{\partial P'}{\partial Re} = \frac{\partial}{\partial Re}\left\{\begin{aligned} &\int_0^{\ell_1} \frac{f_{1\phi}}{2} Re^2\, d\ell + \int_0^{\ell_1} g' d\ell \\ &+ \int_{\ell_1}^{\ell} \frac{f_{2\phi}}{2} Re^2\, d\ell + \int_{\ell_1}^{\ell} Re^2 \frac{\partial}{\partial \ell}\left[\frac{(1-x)^2}{(1-\alpha)} + \frac{\rho_l}{\rho_v}\frac{x^2}{\alpha}\right] d\ell \\ &+ \int_{\ell_1}^{\ell}\left[\alpha\left(\frac{\rho_v}{\rho_l} - 1\right) + 1\right] g' d\ell \end{aligned}\right\} = 0 \qquad 111$$

3.1.2 The Single-phase Region

The single-phase portion of Equation 111 is

$$\frac{\partial P'_{1\phi}}{\partial Re} = \frac{\partial}{\partial Re}\left\{\int_0^{\ell_1} \frac{f_{1\phi}}{2} Re^2\, d\ell + \int_0^{\ell_1} g' d\ell\right\} \qquad 112$$

Assuming that both the friction factor and Reynolds number are independent of the spatial coordinate, Equation 112 may be reduced to

$$\frac{\partial P'_{1\phi}}{\partial Re} = \frac{\partial}{\partial Re}\left\{\frac{f_{1\phi}\ell_1}{2} Re^2 + g'\ell_1\right\} \qquad 113$$

The bulk temperature in the single-phase region is found through an energy balance.

$$\begin{aligned} T(z) &= T_i + \frac{qP_h L_1}{GA_{xs}C_p} \\ &= T_i + \frac{4}{Re\,Pr}\frac{qd}{k}\ell_1 \end{aligned} \qquad 114$$

The onset of net vapor generation is strongly dependent on the local subcooling. For high mass flux systems it is imperative to allow the saturation temperature change with the local pressure since there is often significant pressure changes from the inlet to outlet. Assuming that the saturation temperature is a linear function of pressure over a small range of pressure, the saturation temperature can be approximated by

$$T_s = T_{si} + \frac{dT_s}{dP}\Delta P \qquad 115$$

where the pressure drop is modeled with the definition of the friction factor.

$$\begin{aligned}\Delta P_{1\phi} &= \frac{f_{1\phi}\ell_1}{2}\frac{G^2}{\rho_l} + \rho_l g \ell_1 \\ &= \frac{f_{1\phi}\ell_1}{2}\frac{\mu^2}{d^2\rho_l}Re^2 + \rho_l g \ell_1\end{aligned} \qquad 116$$

A simple form of the friction factor will be used to keep the derivation as simple as possible [Blasius, 1913].

$$f_{1\phi} = 0.3164 Re^{-0.25} \qquad 117$$

The equations for the saturation temperature can be put in non-dimensional form with the definition of P′ and with the following definition.

$$T_p^* = \frac{\mu^2}{\lambda_i d^2 \rho_l}\frac{\partial T_s}{\partial P} \qquad 118$$

Equation 115 then becomes

$$\begin{aligned}T_s &= T_{si} - \left(\frac{\lambda_i d^2 \rho_l}{\mu^2}\right)T_p^*\left[(0.3164\,Re^{-0.25})\frac{\ell_1}{2}\left(\frac{\mu^2}{d^2\rho_l}\right)Re^2 + \left(\frac{\mu^2}{d^2\rho_l}\right)g'\ell_1\right] \\ &= T_{si} - \lambda_i T_p^* \ell_1 [0.1582\,Re^{7/4} + g']\end{aligned} \qquad 119$$

The subcooling profile is found by combining Equations 114 and 119.

$$\begin{aligned}\lambda(z) &= T_s(z) - T(z) \\ &= T_{si} - \lambda_i T_p^*[0.1582\ell_1 Re^{7/4} + g'\ell_1] - T_i - \frac{4}{Re\,Pr}\frac{qd}{k}\ell_1 \\ &= \lambda_i\left[1 - \ell_1\left(T_p^*[0.1582\,Re^{7/4} + g'] + \frac{4}{Re\,Pr}\frac{qd}{k\lambda_i}\right)\right] \\ &= \lambda_i\left[1 - \ell_1\left(T_p^*[0.1582\,Re^{7/4} + g'] + \frac{4Nu_{si}}{Re\,Pr}\right)\right]\end{aligned} \qquad 120$$

where

$$Nu_{si} = \frac{qd}{k\lambda_i} \qquad 121$$

is the Nusselt number based on the inlet subcooling.

Assuming that the effects on the channel pressure due to partially developed boiling are negligible, the end of the single-phase region corresponds to ONVG. According to Saha & Zuber [1974], ONVG occurs when the local Stanton number is equal to 0.0065 for Peclet numbers greater than 70,000. This criteria may be manipulated with the result from the subcooling profile to yield

$$\begin{aligned} & St = 0.0065 \\ & \frac{qd}{k\lambda(z)} = 0.0065\,Re\,Pr \\ & Nu_{si} = 0.0065\,Re\,Pr\left[1 - \ell_1\left(T_p^*[0.1582\,Re^{7/4} + g'] + \frac{4Nu_{si}}{Re\,Pr}\right)\right] \end{aligned} \qquad 122$$

which may be solved for the single-phase L/d ratio, ℓ_1.

$$\begin{aligned} & \ell_1\left(T_p^*[0.1582\,Re^{7/4} + g'] + \frac{4Nu_{si}}{Re\,Pr}\right) = 1 - \frac{Nu_{si}}{0.0065\,Re\,Pr} \\ & \ell_1 = \frac{0.0065\,Re\,Pr - Nu_{si}}{0.001T_p^*\,Pr\,Re^{11/4} + 0.0065T_p^*\,Re\,Pr\,g' + 0.026Nu_{si}} \end{aligned} \qquad 123$$

Once the single-phase length is known, the pressure drop in this region can be evaluated by combining Equations 116 and 117 with the definition of P′.

$$\begin{aligned} & P'_{1\phi} = 0.1582\,Re^{7/4}\,\ell_1 + g'\ell_1 \\ & = (0.1582\,Re^{7/4} + g')\ell_1 \end{aligned} \qquad 124$$

The derivative of the single-phase term from Equation 112 may then be evaluated.

$$\begin{aligned}\frac{\partial P'_{1\phi}}{\partial \mathrm{Re}} &= 0.1582\left(\frac{7}{4}\ell_1 \mathrm{Re}^{3/4} + \mathrm{Re}^{7/4}\frac{\partial \ell_1}{\partial \mathrm{Re}}\right) + g'\frac{\partial \ell_1}{\partial \mathrm{Re}} \\ &= 0.2769\ell_1 \mathrm{Re}^{3/4} + \frac{P'_{1\phi}}{\ell_1}\frac{\partial \ell_1}{\partial \mathrm{Re}}\end{aligned} \qquad 125$$

The derivative of ℓ_1 with respect to the Reynolds number is

$$\frac{\partial \ell_1}{\partial \mathrm{Re}} = \frac{\ell_1[1 - \ell_1(0.423 T_p^* \mathrm{Re}^{7/4} + g')]}{\mathrm{Re} - \dfrac{\mathrm{Nu}_{si}}{0.0065\,\mathrm{Pr}}} \qquad 126$$

3.1.3 The Two Phase Region

The two phase portion of Equation 111 is

$$\begin{aligned}\frac{\partial P'_{2\phi}}{\partial \mathrm{Re}} &= \frac{\partial}{\partial \mathrm{Re}}\left\{P'_{2\phi,f} + P'_{2\phi,a} + P'_{2\phi,g}\right\} \\ &= \frac{\partial}{\partial \mathrm{Re}}\left\{\int_{\ell_1}^{\ell} \frac{f_{2\phi}}{2}\mathrm{Re}^2\, d\ell + \int_{\ell_1}^{\ell} \mathrm{Re}^2 \frac{\partial}{\partial \ell}\left[\frac{(1-x)^2}{(1-\alpha)} + \frac{\rho_l}{\rho_v}\frac{x^2}{\alpha}\right] d\ell + \int_{\ell_1}^{\ell}\left[\alpha\left(\frac{\rho_v}{\rho_l} - 1\right) + 1\right] g'\, d\ell\right\}\end{aligned} \qquad 127$$

The pressure drop in the two phase region consists of a two-phase friction term and an acceleration term. The frictional term is similar to the single-phase frictional term, except the friction factor is a two-phase friction factor. Using Avdeev's definition in Equation 33,

$$f_{2\phi} = \left[1.74 - 0.87\ln\left(\frac{1}{3.9R} + \frac{49}{\mathrm{Re}^{0.91}}\right)\right]^{-2} \qquad 128$$

The R parameter as defined by Avdeev is the ratio of the channel radius to bubble diameter. Although a correlation for R is presented by Avdeev, it is more complicated than the present analysis warrants. Instead, the bubble departure diameter from Levy's [1967] paper will be used to model R. Levy's model states that

$$d_b = 0.015\sqrt{\frac{\sigma d}{\tau_w}} = 0.015\sqrt{\frac{2\sigma d\rho_l}{fG^2}} \qquad 129$$

Again using the simple friction factor correlation in Equation 117, the bubble departure diameter can be expressed as

$$d_b = 0.0377\sqrt{\frac{\sigma d^3\rho_l}{\mu^2}}\,Re^{-7/8} \qquad 130$$

The R parameter is therefore

$$\begin{aligned} R &= \frac{d}{2d_b} \\ &= \frac{d}{0.0754\sqrt{\frac{\sigma d^3\rho_l}{\mu^2}}\,Re^{-7/8}} \\ &= \frac{13.3\mu\,Re^{7/8}}{\sqrt{\sigma d\rho_l}} \\ &= 13.3M_0\,Re^{7/8} \end{aligned} \qquad 131$$

where the dimensionless group, M_0, is defined as

$$M_0 = \frac{\mu}{\sqrt{\sigma d\rho_l}} \qquad 132$$

Using Equation 131 in the two-phase friction factor of Equation 33 gives

$$f_{2\phi} = \left[1.74 - 0.87\ln\left(\frac{0.019}{M_0\,Re^{7/8}} + \frac{49}{Re^{0.91}}\right)\right]^{-2} \qquad 133$$

which is a function only of Reynolds number. Since the two-phase friction factor is independent of spatial considerations,

$$P'_{2\phi,f} = \int_{\ell_1}^{\ell}\frac{f_{2\phi}}{2}Re^2\,d\ell = Re^2\,f_{2\phi}(\ell-\ell_1) \qquad 134$$

Taking the derivative of Equation 134 with respect to the Reynolds number gives

$$\frac{\partial P'_{2\phi,f}}{\partial \mathrm{Re}} = \frac{1}{2}\frac{\partial}{\partial \mathrm{Re}}\left[(\ell-\ell_1) f_{2\phi}\mathrm{Re}^2\right]$$

$$= (\ell-\ell_1) f_{2\phi}\mathrm{Re} + \frac{\mathrm{Re}^2 f_{2\phi}}{2}\left[\frac{(\ell-\ell_1)}{f_{2\phi}}\frac{\partial f_{2\phi}}{\partial \mathrm{Re}} + \frac{\partial \ell_1}{\partial \mathrm{Re}}\right] \qquad 135$$

The derivative of ℓ_1 with respect to Reynolds number is given in Equation 126. The derivative of $f_{2\phi}$ with respect to the Reynolds number is

$$\frac{\partial f_{2\phi}}{\partial \mathrm{Re}} = \frac{1.52 f_{2\phi}^{3/2}}{\mathrm{Re}^2}\left[\frac{\mathrm{Re}^{1.02} + 5247 M_0}{\mathrm{Re}^{1.04} + 5051 M_0}\right] \qquad 136$$

The two-phase acceleration portion of Equation 106 is

$$\frac{\partial P'_{2\phi,a}}{\partial \mathrm{Re}} = \frac{\partial}{\partial \mathrm{Re}}\int_{\ell_1}^{\ell} \mathrm{Re}^2 \frac{\partial}{\partial \ell}\left[\frac{(1-x)^2}{(1-\alpha)} + \frac{\rho_l}{\rho_v}\frac{x^2}{\alpha}\right] d\ell \qquad 137$$

Assuming that the quality at ONVG is << 1 and using the definition of P′, the non-dimensional acceleration pressure drop can be expressed as

$$P'_{2\phi,a} = \mathrm{Re}^2\left[\frac{[1-x(\ell)]^2}{[1-\alpha(\ell)]} + \frac{\rho_l}{\rho_v}\frac{x(\ell)^2}{\alpha(\ell)} - 1\right] \qquad 138$$

Henceforth, the symbols x and α will refer to the quality and void at the channel exit.

The derivative of $P'_{2\phi,a}$ with respect to Reynolds number is

$$\frac{\partial P'_{2\phi,a}}{\partial \mathrm{Re}} = 2\mathrm{Re}\left[\frac{(1-x)^2}{(1-\alpha)} + \frac{\rho_l}{\rho_v}\frac{x^2}{\alpha} - 1\right]$$

$$+\mathrm{Re}^2\left\{2\frac{\partial x}{\partial \mathrm{Re}}\left[\frac{\rho_l}{\rho_v}\frac{x}{\alpha} - \frac{(1-x)}{(1-\alpha)}\right] + \frac{\partial \alpha}{\partial \mathrm{Re}}\left[\frac{(1-x)^2}{(1-\alpha)^2} - \frac{\rho_l}{\rho_v}\frac{x^2}{\alpha^2}\right]\right\} \qquad 139$$

To keep the analysis as simple as possible without compromising the physics, the drift-flux model is used to model the quality and void at the channel exit. According to Equation 15, the exit quality is

$$x = \frac{C_p \lambda_{ONVG}[z^+ - \tanh(z^+)]}{h_{fg} + C_p \lambda_{ONVG}[1 - \tanh(z^+)]} \qquad 15$$

where the parameter z^+ is the fractional distance between the point of ONVG and the point of bulk saturation.

$$z^+ = \frac{z - z_{ONVG}}{z_{sat} - z_{ONVG}} = \frac{\ell - \ell_{ONVG}}{\ell_s - \ell_{ONVG}} \qquad 140$$

Using the Saha & Zuber correlation in Equation 23 to replace the subcooling in Equation 15 yields

$$\begin{aligned} x &= \frac{q[z^+ - \tanh(z^+)]}{0.0065\mathrm{Re}\frac{\mu}{d}\left[h_{fg} + \frac{qd}{0.0065\mathrm{Re}\mu}[1 - \tanh(z^+)]\right]} \\ &= \frac{M_1[z^+ - \tanh(z^+)]}{0.0065\mathrm{Re} + M_1[1 - \tanh(z^+)]} \end{aligned} \qquad 141$$

where the dimensionless constant M_1 is defined as

$$M_1 = \frac{qd}{\mu h_{fg}} \qquad 142$$

The term ℓ_{ONVG} is equivalent to the previously derived ℓ_1. The saturation length, ℓ_s, can be derived similarly, but some approximation must be made for the exit pressure so that the saturation temperature can be modeled. Since the demand curve minimum in this analysis is usually associated with small exit qualities, it is assumed that the single-phase approximation of the pressure profile is valid. Figure 10 through Figure 20 show that the pressure at the demand curve minimum is close to that expected in a fully single-phase flow.

$$T(z) = T_s$$

$$T_i + \frac{4}{\mathrm{Re\,Pr}}\frac{qd}{k}\ell_s = T_{si} - \lambda_i T_p^* \ell_s [0.1582\,\mathrm{Re}^{7/4} + g']$$

$$\ell_s = \frac{\lambda_i}{\frac{4}{\mathrm{Re\,Pr}}\frac{qd}{k} + \lambda_i T_p^* [0.1582\,\mathrm{Re}^{7/4} + g']} \qquad 143$$

$$\ell_s = \frac{1}{\frac{4\mathrm{Nu}_{si}}{\mathrm{Re\,Pr}} + T_p^* [0.1582\,\mathrm{Re}^{7/4} + g']}$$

The exit void fraction is also taken from Kroeger & Zuber's [1968] analysis.

$$\alpha = \frac{x}{C_0\left[\frac{x\Delta\rho}{\rho_l} + \frac{\rho_v}{\rho_l}\right] + \frac{1.41 M_2}{\mathrm{Re}}} \qquad 144$$

where the dimensionless constant M_2 is defined as

$$M_2 = \frac{\rho_v d}{\mu}\left[\frac{\sigma g \Delta\rho}{\rho_l^2}\right]^{1/4} \qquad 145$$

The exit quality and void fraction are now developed, but the derivatives of both variables must be considered to complete the derivation. The variables in the expression for the exit quality are the Reynolds number and z^+. z^+ is also a function of Reynolds number and will be considered separately.

$$\frac{\partial x}{\partial \mathrm{Re}} = x\left\{\frac{\frac{\partial z^+}{\partial \mathrm{Re}}[1 - \mathrm{sech}^2(z^+)]}{z^+ - \tanh(z^+)} - \frac{0.0065 - M_1\,\mathrm{sech}^2(z^+)\frac{\partial z^+}{\partial \mathrm{Re}}}{0.0065\mathrm{Re} + M_1[1 - \tanh(z^+)]}\right\} \qquad 146$$

As stated previously, z^+ is the fractional distance between the point of ONVG and the point of bulk saturation. Since the local z/d is the exit L/d for this case, ℓ is known and z^+ is only dependent on the single-phase and saturation lengths.

$$\frac{\partial z^+}{\partial \mathrm{Re}} = z^+ \left\{ \frac{\partial \ell_1}{\partial \mathrm{Re}} \left[\frac{\ell - \ell_1 - 1}{\ell - \ell_1} \right] - \frac{\partial \ell_s}{\partial \mathrm{Re}} \right\} \qquad 147$$

The single-phase L/d, ℓ_1, the saturation length, ℓ_s, and the derivative of the single-phase length with respect to the Reynolds number are already given in Equations 123, 143, and 126, respectively. The derivative of the saturation length is

$$\frac{\partial \ell_s}{\partial \mathrm{Re}} = \ell_s^2 \left[\frac{4\mathrm{Nu}_{si}}{\mathrm{Re}^2\,\mathrm{Pr}} - 0.277 T_p^* \,\mathrm{Re}^{3/4} \right] \qquad 148$$

The derivative of the exit quality is now complete. The exit void fraction is dependent both on the Reynolds number and the exit quality, and its derivative can be expressed in terms of these quantities.

$$\frac{\partial \alpha}{\partial \mathrm{Re}} = \frac{\alpha}{x}\frac{\partial x}{\partial \mathrm{Re}} + \frac{\alpha^2}{x}\left[\frac{C_0 \Delta\rho}{\rho_l}\frac{\partial x}{\partial \mathrm{Re}} - 1.41\frac{M_2}{\mathrm{Re}^2} \right] \qquad 149$$

The two-phase gravitational part of Equation 106 is

$$P'_{2\phi,g} = \int_{\ell_1}^{\ell} \left[\alpha\left(\frac{\rho_v}{\rho_l} - 1 \right) + 1 \right] g' d\ell \qquad 150$$

Assuming an average value for void fraction at $\alpha_{exit}/2$, this reduces to

$$P'_{2\phi,g} = \left[\frac{\alpha}{2}\left(\frac{\rho_v}{\rho_l} - 1 \right) + 1 \right] g'(\ell - \ell_1) \qquad 151$$

The derivative of $P'_{2\phi,g}$ with respect to Reynolds number is therefore

$$\frac{\partial P'_{2\phi,g}}{\partial \mathrm{Re}} = g' \left\{ \frac{\ell - \ell_1}{2}\left(\frac{\rho_v}{\rho_l} - 1 \right)\frac{\partial \alpha}{\partial \mathrm{Re}} - \left[\frac{\alpha}{2}\left(\frac{\rho_v}{\rho_l} - 1 \right) + 1 \right]\frac{\partial \ell_1}{\partial \mathrm{Re}} \right\} \qquad 152$$

The equation for the minimum in the demand characteristic is now completely defined. A small subroutine that uses the above formulas to determine the minimum in the demand curve is included in Appendix A. To ensure that the model is capable of predicting the demand curve minimum it is compared to a subset of the ANS flow excursion database [Siman-Tov, et al, 1995]. The database used for this comparison consists of 441 data points from 15 different investigations. It is limited to those flow excursion data points that have Pe > 70,000. Table 5 lists the range of data used in the database.

Table 5. Parameter Range for the Comparison Database.

Parameter	Minimum	Maximum
L/d Ratio	50	444
Mass Flux (kg/m^2 s)	1,049	25,074
Exit Pressure (MPa)	0.100	1.763
Average Heat Flux (MW/m^2)	0.60	19.0
Exit Subcooling (°C)	0.14	65.4
Inlet Temperature (°C)	20.0	115.0

Figure 40 shows that the model is capable of predicting the minimum in the pressure demand characteristic for the database. The model predicts critical Reynolds numbers that are about 0.8% high with a standard deviation of about 12%. The average error is the average of

$$\text{Error} = \frac{(\text{Re}_{\text{Predicted}} - \text{Re}_{\text{Measured}})}{\text{Re}_{\text{Measured}}} \qquad 153$$

for the entire database.

3.2 A Comparison Between ONVG and Flow Excursion

Since ONVG and the demand curve minimum are physically distinct phenomena, it is possible that using an ONVG correlation for predicting the demand curve minimum will lead to significant errors in certain situations. However, these regions are not well defined. In order to get

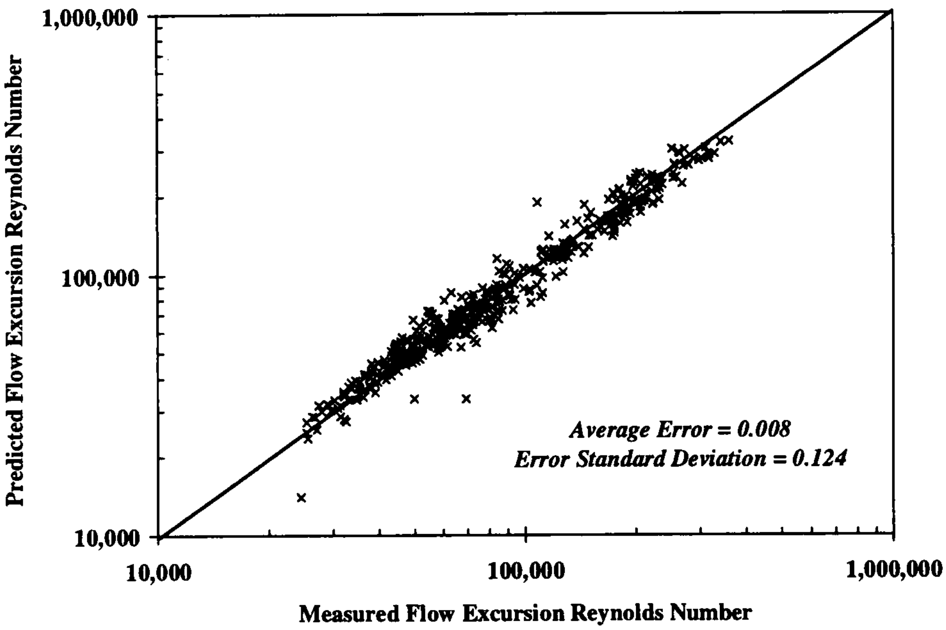

Figure 40. Model Comparison for Flow Excursion Database.

a more precise identification of the flow situations where ONVG and the demand curve minimum nearly coincide, a numerical regression experiment is conducted.

Six input parameters are considered for the experiment: inlet subcooling, inlet pressure, equivalent diameter, Reynolds number, heat flux, and the angle from vertical. Some physically significant interaction effects are also included: exit subcooling, subcooling gradient, pressure gradient, and the length to diameter ratio. The six main factors are chosen at random for each of 2000 trials. The range of each of the input parameters is shown in Table 6.

The response for the experiment is the two phase length to diameter ratio.

$$\ell_2 = \ell - \ell_1 \tag{154}$$

Table 6. Parameter Levels for the Factorial Experiment.

Parameter	Low Level	High Level
Primary Factors		
Inlet Pressure (MPa)	0.106	8.000
Inlet Subcooling (°C)	7	267
Heat Flux (MW/m^2)	1	12
Reynolds Number	45,000	1,000,000
Equivalent Diameter (m)	0.001	0.05
Angle from Vertical (rad)	0	π
Interaction Factors		
Exit Subcooling (°C)	0.4	131.0
Subcooling Gradient (°C/m)	5	728
Pressure Gradient (MPa/m)	0.2	20.9
Length to diameter Ratio	26	1900

Before performing the regression, the parameters are scaled so that the predicted effects are of the same order of magnitude regardless of the magnitude of the actual parameter. Table 7 gives the calculated effects.

Many of the calculated effects require little explanation. The pressure effect is large, but expected since a high pressure moves the vapor density toward the liquid density producing less void for the same mass quality. The diameter effect is explained by noting that a larger diameter leads to a larger cross sectional area and less liquid acceleration as void is produced (the parameter R is larger for a given average bubble diameter). The L/d ratio effect is also expected due to the fact that the single-phase $\partial P'/\partial Re$, which must be overwhelmed by the two phase $\partial P'/\partial Re$, is proportional to the single-phase L/d.

The remaining calculated effects in Table 7 may be interpreted with the schematic of the subcooling profile in Figure 41 and Equations 120, 140, and 141, reproduced here for convenience.

$$z^+ = \frac{z - z_{ONVG}}{z_{sat} - z_{ONVG}} = \frac{\ell - \ell_{ONVG}}{\ell_s - \ell_{ONVG}} \qquad 140$$

Table 7. Analysis of Experimental Results.

Parameter	Effect	Standard Error
Single-phase Pressure Gradient	-23.03	0.95
Exit Subcooling	-14.58	0.61
Pressure	12.30	0.23
Inlet Subcooling	-10.41	0.39
Subcooling Gradient	8.32	1.02
Reynolds Number	-2.92	0.36
Equivalent Diameter	2.55	0.38
Length to Diameter Ratio	1.98	0.76
Heat Flux	-1.30	0.38
Angle from Vertical	-0.59	0.18

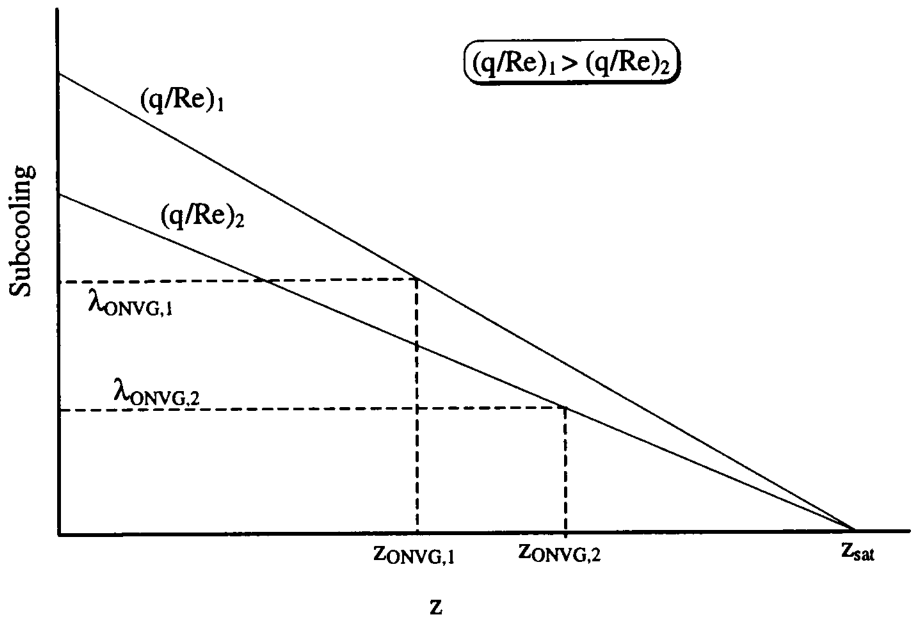

Figure 41. Schematic Representation of the Subcooling Profile in a Channel.

$$x = \frac{C_p \lambda_{ONVG}[z^+ - \tanh(z^+)]}{h_{fg} + C_p \lambda_{ONVG}[1 - \tanh(z^+)]} \qquad 141$$

$$\lambda(z) = \left[1 - \ell_1 \left(T_p^* [0.1582\, \mathrm{Re}^{7/4} + g'] + \frac{4\mathrm{Nu}_{si}}{\mathrm{Re\,Pr}} \right)\right] \qquad 120$$

The effects of Reynolds number and heat flux are both negative. This can be explained by examining Equation 141 and Figure 41. For the moment, assume that the subcooling profile is controlled by the bulk temperature profile, $4Nu_{si}$ / Pe. When the heat flux is increased, the subcooling at ONVG is also increased producing two competing effects. First, the length z_{SAT} - z_{ONVG} is increased which retards the void development due to the dependence of z+ and increases the two-phase length. Second, the exit quality is increased which produces a greater acceleration pressure gradient and reduces the two-phase length. Since the calculated effect is negative, the latter effect is obviously the strongest.

The Reynolds number dependence is opposite to the heat flux. When the Reynolds number is increased, the subcooling at ONVG is decreased. The two-phase length is decreased due to the decreasing distance between z_{SAT} and z_{ONVG}, but increased due to the smaller exit quality. According to the analysis of the heat flux effect, the latter should dominate and the Reynolds number effect should be positive. However, the Reynolds number also effects the subcooling profile through the pressure gradient as shown in Equation 120. A large pressure gradient moves the lower subcooling profile toward the upper profile *without changing the subcooling at ONVG.* A large pressure gradient thus decreases the distance between z_{SAT} and z_{ONVG} while holding the exit quality constant, resulting in a reduced two-phase length. The Reynolds number effect is thus negative and small due to compensating effects, while the effect of the pressure gradient, which is controlled primarily by the Reynolds number, is large and negative.

The two most important parameters in determining the error associated with predicting the demand curve minimum with an ONVG correlation are the system pressure and pressure gradient (and therefore Reynolds number). As shown in Figure 42, the error is greatest when the Reynolds number is small (less than about 4 x 10^5) and the system pressure is large (greater than about 3 MPa).

Finally, the relationship between the exit subcooling and the two-phase length is worth noting. The exit subcooling will be small for those flow situations that require large exit qualities to produce the demand curve minimum. Large exit qualities are usually associated with large two-phase lengths. Hence, there is a correlation between the exit subcooling and the two phase length.

Although the relationship between the two-phase length and exit subcooling is not a direct cause-and-effect in the way that the two-phase length is correlated with Reynolds number or heat flux, it does have important practical application. Siman-Tov, et al [1995] recently suggested that the Saha & Zuber [1974] correlation for ONVG in Equation 23 can be modified with a stronger subcooling dependence to produce a correlation for the demand curve minimum.

$$St_{FE} = \frac{q}{GC_p\lambda} = 0.0065\left(0.55 + \frac{11.21}{\lambda}\right) \qquad 155$$

Considering the strong relationship between exit subcooling and two-phase length indicated in Table 7, it is not surprising that the modification in Equation 155 allows the extension of an ONVG correlation to the demand curve minimum for reasonably large L/d.

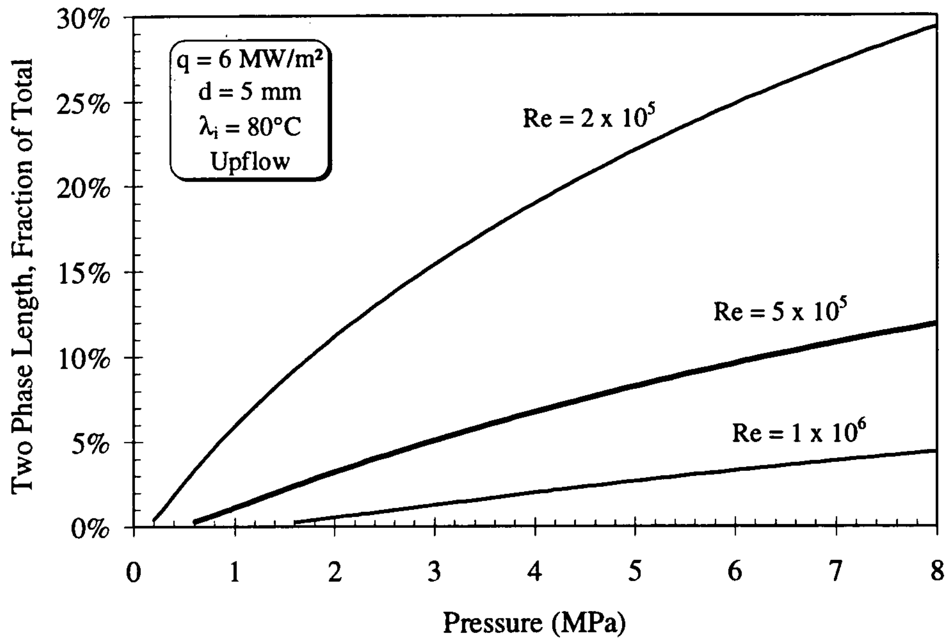

Figure 42. The Relationship Between the Two Phase Length, System Inlet Pressure, and Reynolds Number.

3.3 Relative Importance of Shear, Gravitational, and Acceleration Effects on the Channel Pressure Drop

An important consideration to the designer is the relative importance of the viscous, acceleration, and gravitational pressure gradients. For many flow situations only one of these effects dominates the pressure and velocity field. For example, the pressure gradient due to wall shear for an ANS channel in normal operation (25,000 kg/m² s mass flux) is much larger than that due to gravity.

For high velocity flows beyond ONVG, the acceleration pressure gradient is always important. The regions where it is less important are the same as those found in the previous section with large two phase lengths. For flow conditions with large acceleration pressure gradients, the two phase length will be small.

A simple comparison can be made between the frictional and gravitational effects by using the non-dimensional form of the single-phase pressure drop in Equation 124. By rearranging this formula, it can be seen that the gravitational effects may be safely ignored if

$$Re \gg (6.32g')^{4/7} \qquad 156$$

This criterion is based on single-phase flow correlations, but the gravitational effect decreases as void is produced in a channel, while the frictional effect increases. Therefore, the criterion will be conservative for two-phase flow. Figure 43 shows the Reynolds number locus where the frictional and gravitational effects on the local pressure gradient are equal using water at 150°C as the working fluid. At ANS conditions with a 1.3 mm gap, the nominal Reynolds number of about $2x10^5$ is an order of magnitude greater than the predicted locus. Therefore, the gravitational effects are not significant at steady state conditions.

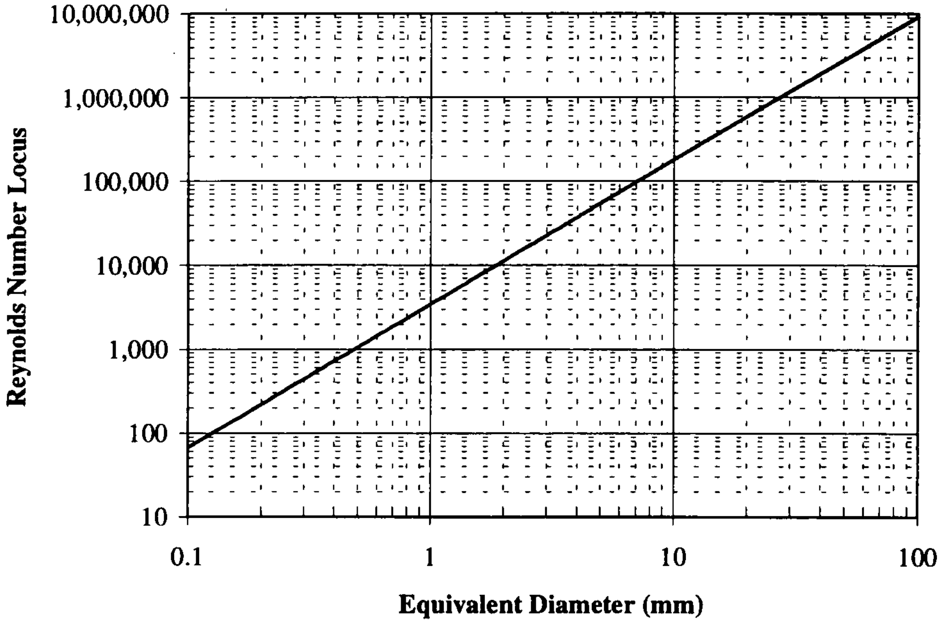

Figure 43. Reynolds Number Where Frictional and Gravitational Effects Are Equal.

Conclusion

One of the most efficient designs for removing large heat loads is a parallel channel assembly with a small equivalent diameter and large mass flux. This design is found in system plans for the Advanced Neutron Source reactor, hypersonic aircraft, beam dumps in fusion energy, spallation source cooling, and plasma arc torch cooling. The design limit for channels of this type is usually associated with the minimum in the pressure demand characteristic of a heated channel. A good method for predicting this limit is necessary to ensure that the designs have adequate margin to failure.

For the conditions of the Advanced Neutron Source reactor fuel cooling channels, it is recommended that the drift-flux model developed by Avdeev [1982-1988] be used to predict the local pressure gradient. This model is based on local conditions and is shown to accurately predict the data taken at the THTL facility. The model predictions are about 6% high on average with a standard deviation of 0.10 in the single-phase and partially developed subcooled boiling regions. When the fully developed boiling region is included, the average prediction is 13% high with a standard deviation of 0.12.

Traditionally, the bubble layer in the region from IB to ONVG is treated as a roughness effect despite the fact that bubbles are known to grow and collapse with high frequency in the wall region. Three mechanistic approaches that may be used to predict the increase in wall shear due to bubble ebullition are developed. These models have functionality based on flow physics and are shown to produce trends similar to the model of Avdeev [1982-1988] which is known to follow existing data well. These models should be the basis for future wall shear stress modeling in the bubble boundary layer. These models can be extended to fully developed boiling when more information regarding the nature of the velocity profile in these flows becomes available.

The condition of the bubble boundary layer is directly related to the local pressure gradient and is sensitive to local flow conditions. It is shown that the combination of high heat flux, high mass flux, and small equivalent diameter leads to the unusual condition that the bubble departure size and the laminar sublayer are roughly equal based on conventional models. In addition, it is shown experimentally that bubble ebullition at the channel surface of the THTL test section disrupts the oxide layer and creates a surface with a roughness scale two or three times the predicted laminar sublayer thickness. However, this region is small and has not been found to have a large effect on the total system pressure drop.

Because ONVG predictions are much simpler than demand curve minimum predictions, they are often used as conservative estimates of the demand curve minimum. It is shown that for low pressure and high Reynolds number flows, this is a good approximation since the demand curve minimum will follow the point of ONVG closely. Alternatively, conditions of high pressure and low Reynolds number may lead to predictions that are overly conservative.

Conventional models for predicting subcooled boiling pressure gradients are very empirical. Future work should integrate models with sound physical basis to minimize empiricism in engineering calculations of this type. The mechanistic models developed herein could easily be extended beyond ONVG with an appropriate experimental database. These models use consistent expressions for fluid dynamic and thermal effects in the boundary layer and link micro models for bubble ebullition to macro models for heat transfer and fluid flow. This is a very significant improvement over conventional modeling techniques for subcooled boiling flows.

List of References

List of References

Ahmad, S.Y., 1970, "Axial Distribution Of Bulk Temperature And Void Fraction In A Heated Channel With Inlet Subcooling," *Journal Of Heat Transfer*, 92(4), 595-609.

Avdeev, A.A., 1982, "The Reynolds Analogy For Nondevelooped Surface Boiling Under Forced Motion Conditions," *Thermal Engineering*, 29(3).

Avdeev, A.A., 1986, "Application Of The Reynolds Analogy To The Investigation Of Surface Boiling In Conditions Of Forced Motion," *High Temperature*, 24(1), 111-119.

Avdeev, A.A., And Pekhterev, V.P., 1986, "Void Fraction With Boiling Of Subcooled Liquid In Channels With Different Laws Of Heating," *Thermal Engineering*, 33(10).

Avdeev, A.A., And Pekhterev, V.P., 1987, "A Criterial Equation For Calculation For Boiling Flows Of Subcooled Liquid," *Thermal Engineering*, 34(2).

Avdeev, A.A., 1988, "The Boundaries Of The Region Of The Effect Of Surface Boiling On Void Fraction And Hydraulic Resistance," *Thermal Engineering*, 35(9).

Bergles, A.E., And Rohsenow, W.M., 1964, "The Determination Of Forced Convection Surface Boiling Heat Transfer," *Journal Of Heat Transfer*, 86, 365-372.

Bibeau, E. L., And Salcudean, M., 1994, "A Study Of Bubble Ebullition In Forced-Convective Subcooled Nucleate Boiling At Low Pressure," *Int. J. Heat Mass Transfer*, 37(15), 2245-2259.

Blasius, H., 1913, "Das Ähnlichkeitsgesetz Bei Reibungsvorgängen In Flussikeiten," *Forsch. Arb. Ing. Wes.*, No. 134, Berlin.

Carey, V., 1992, Liquid-Vapor Phase-Change Phenomena, Hemisphere, Washington.

Carlson, K.E., et al, 1990, RELAP5-MOD3 Code Manual Volume IV: Models And Correlations. NUREG/CR-5535.

Crabtree, J.A., And Siman-Tov, M., 1993, "Thermophysical Properties Of Saturated Light And Heavy Water For Advanced Neutron Source Applications," ORNL/TM-12322.

Currie, I.G., 1974, Fundamental Mechanics of Fluids, McGraw-Hill, Inc.

Felde, et al, 1994, "Advanced Neutron Source Reactor Thermal-Hydraulic Test Loop Facility Description," ORNL/TM-12397.

Filonenko, G.K., 1954, "Hydraulic Resistance In Pipes," *Teploenergetika*, 1(4), 40-44.

Forster, H.K., And Greif, R., 1959, "Heat Transfer To A Boiling Liquid - Mechanisms And Correlations," *Journal Of Heat Transfer*, 81, 45-53.

Griffith, P., Clark, J. A., Rohsenow, W. M., 1958, "Void Volumes In Subcooled Boiling Systems," MIT Technical Report No. 12.

Gunther, F.C., 1951, "Photographic Study Of Surface Boiling Heat Transfer To Water With Forced Convection," *ASME Transactions*, 73, 115-123.

Hahne, E., et al, 1993, "A New Pressure Drop Correlation For Subcooled Flow Boiling Of Refrigerants," *Int. J. Heat Mass Transfer*, 36(17), 4267-4274.

Han, C.Y., And Griffith, P., 1965, "The Mechanism Of Heat Transfer In Nucleate Pool Boiling, Part I, Bubble Initiation, Growth, And Departure," *Int. J. Heat Mass Transfer*, 8(6), 887-904.

Hirata, M., And Nishiwaki, N., 1963, "Skin Friction And Heat Transfer For Liquid Flow Over A Porous Wall With Gas Injection," *Int. J. Heat Mass Transfer*, 6, 941-949.

Hoffman, M.A., And Wong, C.F., 1992, "Prediction Of Pressure Drops In Forced Convection Subcooled Boiling Water Flows," *Int. J. Heat Mass Transfer*, 35, 3291-3299.

Holman, J.P., 1990, Heat Transfer, 7th Edition, McGraw-Hill, Inc.

Hsu, Y.Y., And Graham, R.W., 1986, Transport Processes In Boiling And Two-Phase Systems, American Nuclear Society.

Jia, D. And Schrock, V.E., 1986, "A Generalized Procedure For Predicting The Pressure Drop In A Subcooled Boiling Channel," The 4th International Symposium On Multiphase Transport And Particulate Phenomena, Miami.

Kroeger, P.G., And Zuber, N., 1968, "An Analysis Of The Effects Of Various Parameters On The Average Void Fractions In Subcooled Boiling," *Int. J. Heat Mass Transfer*, 11, 211-213.

Lahey, R.T., Jr., 1974, "A Mechanistic Subcooled Boiling Model," Rensselaer Polytechnic Institute, Troy, NY.

Larson, P.S., And Tong, L.S., 1969, "Void Fractions In Subcooled Flow Boiling," *Journal Of Heat Transfer*, November, 471-476.

Ledinegg, M., 1938, "Instability Of Flow During Natural And Forced Circulation," *Die Warme*, Vol. 61(8).

Levy, S., 1967, "Forced Convection Subcooled Boiling-Prediction Of Vapor Volumetric Fraction," *Int. J. Heat Mass Transfer*, 10, 951-965.

Mikheev, M.A., And Mikheeva, I.M., 1973, Principles Of Heat Transfer [In Russian], Energiya, Moscow.

Owens, W.L., And Schrock, V.E., 1960, "Local Pressure Gradients For Subcooled Boiling Of Water In Vertical Tubes," ASME Paper 60-WA-249.

Maitra, D., And Raju, K.S., 1975, "Vapour Void Fraction In Subcooled Flow Boiling," *Nuclear Engineering And Design*, 32, 20-28.

Reynolds, J.B., 1954, "Local Boiling Pressure Drop," ANL-5178.

Riemke, R.A., 1993, "Modification To Unal's Subcooled Flow Boiling Bubble Model," *Nuclear Technology*, 102, 416-417.

Rohde, R.R., 1962, "Boiling Water Reactor Technology, Status Of The Art Report," *Heat Transfer And Hydraulics*, Vol. I, ANL-6561.

Rouhani, S.Z., And Axelson, E., 1970, "Calculation Of Void Volume Fraction In The Subcooled And Quality Boiling Regions," *Int. J. Heat Mass Transfer*, 13, 383-393.

Saha, P. And Zuber, N., 1974, "Point Of Net Vapor Generation And Vapor Void Fraction In Subcooled Boiling," Proc. Of The 5th International Heat Transfer Conference, Japan, 4, 175-179.

Schlichting, H., 1979, Boundary-Layer Theory, 7th Edition, McGraw-Hill, Inc.

Shin, T.S., And Jones, O.C., 1993, "Nucleation And Flashing In Nozzles - 1: A Distributed Nucleation Model," *Int. J. Multiphase Flow*, 19(6), 943-964.

Siman-Tov, M., et al, 1995, "Static Flow Instability In Subcooled Flow Boiling In Parallel Channels," 2nd International Conference on Multiphase Flow, April 3-7, Kyoto, Japan.

Siman-Tov, M., et al., 1991, "Thermal-Hydraulic Correlations For The Advanced Neutron Source Reactor Fuel Element Design And Analysis," ASME Winter Annual Meeting, December 1 - 6, Atlanta, GA.

van Stralen, et al, 1975, "Bubble Growth Rates In Pure And Binary Systems: Combined Effect Of Relaxation And Evaporation Microlayers," *Int. J. Heat Mass Transfer*, 18, 453-467.

Sultan And Judd, 1978, "Spatial Distribution Of Active Sites And Bubble Flux Density," *Transactions Of The ASME*, 100, Feb.

Tarasova, N.V., And Orlov, V.M., 1962, "An Investigation Into Hydraulic Resistance With Surface Boiling Of Water In A Tube," *Teploenergetika*, 6, 48-52.

Tarasova, N.V., et al, 1966, "Pressure Drop Of Boiling Subcooled Water And Steam-Water Mixture Flowing In Heated Channels," Proc. 3rd Int. Heat Transfer Conference, Chicago, Vol. 4, Paper 113, 178-183.

Unal, H. C., 1976, "Maximum Bubble Diameter, Maximum Bubble Growth Time And Bubble Growth Rate During The Subcooled Nucleate Flow Boiling Of Water Up To 17.7 MPa," *Int. J. Heat Mass Transfer*, 19, 643-649.

Wallis, G., 1969, One-Dimensional Two Phase Flow. McGraw-Hill, Inc.

White, F.M., 1991, Viscous Fluid Flow, McGraw-Hill, Inc.

Yoder, G. L., With Dixon J. R., Elkassabgi, Y., Felde, D. K., Giles, G. E., Harrington, R. M., Morris, D. G., Nelson, W. R., Ruggles, A. E., Siman-Tov, M., Stovall, T. K., 1994, "Steady State Thermal-Hydraulic Design Analysis Of The Advanced Neutron Source Reactor," ORNL/TM-12398.

Zeng, L.Z., et al, 1993, "A Unified Model For The Prediction Of Bubble Detachment Diameters In Boiling Systems -- II. Flow Boiling," *Int. J. Heat Mass Transfer*, 36, 2271-2279.

Zuber, N., And Findlay, J.A., 1964, "The Effects Of Non-Uniform Flow And Concentration Distributions And The Effect Of The Local Relative Velocity On The Average Volumetric Concentration In Two-Phase Flow," GEAP-4542, General Electric Co.

Appendices

Appendix A

Program Description and Listing

Appendix A. Program Description and Listing

The following program is written in FORTRAN and was used to calculate the pressure drop in a THTL channel. Many variations of the program were used during this project, this being a representative sample. The function of the main program is simply to read the appropriate input data (test section specifications, mass flux, and heat flux) and send it to the subroutine MatchPexit. The function of MatchPexit is to find the inlet pressure necessary to match the given exit pressure. Once a new best guess for the inlet pressure is found, the subroutine calls the subroutine FEM, which marches down the channel and calculates the exit pressure.

A.1 Pressure Drop

A.1.1 Main Program

```
program dp
c
      real*8 tin, pin, pout
      real*8 dpm, dpc, pinlet, pexit
      real*8 gap, span, g, angle, c(17),
     1          length, qf(9)
      character*10 test

        length = .507
        angle = 0.0
c
        open (unit=20,file='datapts',status='old')
        open (unit=21,file='predict',status='new')
c
        do 2 i = 1,17
          read (20,200) test, gap, span, g, tin, pin, pout,
     1            qf(1), qf(2), qf(3), qf(4), qf(5), qf(6),
     2            qf(7), qf(8), qf(9)
          dpm = (pin - pout) / 1.0d6
```

```
c
        call matchpexit (tin, pin, pout, pinlet, pexit,
   1                  gap, span, qf, g, angle, c, length)
c
        dpc = (pinlet - pexit) / 1.0d6
        write (21,210) test, g, pin, pout, dpm, pinlet, pexit, dpc
c
 2     continue
c
       data c(1)/1.0/c(2)/-.7/c(3)/-1.28/c(4)/6.28/c(5)/3.9/
   1     c(6)/12.0/c(7)/.524/c(8)/2.0/c(9)/.93/c(10)/.065/
   2     c(11)/.25/c(12)/.007/c(13)/.25/c(14)/-.3/c(15)/-.5/
   3     c(16)/.48/c(17)/1.2/
c
200   format (a10,1x,f8.6,1x,f6.4,1x,f8.2,1x,f8.5,1x,f7.0,1x,
   1          f7.0,1x,f8.0,1x,f8.0,1x,f8.0,1x,f8.0,1x,f8.0,
   2          1x,f8.0,1x,f8.0,1x,f8.0,1x,f8.0)
210   format (a10,2x,f8.2,2x,f10.2,2x,f10.2,2x,f6.4,2x,
   1          f10.2,2x,f10.2,2x,f6.4)
      stop
      end
c
```

A.1.2 Subroutine MatchPexit

This subroutine is responsible for ensuring that the calculated exit pressure matches the given inlet pressure. It uses the secant iterative method along with subroutine FEM to accomplish its task.

```
     subroutine matchpexit (tin, pin, pexit, p2, pout,
   1                  gap, span, qf, g, angle, c, length)
c
      real*8 tin, pin, pexit, p1, p2, pout, ep1, ep2, dpde
      real*8 gap, span, qf, g, angle, c(17), length
      integer i
c
       p1 = pin
       call fem (tin, p1, pout,
   1                  gap, span, qf, g, angle, c, length)
       ep1 = (pout - pexit) / pexit
c
c
       p2 = p1 * 1.1
       call fem (tin, p2, pout,
   1                  gap, span, qf, g, angle, c, length)
```

```
      ep2 = (pout - pexit) / pexit
c
      i = 0
      do while ((abs(ep2) .ge. .0001) .and. (i .lt. 30))
        i = i + 1
        dpde = (p2 - p1) / (ep2 - ep1)
        p1 = p2
        ep1 = ep2
        p2 = p2 - dpde * ep2
        call fem (tin, p2, pout,
     1              gap, span, qf, g, angle, c, length)
        ep2 = (pout - pexit) / pexit
      end do
      print *, g, i, ep2
c
    return
    end
```

A.1.3 Subroutine FEM

This subroutine calculates the exit pressure based on the channel characteristics and flow conditions. The subroutine uses segment lengths of 5 mm, 1 mm, and 0.5 mm for the single-phase region, partially developed boiling region, and fully developed boiling region, respectively. This subroutine also determines the positions where transition to a new region occurs.

```
    subroutine fem (tin, pin, p2,
     1              gap, span, qf, g, angle, c, length)
c
    real*8 tin, pin, p2, t1, t2, p1, x1, x2, v1, v2, q
    real*8 r, ra, a, dh, z, lseg, zib, zosv, dtib, st, dtwall, dtw
    real*8 gap, span, qf(9), g, angle, c(17), length, lq(9), de
    real*8 ib, superheat, hf, cond, tsat
    integer j
c
      lseg = .005
      de = 2.0 * gap
      zib = 1.0
      zosv = 1.0
      z = 0.0
      p2 = pin
      t2 = tin
      x2 = 0.0
      v2 = 0.0
      do while (z .lt. length)
```

```
      z = z + lseg
      j = 1
      p1 = p2
      t1 = t2
      x1 = x2
      v1 = v2
      do while (lq(j) .le. z)
        j = j + 1
      end do
      q = qf(j)
      if (z .le. zib) then
c
c           calculate single-phase quantities
              call singlephase (t1, p1, t2, p2, lseg, dtw,
     1                 gap, span, q, g, angle, c)
c
c           test for transition to pdb
              dtib = ib(p2, q)
        if (dtib .le. dtw) then
          if (lseg .gt. .001) then
            z = z - lseg
            lseg = .001
            t2 = t1
            p2 = p1
          else
            zib = z
          end if
        end if

      else if (z .le. zosv) then
c
        call pdb (t1, x1, v1, p1, lseg,
     1         t2, x2, v2, p2,
     2              gap, span, q, g, angle, c)
c
        st = q / (g * cp(t2) * (tsat(p2) - t2))
        r = 10.0**((st**c(2) + c(3)) / c(4))
        dtwall = superheat(p2, q)
        dh = hf(tsat(p2)) - hf(t2)
        a = g * de * dh / (2.0 * cond(t2) * dtwall)
        ra = c(8) * (c(9) + c(10) * a**c(11))**(1 / c(11))
c
        if (ra .ge. r) then
          if (lseg .gt. .0005) then
            lseg = .0005
            t2 = t1
            p2 = p1
            x2 = x1
            v2 = v1
          else
            zosv = z
```

```
          end if
        end if
c
      else
c
        call fdb (t1, x1, v1, p1, lseg,
  1              t2, x2, v2, p2,
  2                   gap, span, q, g, angle, c)
c
      end if
c
      if (z + lseg .ge. length) then
        lseg = length - z
      end if
c
    end do
    data lq(1)/.0825/lq(2)/.22/lq(3)/.34/lq(4)/.4/lq(5)/.44/
  1      lq(6)/.47/lq(7)/.485/lq(8)/.495/lq(9)/1.0/
  return
  end
c
```

A.1.4 Subroutine SinglePhase

This subroutine calculates the exit temperature and pressure of a segment length in single-phase flow.

```
  subroutine singlephase (tin, pin, tout, pout, lseg, dtw,
  1                 gap, span, q, g, angle, c)
    real*8 tin, pin, tout, pout, lseg, dtw
    real*8 gap, span, q, g, angle, c(17), ph, axs, de
    real*8 tb, tw, gradpf, gradpg, gradpa, gradp, f
    real*8 cp, densf, tsat
c
    ph = 2.0 * span
    axs = gap * span
    de = 2.0 * gap
c
    tout = tin + (q * ph * lseg) / (g * axs * cp(tin))
    tb = (tin + tout) / 2.0
    tout = tin + (q * ph * lseg) / (g * axs * cp(tb))
    tb = (tin + tout) / 2.0
c
    call petukhov (tb, tw, q, g, de, gap, span, c)
c
    call filonenko (f, tb, tw, g, de, gap, span, c)
c
    gradpf = .5 * f / de * g**2 / densf(tb)
```

```
      gradpg = 9.81 * densf(tb) * cos(angle)
      gradpa = g**2 * (1 / densf(tout) - 1 / densf(tin)) / lseg
c
      gradp = gradpf + gradpg + gradpa
      pout = pin - lseg * (gradpf + gradpg + gradpa)
      if (pout .lt. 101000.0) pout = 101000.0
c
      dtw = tw - tsat(pout)
c
     return
     end
c
```

A.1.5 Subroutine Filonenko

This subroutine calculates the Filonenko friction factor [Filonenko, 1954].

```
     subroutine filonenko (f, tb, tw, g, de, gap, span, c)
c
      real*8 f, tb, tw, g, de, gap, span, c(17)
      real*8 re, ratio
      real*8 visc
c
      re = g * de / visc(tb)
c
      f = c(1) / (1.82 * log10(re) - 1.64)**2
c
      f = f * (1.0875 - .1125 * gap / span)
c
      if (tw .gt. 0.0) then
       ratio = visc(tw) / visc(tb)
       if (ratio .lt. .35) ratio = .35
       if (ratio .gt. 2.0) ratio = 2.0
c        f = f * (7.0 - 1.0 / ratio) / 6.0
      endif
c
     return
     end
c
c
```

A.1.6 Subroutine Petukhov

This subroutine calcultes the Petukhov single-phase heat transfer coefficient.

```
      subroutine petukhov (tb, tw, q, g, de, gap, span, c)
c
        real*8 tb, tw, q, g, de, gap, span, c(17)
        real*8 re, ff, htct, htcb, htciso, e0, e1, dtde
        real*8 t0, t1, p
        real*8 visc, cond, cp
        integer i
c
        re = g * de / visc(tb)
        tw = 0.0
        p = cp(tb) * visc(tb) / cond(tb)
        call filonenko (ff, tb, tw, g, de, gap, span, c)
        htct = (cond(tb) / de) * (ff / 8.0) * re * p
        htcb = (1.0 + 3.4 * ff) + (11.7 + 1.8 * p**(-0.333)) *
     1        (ff / 8.0)**.5 * (p**0.666 - 1.0)
        htciso = htct / htcb
c
        t0 = tb + q / htciso
        e0 = q - htciso * (visc(tb) / visc(t0))**.11 * (t0 - tb)
c
        t1 = t0 + 5.0
        e1 = q - htciso * (visc(tb) / visc(t1))**.11 * (t1 - tb)
c
        i = 0
        do while ((abs(e1) .gt. .0001) .and. (i .lt. 20))
          dtde = (t0 - t1) / (e0 - e1)
          t0 = t1
          e0 = e1
          t1 = t1 - e1 * dtde
          e1 = q - htciso * (visc(tb) / visc(t1))**.11 * (t1 - tb)
          i = i + 1
        end do
c
        tw = t1
c
      return
      end
c
```

A.1.7 Function SuperHeat

This function calculates the superheat (T_w - T_{sat}) for a given pressure and temperature.

```
      real*8 function superheat (p, q)
c
        real*8 p, pbar, q
```

```
c
      pbar = p / 10.0**5
      superheat = (q**.33) * ((1.0 - .0045 * pbar) /
     1            (3.4 * (pbar**.18)))
     return
     end
c
```

A.1.8 Function IB

This function calculates the wall superheat necessary for the incipience of boiling.

```
      real*8 function ib (p, qw)
c
        real*8 p, qw, q, a, b
        q = qw / 10.0**6
        a = q / (1.7978e-9 * p**1.156)
        b = p**0.0234 / 2.8285
        ib = a**b / 1.8
c
      return
      end
```

A.1.9 Subroutine PDB

This subroutine calculates the exit void, quality, and pressure for the given segment length when the flow conditions are beyond IB but before ONVG. The actual calculations are done in PDBcalc, but this subroutine is the controlling loop. Its responsibility is to divide the segment length into as many sub-segments as necessary to achieve convergence. The criteria for convergence is when the exit void and pressure for a calcuation using n sub-segments is within 0.01% of the void and pressure for a calculation using n-1 sub-segments.

```
      subroutine pdb (tin, xin, vin, pin, lseg,
     1              t2, x2, void2, p2,
     2                 gap, span, q, g, angle, c)
c
      real*8 tin, pin, xin, vin, lseg
      real*8 t0, p0, x0, void0
```

```
      real*8 p1, void1
      real*8 t2, p2, x2, void2
      real*8 ev, ep
      real*8 gap, span, q, g, angle, c(17)
      integer k, j
c
c
        k = 0
        t2 = tin
        p2 = pin
        x2 = xin
        void2 = vin
        ev = 1.0
        ep = 1.0
        do while (((ev .gt. .0001) .or. (ep .gt. .0001))
     1           .and. (k .lt. 100))
          k = k + 1
          void1 = void2
          p1 = p2
          t2 = tin
          p2 = pin
          x2 = xin
          void2 = vin
          do 10 j=1, k
            t0 = t2
            p0 = p2
            x0 = x2
            void0 = void2
            call pdbcalc (t0, x0, void0, p0, lseg / k,
     1                    t2, x2, void2, p2,
     2                    gap, span, q, g, angle, c )
 10       continue
          ev = abs(void2 - void1) / void2
          ep = abs(p2 - p1) / p2
        end do
c
      return
      end
c
```

A.1.10 Subroutine PDBcalc

This subroutine calculates the temperature, quality, void, and pressure at the exit of a sub-segment given the same parameters at the sub-segment inlet. This subroutine is used when the flow conditions are beyond IB but before ONVG.

```
      subroutine pdbcalc (tin, x0, void0, pin, lseg,
```

```
     1               tout, x, void, pout,
     2                 gap, span, q, g, angle, c)
c
      real*8 tin, x0, void0, pin, lseg
      real*8 tout, x, void, pout, ph, axs, de
      real*8 p, tb, dtwall, tw, st, r, re, f
      real*8 rho2, gradpf, gradpg, gradpa, gradp
      real*8 af0, af1, ag0, ag1
      real*8 gap, span, q, g, angle, c(17)
      real*8 cp, tsat, superheat, visc, densf, densg
c
      p = pin
c
      ph = 2.0 * span
      axs = gap * span
      de = 2.0 * gap
c
c       bulk and exit temperatures
      tout = tin + (q * ph * lseg) / (g * axs * cp(tin))
      tb = (tin + tout) / 2
      tout = tin + (q * ph * lseg) / (g * axs * cp(tb))
      tb = (tin + tout) / 2
      if (tb .ge. tsat(p)) tb = .99 * tsat(p)
c
c       wall temperature
      call petukhov (tb, tw, q, g, de, gap, span, c)
      dtwall = superheat(p, q)
      if (tw .gt. tsat(p) + dtwall) tw = tsat(p) + dtwall
c
c       bubble size
      st = q / (g * cp(tb) * (tsat(p) - tb))
      r = 10.0**((st**c(2) + c(3)) / c(4))
c
c       friction factor
      re = g * de / visc(tb)
      call f2phase (f, r, re, c)
c
c         void fraction
      void = 2.0 * c(7) / r
c
c       quality
      rho2 = densg(tb) * void + densf(tb) * (1.0 - void)
      x = c(6) * (f / 8.0)**0.5 * densg(tb) * void / rho2
c
c      frictional pressure gradient
      gradpf = .5 * f / de * g**2 / densf(tb)
c
c      gravitational pressure gradient
      gradpg = 9.81 * densf(tb) * cos(angle)
c
c      acceleration pressure gradient
```

```
      ag1 = x**2 / (densg(tb) * void)
      af1 = (1.0 - x)**2 / ((1.0 - void) * densf(tb))
      af0 = (1.0 - x0)**2 / ((1.0 - void0) * densf(tin))
      if (void0 .gt. 0.0) then
        ag0 = x0**2 / (densg(tin) * void0)
      else
        ag0 = 0.0
      endif
      gradpa = g**2 * (af1 + ag1 - (af0 + ag0)) / lseg
c
c       exit pressure
      gradp = gradpf + gradpg + gradpa
      pout = pin - lseg * (gradpf + gradpg + gradpa)
      if (pout .lt. 101000.0) pout = 101000.0
c
    return
    end
c
```

A.1.11 Subroutine FDB

This subroutine calculates the exit void, quality, and pressure for the given segment length when the flow conditions are beyond ONVG. The actual calculations are done in FDBcalc, but this subroutine is the controlling loop. Its responsibility is to divide the segment length into as many sub-segments as necessary to achieve convergence. The criteria for convergence is when the exit void and pressure for a calcuation using n sub-segments is within 0.01% of the exit void and pressure for a calculation using n-1 sub-segments.

```
subroutine fdb (tin, xin, vin, pin, lseg,
   1            t2, x2, void2, p2,
   2                 gap, span, q, g, angle, c)
c    initial conditions/definitions
c
      real*8 tin, pin, xin, vin, lseg
      real*8 gap, span, q, g, angle, c(17)
      real*8 t0, p0, x0, void0
      real*8 p1, void1
      real*8 t2, p2, x2, void2
      real*8 ev, ep
      integer k, j
c
      k = 0
```

```
        t2 = tin
        p2 = pin
        x2 = xin
        void2 = vin
        ev = 1.0
        ep = 1.0
        do while (((ev .gt. 0.0001) .or. (ep .gt. 0.0001))
     1             .and. (k .lt. 100))
          k = k + 1
          void1 = void2
          p1 = p2
          t2 = tin
          p2 = pin
          x2 = xin
          void2 = vin
c
          do 5 j=1,k
            t0 = t2
            p0 = p2
            x0 = x2
            void0 = void2
            call fdbcalc (t0, x0, void0, p0, lseg / k,
     1                    t2, x2, void2, p2,
     2                    gap, span, q, g, angle, c )
 5        continue
c
          ev = abs(void2 - void1) / void2
          ep = abs(p2 - p1) / p2
        end do
c
      return
      end
c
```

A.1.12 Subroutine FDBcalc

This subroutine calculates the temperature, quality, void, and pressure at the exit of a sub-segment given the same parameters at the sub-segment inlet. This subroutine is used when the flow conditions are beyond ONVG.

```
      subroutine fdbcalc (t0, x0, void0, p0, lseg,
     1                    tout, x, void, pout,
     2                    gap, span, q, g, angle, c )
c
        real*8 t0, x0, void0, p0, lseg
        real*8 gap, span, q, g, angle, c(17)
        real*8 tout, x, void, pout, de, ph, axs
```

```
      real*8 gl, dtwall, tw, p, dh, a, r, voidc, re, f, tb
      real*8 stcore, qcore, stcond, qcond, term1, term2
      real*8 dtdz, dxdz, wt, rho2, xw, term3, af0, af1
      real*8 ag0, ag1, gradpf, gradpg, gradpa, gradp
      real*8 superheat, tsat, hf, cond, visc, cp, hfg, densf,
     1     densg
c
      ph = 2.0 * span
      axs = gap * span
      de = 2.0 * gap
c
      p = p0
      tb = t0
      void = void0
      x = x0
c
      gl = g * (1.0 - x) / (1.0 - void)
c
c       wall temperature
      dtwall = superheat(p, q)
      tw = tsat(p) + dtwall
c
c         bubble size
      dh = hf(tsat(p)) - hf(tb)
      a = (g * de * dh) / (2 * cond(tb) * dtwall)
      if (a .lt. 5723.0) a = 5723.0
      r = c(8) * (c(9) + c(10) * a**c(11))**(1 / c(11))
c
c       initial void fraction in the liquid core region
      voidc = (void - c(7) * 2 / r) / (1 - 2 / r)
      if (voidc .lt. 0.0) voidc = 0
c
c       friction factor & reynolds number
      re = g * de / visc(tb)
      call f2phase (f, r, re, c)
c
c      heat flux to the liquid core region
      stcore = (c(4) * log10(r)- c(3))**(1 / c(2))
      qcore = gl * dh * stcore
      if (qcore .gt. q) then
        qcore = q
      elseif (qcore .lt. 0.0) then
        qcore = 0.0
      endif
c
c       condensation heat flux
      term1 = c(12) * voidc * r * (void / (1 - void))**c(13)
      term2 = (1.0 - 2.0 / r) * (re**c(14)) * (pr(tb)**c(15))
      stcond = term1 * term2
      qcond = gl * dh * stcond
      if (qcond .lt. 0.0) qcond = 0.0
```

```
c
c       new temperature estimates
        dtdz = (qcore + qcond) * ph / (g * axs * cp(tb))
        tb = t0 + dtdz * lseg / 2.0
        tout = t0 + dtdz * lseg
        if (tb .gt. tsat(p)) tb = tsat(p)
        if (tout .gt. tsat(p)) tout = tsat(p)
c
c       new quality estimate
        dxdz = ph * (q - qcore - qcond) / (g * axs * hfg(tb))
        x = x + dxdz * lseg
        if (x .lt. 0.0) x = 0.0
        if (x .gt. .99) x = 0.99
c
c       new void fraction estimate
        wt = c(16) * (9.81 * de / 2.0 * (1.0 - densg(tb) / densf(tb)))
        rho2 = densg(tb) * void + densf(tb) * (1.0 - void)
        xw = c(6) * (f / 8.0)**0.5 * densg(tb) * 2.0 / r * c(7) / rho2

        term1 = (1.0 - x) * densg(tb) / densf(tb)
        term2 = xw / c(7)
        term3 = (1.0 - 2.0 / r) * densg(tb) * wt / g

        voidc = (x - xw) / (c(17) * (x + term1 - term2) + term3)
        void = voidc * (1.0 - 2.0 / r) + c(7) * 2 / r
        if (void .lt. 0.0) void = 0.0
        if (void .gt. .99) void = .99
c
c       frictional pressure gradient
        call f2phase (f, r, re, c)
        gradpf = (f / de) * .5 * g**2 / (densf(tb))
c
c       gravitational pressure gradient
        rho2 = void * densg(tb) + (1.0 - void) * densf(tb)
        gradpg = 9.81 * cos(angle) * rho2
c
c       acceleration pressure gradient
        ag1 = x**2 / (densg(tout) * void)
        af1 = (1.0 - x)**2 / ((1.0 - void) * densf(tout))

        af0 = (1.0 - x0)**2 / ((1.0 - void0) * densf(t0))
        if (void0 .gt. 0.0) then
          ag0 = x0**2 / (densg(t0) * void0)
        else
          ag0 = 0.0
        endif
        gradpa = g**2 * (af1 + ag1 - (af0 + ag0)) / lseg
c
c       exit pressure
        gradp = gradpa + gradpg + gradpf
        pout = p0 - gradp * lseg
```

```
      if (pout .lt. 101000.0) pout = 101000.0
c
     return
     end
c
```

A.1.13 Subroutine f2Phase

This subroutine calculates the two-phase friction factor.

```
     subroutine f2phase (f, r, re, c)
c
      real*8 f, r, re, cf, c(17)
c
      cf = 1.0 / (c(5) * r) + 49.0 / re**.91
c
      f = c(1) * 1.33 * (1.74 - 2 * log10(cf))**(-2.0)
c
     return
     end
c
```

A.1.14 Fluid Property Functions

The following functions are used to determine fluid properties as a function of temperature. They are based on empirical functions developed by Crabtree and Siman-Tov [1993].

```
real*8 function cond (tc)
c     h2o saturated liquid thermal conductivity (w/m k)
c
      real*8 tc, t, a, b, m, d
c
      if (tc .lt. 20.0) then
        t = 20.0
      else if (tc .gt. 300.0) then
        t = 300.0
      else
        t = tc
      end if
c
      a = .5677829144
      b = .0018774171
      m = -.000008179
      d = 5.66294775d-09
```

```
c
      cond = (a + b * t + m * t**2 + d * t**3)
c
      return
      end
c
      real*8 function cp (tc)
c       h2o saturated liquid specific heat (j/kg k)
c
        real*8 tc, t, a, b, m, d
c
        if (tc .lt. 20.0) then
          t = 20.0
        else if (tc .gt. 300.0) then
          t = 300.0
        else
          t = tc
        end if
c
        a = 17.48908904
        b = -.00167507
        m = -.03189591
        d = -.0000028748
c
        cp = 1000.0 * ((a + m * t) / (1 + b * t + d * t**2))**(.5)
      return
      end
c
      real*8 function densf (tc)
c         h2o saturated liquid density (kg/m^3)
c
        real*8 tc, t, a, b, m, tf
c
        if (tc .lt. 20.0) then
          t = 20.0
        else if (tc .gt. 300.0) then
          t = 300.0
        else
          t = tc
        end if
c
        a = 1004.789042
        b = -.046283
        m = -.00079738
        tf = 1.8 * t + 32
c
        densf = (a + b * tf + m * t**2)
c
      return
      end
c
```

```
      real*8 function densg (tc)
c        h2o saturated vapor density (kg/m^3)
c
        real*8 tc, t, a, b, m, d, e, f, g, h
c
        if (tc .lt. 20.0) then
          t = 20.0
        else if (tc .gt. 300.0) then
          t = 300.0
        else
          t = tc
        end if
c
        a = -.0004375094
        b = -.0069477
        m = .0007662589
        d = .00002418897
        e = -.00000596392
        f = -.00000004227966
        g = .0000002867976
        h = 2.594175d-11

        densg = ((a + m * t + e * t**2 + g * t**3) /
     1        (1 + b * t + d * t**2 + f * t**3 + h * t**4))
c
      return
      end
c
      real*8 function hf (tc)
c   h2o saturated liquid enthalpy
        real*8 tc, t, a, b, m, d, e
c
        if (tc .lt. 20.0) then
          t = 20.0
        else if (tc .gt. 300.0) then
          t = 300.0
        else
          t = tc
        end if
c
        a = .786889159
        b = 4.16304256
        m = -.007798602
        d = -.001874457
        e = -.0000003334
        hf = 1000.0*(a+b*t+m*t**2)/(1.0+d*t+e*t**2)
c
      return
      end
c
      real*8 function hfg (tc)
```

```
c     h2o latent heat of vaporization (k/kg)
c
        real*8 tc, t, a, b, m, d
c
        if (tc .lt. 20.0) then
          t = 20.0
        else if (tc .gt. 300.0) then
          t = 300.0
        else
          t = tc
        end if
c
        a = 6254828.56
        b = -11742.337953
        m = 6.336845
        d = -.049241
c
        hfg = 1000.0 * (a + b * t + m * t**2 + d * t**3)**0.5
c
      return
      end
c
      real*8 function hg (tc)
c  h2o saturated latent heat (j/kg)
        real*8 tc, t, a, b, m, d
c
        if (tc .lt. 20.0) then
          t = 20.0
        else if (tc .gt. 300.0) then
          t = 300.0
        else
          t = tc
        end if
c
        a = 2488.301071
        b = .00062698272
        m = -.00003953072
        d = 3.562872385
c
        hg = 1000.0*(a+b*t**2.5 + m * t**3 + d * t**0.5 * dlog(t))
c
      return
      end
c
      real*8 function pr (t)
c       prandtl number
      real*8 t, cp, visc, cond
c
        pr = cp(t) * visc(t) / cond(t)
c
      return
```

```
      end
c
      real*8 function psat (tc)
c       h2o saturation pressure (mpa)
c
        real*8 tc, t, a, b, m, d, e, f
c
        if (tc .lt. 20.0) then
          t = 20.0
        else if (tc .gt. 300.0) then
          t = 300.0
        else
          t = tc
        end if
c
        a = -7.395489709
        b = .004884152
        m = .036337285
        d = .00000430896
        e = .00002651419
        f = -.00000000414934
c
        psat = exp((a + m * t + e * t**2) /
     1            (1 + b * t + d * t**2 + f * t**3))
      return
      end
c
      real*8 function sftens (tc)
c       h2o surface tension (n/m)
c
        real*8 tc, t, a, b, m, x
c
        if (tc .lt. 20.0) then
          t = 20.0
        else if (tc .gt. 300.0) then
          t = 300.0
        else
          t = tc
        end if
c
        a = .2358
        b = 1.256
        m = -.625
        x = (373.99 - t) / 647.15
c
        if (t .gt. 373.99) then x = 0
c
        sftens = a * x**b * (1 + m * x)
c
      return
      end
```

```
c
      real*8 function tsat (pc)
c       saturation temperature (°m) as a real*8 function of pressure (mpa)
c
        real*8 pc, p, a, b, m, d
c
        if (pc .lt. 2500.0) then
          p = 0.025000
        else if (pc .gt. 8500000.0) then
          p = 8.5000000
        else
          p = pc / 1.0e6
        end if
c
        a = 179.9600321
        b = -.106303
        m = 24.2278298
        d = .0002951
c
        tsat = (a + m * dlog(p)) / (1 + b * dlog(p) +
     1        d * dlog(p)**2)
c
      return
      end
c
      real*8 function visc (tc)
c      h2o saturated liquid dynamic viscosity (pa s) or (kg/m s)
c
        real*8 tc, t, a, b, m, d
c
        if (tc .lt. 20.0) then
          t = 20.0
        else if (tc .gt. 300.0) then
          t = 300.0
        else
          t = tc
        end if
c
        a = -6.325203964
        b = .008705317
        m = -.088832314
        d = -.0000009657
c
        visc = exp((a + m * t) / (1.0 + b * t + d * t**2))
c
      return
      end
```

A.2 Demand Curve Minimum

```
Function ReCrit (ReNom, Pr, Nu, Tp, M0, M1, rd, rv, l, M2)

  Re1 = ReNom * .98
  E1 = dPdReOSV(Re1, Pr, Nu, Tp, M0, M1, rd, rv, l, M2)

  Re2 = ReNom * 1.02
  E2 = dPdReOSV(Re2, Pr, Nu, Tp, M0, M1, rd, rv, l, M2)
  i = 0
  Do
    i = i + 1
    dRdE = (Re2 - Re1) / (E2 - E1)
    E1 = E2: Re1 = Re2
    Re0 = Re2 - .1 * dRdE * E2
    If Re0 < 0 Or Re0 > 2 * ReNom Then
      Re2 = Re2 / 2
    Else
      Re2 = Re0
    End If
    E2 = dPdReOSV(Re2, Pr, Nu, Tp, M0, M1, rd, rv, l, M2)
  Loop Until Abs(E2) < .001 Or i > 500

  ReCrit = Re2
  Iters.Caption = i
End Function


Function dPdReOSV (Re, Pr, Nu, Tp, M0, M1, rd, rv, l, M2)

  'Single-phase Length
  A1 = .0065 * Re * Pr - Nu
  A2 = .001 * Re ^ (11 / 4) * Pr * Tp + .026 * Nu
  l1 = A1 / A2

  'Single-phase gradient
  If l1 < l Then
    A1 = .1582 * Nu
    A2 = .001 * Re ^ 2 * Pr * Tp + .026 * Nu * Re ^ -.75
    A3 = .00046 * Nu * Pr * Re ^ (-15 / 4) - .0715 * Nu ^ 2 * Re ^ (-19 / 4)
    A4 = (.001 * Pr * Tp + .026 * Nu * Re ^ (-11 / 4)) ^ 2
    dP1dRe = (A1 / A2 + A3 / A4)

  'Two Phase Gradient

  'Two-Phase Friction Factor
    f = (1.74 - .87 * Log(.0097 / (M0 * Re ^ (7 / 8)) + 49 / Re ^ .91)) ^ -2

  'Derivative of single-phase length wrt Re
    dl1dRe = l1 * (1 - .423 * l1 * Re ^ (7 / 4) * Tp) / (Re - Nu / (.0065 * Pr))
```

```
'Derivative of f wrt Re
   A1 = (Re ^ 1.02 + 5247 * M0) / (Re ^ 1.04 + 5051 * M0)
   dfdRe = 1.52 * f ^ (3 / 2) * A1 / Re ^ 2

'Two Phase Friction Gradient
   A1 = (l1 - l) * f * Re
   A2 = Re ^ 2 * f / 2
   A3 = (l1 - l) / f * dfdRe + dl1dRe
   dP2fdRe = A1 + A2 * A3

'Two Phase Acceleration Gradient
   Co = 1.13

'Saturation length
   ls = 1 / (4 * Nu / (Re * Pr) + .1582 * Re ^ (7 / 4) * Tp)
   dlsdRe = ls ^ 2 * (4 * Nu / (Re ^ 2 * Pr) + .277 * Re ^ (3 / 4) * Tp)

   z = (l - l1) / (ls - l1)
   dzdRe = z * (dl1dRe * (l - l1 - 1) / (l - l1) - dlsdRe)

   x = M1 * (z - Tanh(z)) / (.0065 * Re + M1 * (1 - Tanh(z)))
   A1 = dzdRe * (1 - Sech(z) ^ 2) / (z - Tanh(z))
   A2 = (.0065 - M1 * Sech(z) ^ 2 * dzdRe) / (.0065 * Re + M1 * (1 - Tanh(z)))
   dxdRe = x * (A1 - A2)

   v = x / (Co * (x * rd + rv) + 1.41 * M2 / Re)
   A1 = v / x * dxdRe
   A2 = v ^ 2 / x * (Co * rd * dxdRe - 1.41 * M2 / Re ^ 2)
   dvdRe = A1 + A2

   A1 = (1 - x) ^ 2 / (1 - v) + (1 / rv) * x ^ 2 / v - 1
   A2 = 2 * dxdRe * (1 / rv * x / v - (1 - x) / (1 - v))
   A3 = dvdRe * ((1 - x) ^ 2 / (1 - v) ^ 2 - 1 / rv * x ^ 2 / v ^ 2)
   dP2adRe = -Abs(2 * Re * A1 + Re ^ 2 * (A2 + A3))
   If v > .65 Then dP2adRe = -100000000# * (1 + 10 * Rnd)

 Else
   l1 = l
   dP1dRe = 7 / 4 * .1582 * l1 * Re ^ (3 / 4)
   dP2fdRe = 0
   dP2adRe = 0
 End If

 dPdReOSV = dP1dRe + dP2fdRe + dP2adRe

End Function
```

Appendix B

RELAP5/MOD3 Input Deck

Appendix B. RELAP5/MOD3 Input Deck

B.1 Steady State Input Deck

```
=Relap5 ANSR Flow Excursion Model
*
0000001  8 10 22
*
0000100 new    transnt
*
0000101 run
*
0000102 si     si
*
0000105    10.0    15.0    400000.0
*
0000200    0.0
*       MaxTime  Min dt    Max dt   ssdtt MinEd MajEd   Rst
0000201      10.0   1.0e-8    0.001     00003 10000 10000  10000
0000202    130.0    1.0e-8    0.001     00003  2000 60000  60000
0000203    140.0    1.0e-8    0.001     00003  2000 10000  10000
*
*
**************************************************************
*    INLET TIME DEPENDANT VOLUME
0010000    inletvol    tmdpvol
*
*       Axs          L    V
0010101    3.46e-5   0.100  0.0
*       Azi  Vert  Vert L
0010102    0.0  90.0  0.100
*     SurfRuf  Dh    pvbfe
0010103    0.0    0.0    00010
*       ebt
0010200    101
*       Time    Temp      X
0010201    0.0    318.0    0.0
*
*
*
*    INLET TIME DEPENDANT JUNCTION
0020000    inletflo    tmdpjun
*         From          To          Axs
```

```
0020101   001000000   003010001   0.0
*      Mass Flows are specified
0020200   1
*      Time    Mdotl    Mdotg   Mdoti
0020201   0.0     0.7612     0.0    0.0
*
*
0030000   inplenum   branch
*      #junctions    mdot/vel
0030001    1          1
*       Axs       L        Volume
0030101   3.46e-5   0.01       0.0
*       Aximuth     Inclination     elevation
0030102     0.0         90.0          0.01
*       wall rough    Dh           pvbfe
0030103     0.0       0.00272       11000
*        ebt     Temp      X
0030200     101    318.0    0.0
*        from       to      Axs  fflow rflow  fvcahs
0031101     003010002 200010001   0.0 0.0   0.0  000000
*       mdotl   mdotg  mdoti
0031201     0.7612  0.0   0.0
*
*      CORE CHANNEL
2000000   core    pipe
*      # Volumes
2000001   20
*
*       Axs      Volume #
2000101   3.46e-5    20
*        L      Volume #
2000301   0.02535    20
*       Vertical Angle
2000601   90.0        20
*       Rough      Dh        Vol#
2000801   0.14e-6   0.00272    20
*       pvbfe    Volume
2001001    11000    20
*       fvcahs    Jnctn#
2001101    000000    19
*       ebt    Temp     X               #Vols
2001201    101    318.0    0.0 0.0   0.0   0.0   20
*
2001300    1   *0-Velocity, 1-Mass Flow
2001301    0.7612    0.0    0.0    19
*
3000000    oplenum    branch
*       #junctions     mdot/vel
3000001      2            1
*        Axs        L        Volume
3000101   3.46e-5   0.01        0.0
```

```
*       Aximuth      Inclination      elevation
3000102     0.0          90.0           0.01
*      wall rough    Dh            pvbfe
3000103     0.0       0.00272        11000
*      ebt     Temp      X
3000200      101    318.0     0.0
*      from       to       Axs  fflow rflow  fvcahs
3001101      200200002 300010001  0.0 0.0   0.0  000000
3002101      300010002 400000000  0.0 0.0   0.0  000000
*      mdotl  mdotg  mdoti
3001201      0.7612  0.0   0.0
3002201      0.7612  0.0   0.0
*
*     EXIT VOLUME
4000000    exitvol    tmdpvol
*       Axs        L    V
4000101    3.46e-5  0.01  0.0
*       Azi  Vert  Vert L
4000102   0.0  90.0   0.01
*       SurfRuf  Dh    pvbfe
4000103     0.0    0.0   00010
*       ebt
4000200     102
*       Time    Pressure     X
4000201     0.0       1.7e6    0.0
*
*
*      HEAT STRUCTURES
*
*
*
*
*   CORE CHANNEL LEFT BOUNDARY
*      #Axial  #Rad  Rect  IC's  LBound  Rflood RefBound SubIntrvls
12000000   20    5    1    1    0.0    0      1    16
*      MeshLoc Meshformat
12000100    0    2
*       inverval      number
12000101    0.000635      4
*       Comp  intervals
12000201    1    4
*        factor  interval
12000301    1.0     4
*
12000400    0  *0 temps
*        temp     mesh
12000401    318.0   5
*       BoundCond    Inc    BCType SAcode  Ah         HSN
12000501    0            0      0    1    6.44e-4     20
*
12000601    200010000  010000  1     1      6.44e-4      20
```

```
*       Table# Mult    LCoef RCoef  HSN
12000701    101    1.0000  0.0    0.0   20       *.0486
*         Dh    EntrnceL1 EntrnceL2 Grid1 Grid2 Loss1 Loss2 LBF  HSN
12000901    0.0     100.0     100.0    0.0  0.0  0.0  0.0  1.0  20
*
*
*
*  CORE CHANNEL RIGHT BOUNDARY
*     #Axial  #Rad  Rect  IC's  LBound  Rflood RefBound SubIntrvls
12010000   20   5   1   1  0.00381   0    0   16
*      MeshLoc Meshformat
12010100   0   2
*      #intervals   rb
12010101   0.000635    4
*      Comp  intervals
12010201   1    4
*      factor  interval
12010301   1.0    4
*
12010400   0  *0 temps
*       temp    mesh
12010401   318.0   5
*      BoundCond   Inc    BCType SAcode  Ah        HSN
12010501    200010000 010000   1    0    6.44e-4      20
*
12010601   0        0       0   0    6.44e-4       20
*       Table# Mult    LCoef RCoef  HSN
12010701   101    1.0000  0.0     0.0    20 *.0486
*          Dh    EntrnceL1 EntrnceL2 Grid1 Grid2 Loss1 Loss2 LBF  HSN
12010801   0.0     100.0     100.0    0.0  0.0  0.0  0.0  1.0  20
*
*
20100100   tbl/fctn  2   1
*       Conductivity Function
20100101   273.0 870.0 156.93 0.18738 -2.5238e-4 0.0 0.0 0.0 273.0
*
*       Volumetric Heat Capacity
*compxn      temperature          vol ht cap
20100151      271.9               2.429e6
20100152      299.7               2.429e6
20100153      399.7               2.542e6
20100154      499.7               2.666e6
20100155      599.7               2.791e6
20100156      699.7               2.915e6
20100157      799.7               3.039e6
20100158      899.7               3.163e6
20100159      924.7               2.826e6
20100160     1060.8               2.826e6
20100161     1100.                2.826e6
20100162    20000.                2.826e6
*
```

```
*
*   HEATED CHANNEL POWER (WATTS)
20210100    power
20210101       0.0     0.0
20210102      10.0     0.0
20210103     130.0  4443.6
20210104     140.0  4443.6
*
*
*
. The end of the test
```

B.2 Transient Input Deck

```
=Relap5 CF62294 Flow Excursion Model
*
0000100 restart    transnt
*
0000101 run
*
0000102 si     si
*
0000103   596402
*
0000105    10.0    15.0    400000.0
*
0000200    0.0
*       MaxTime  Min dt    Max dt  ssdtt MinEd  MajEd   Rst
0000201      5.0   1.0e-8   0.001  00003  1000   1000   1000
*
0000202    205.0   1.0e-8   0.001  00003  1000  50000  20000
*
*
*
***************************************************************
*   INLET TIME DEPENDANT JUNCTION
0020000    inletflo    tmdpjun
*          From          To         Axs
0020101   001000000   003010001    0.0
*     Mass Flows are specified
0020200    1
*       Time      Mdotl     Mdotg  Mdoti
0020201   0.0      0.7612     0.0    0.0
0020202   5.0      0.7612     0.0    0.0
0020203  205.0     0.1730     0.0    0.0
. The end of the test
```

VITA

Joel Lee McDuffee was born in Gallatin, Tennessee on March 20, 1967. He attended elementary, junior high, and high school in the Shackle Island community near Goodlettsville, Tennessee. He graduated from Beech Senior High School in June, 1985. Joel entered Middle Tennessee State University the following August and graduated with a Bachelor of Science degree in Aerospace Technology in December, 1989. He entered the University of Tennessee in August, 1991 and earned a second Bachelor of Science degree in Nuclear Engineering in 1994. Joel immediately reentered the University of Tennessee and received a Master of Science degree in Engineering Science and Mechanics in December, 1995.

Joel is presently employed by the University of Tennessee as a research assistant. He works primarily at the Thermal Systems Section of the Engineering Technology Division of Oak Ridge National Laboratory.